UNIVERSITY OF CINCINNATI

December 21st , 20 00

I, Boon Kwee Lee **,**
hereby submit this as part of the requirements for the degree of:

Doctorate of Philosophy (Ph.D.)

in:

Electrical Engineering

It is entitled:

Optical Storage in Erbium doped Gallium Nitride
Using Focused Ion Beam Nanofabrication

Approved by:

Dr. Andrew J. Steckl
Dr. Peter B. Kosel
Dr. Fred Beyette
Dr. Joseph T. Boyd

Optical Storage in Erbium doped Gallium Nitride Using Focused Ion Beam Nanofabrication

A dissertation submitted to the

Division of Research and Advanced Studies
of the University of Cincinnati

in partial fulfillment of the
requirements for the degree of

DOCTORATE OF PHILOSOPHY (Ph.D.)

in the Department of Electrical & Computer Engineering and Computer Science
of the College of Engineering

2000

by

BOON KWEE LEE

B.S., University of Tennessee 1990
M.S., University of Cincinnati 1994

Committee Chair: Dr. Andrew J. Steckl

Abstract

In this research, we propose a concept for a high-density, page-oriented data storage using optical upconversion emission from erbium doped gallium nitride (GaN:Er). This alternative storage design is based on nonlinear optical process of rare earth (RE) doped in wide bandgap semiconductor host. Data is recorded with focused ion beam (FIB) write technology and retried as amplitude modulated signal by detecting the incoherent upconversion emission. Writing process with FIB could be implemented with either ion implantation or ion milling approach.

With ion implantation approach, Er ions were implanted by FIB into undoped GaN thin film grown on sapphire or silicone (Si) substrates. Thermal annealing process was applied next to activate the optical properties of implanted Er ions. Information stored as data bits consists of patterns of implanted locations as logic '1' and unimplanted locations as logic '0'. The photon upconversion process in Er ions is utilized to read the stored information. This process makes use of infrared (IR) lasers (840 nm and 1 μm) to excite visible emission (522 and 546 nm). Patterns as small as 0.5 μm were implanted and read. Volumetric optical memory based on GaN:Er semiconductors could in theory approach storage capacity of 10^{12} bits/cm^3.

With ion milling approach, sub-micron patterns were micro-machined on MBE grown in-situ doped GaN:Er film on Si substrate. Data retrieval is accompanied by upconversion emission at 535 and 556 nm upon 1 μm IR laser stimulation. Regions where Er-doped

GaN layer is completely removed (and do not emit) are defined as logic '0', while regions that are not milled (and do emit) are defined as logic '1'. Data patterns with sub-micron bit size (or 100 Mbits/cm^2 density) have been fabricated by FIB milling. Data written by this approach has a theoretical storage capacity approaching 10 Gbits/cm^2.

Our implementation of this proposed optical storage architecture takes advantage of capabilities that is available in the Nanoelectronics Laboratory such as, non-optical recording technique with FIB implantation or milling, liquid alloy ion source fabrication, epitaxial growth of GaN films by molecular beam epitaxy, upconversion optical readout set-up, and visible to IR optical characterization.

Acknowledgments

First and foremost, I would like to dedicate this thesis to my beloved wife, Naoe, and our good luck charm and supercat, Yuki Chan, for their unwavering support, patience, and understanding to help me get through many years of my research work.

I would also like to thank my advisor, Dr. Steckl, whose vision and guidance help me achieve my goals. I would also like to acknowledge the help and friendship of the Nanolab mates who have challenged and encouraged me throughout my endeavor at my doctoral program. They are JD, Vivek, John, Ron, Don, David, Irving, Jay, Robert, Mike, Bob, Jason, Ming, Lin, and Julie. I am thankful especially to Ron and Don for providing me with Er doped GaN samples, to David and Jay for preparing Er LAIS for FIB ion implantation for me, to Irving and Bob for assisting me in the operation of FIB ion milling system, and to Robert for helping me set up LabVIEW integration system.

At last, I would like to thank my Mom, Dad, sisters, and brothers for their continuous support and confidence on me.

This work owes its existence to every one of them.

Table of Contents

List of Tables and Figures

Chapter 1 Introduction

Chapter 2 Optical Data Storage Technology

Chapter 3 Research Objective Technology

<u>Chapter 4</u> Research Objective

Chapter 5 Experimental Results

- **Figure 5.21**: Upconversion intensity per bit with respect to bit density. Intensity pre bit is derived from the total upconversion intensity excited by 2 μm in diameter laser divided by total number of bits covered by the laser beam size. Plot shows the inverse relationship between bit density and intensity emitted by each bit.
- **Figure 5.22**: Upconversion emission intensity versus current bit density (diamond data points). Maximum bit density of ~10 Gbits/cm^2 is projected with current FIB milling parameters. To achieve terabyte storage capacity, an 100X improvement is required.
- **Figure 5.23**: (a) Microphotographs of 1.6 μm pitch and 0.8 μm pitch bit patterns.
  (b) CCD optical image of upconversion emission from 1.6 μm pitch bit pattern

Chapter 1
Introduction

Since humans have mastered the art of communication in the early day, we have been seeking practical way to preserve thought and to exchange knowledge. From stone inscription, script writing to printing press, humans have been able to gradually spread ideas, and gain one another's learning. Learnt information is gradually accumulated, organized, and redistributed. Until the emerging of digital technology, there were no effective means to record and maintain the ever-increasing amount of data available beyond the usual tablet inscription, paper printing, photography, and film. Today data is stored in variety forms, nonetheless, they are generally stored in two basic formats: analog or digital. Analog data is usually stored in the form of picture or image whereas digital data is stored in the form of binary bits. Current predominant methods for data storage are strongly associated with computer applications; thus, we generally think of data storage only in digital sense.

In today information age, endless proliferations of digital technology leads no doubt the parallel ever increasing demand for data storage. Information is now routinely stored, transferred, and accessed in the form of binary bits. To appreciate the need for new data storage methods, we must first comprehend the basis of how data is stored, the materials suitable for storing data, and the competing yet sometime complimenting techniques for data storage systems

1.1 What is Data Storage?

When information is stored in predefined patterns, and can be retrieved in recognizable unaltered fashion in later time; then, we have established some form of data storage systems. Data storing techniques usually involve encoding tactics, choices of media, and storage methods. When designing digital data storage, there are four important parameters that characterize each storage systems. The four parameters are data storage capacity, access time, transfer rate (latency), and cost per bit. The storage capacity is a direct function of storage bit density and the geometrical dimensions of the media. The access time measures how fast a data location can be accessed on the storage media. Access time is usually prescribed by the physical design of the detection system and the relative motion between the readout head and the media. The data transfer rate measures how long the data stream must be stored and retrieved by the storage system as a whole. Transfer rate is determined by storage density, detector sensitivity, tolerance of signal to noise ratio, and the responsiveness of system controller. Finally, the cost of the drive or cost per bit, consists both drive and storage media cost. It is strongly depended on numbers of unit production, complexity of assembly process, and total numbers of component parts involve in an overall system design.

1.2 The Memory Hierarchy

There are no single storage systems that can encompass maximum performance in all four parameters at once. The characteristics of the storage systems are governed by the different emphases on each parameter, each with its own strength and weakness. Each storages employs strategy to create effective memory system that maximizes overall data store-retrieval performance with given set of objective and cost. In modern sequential computer architecture terminology, these memory systems are categorized into three major levels of the storage hierarchy order as shown in Figure 1.1: primary, secondary, and tertiary memory, based upon memory access time by the computer. Generally speaking, there exist a trade-off relationship between the access time and the cost/capacity, which dictates that the faster the accessibility, the higher the cost/capacity.

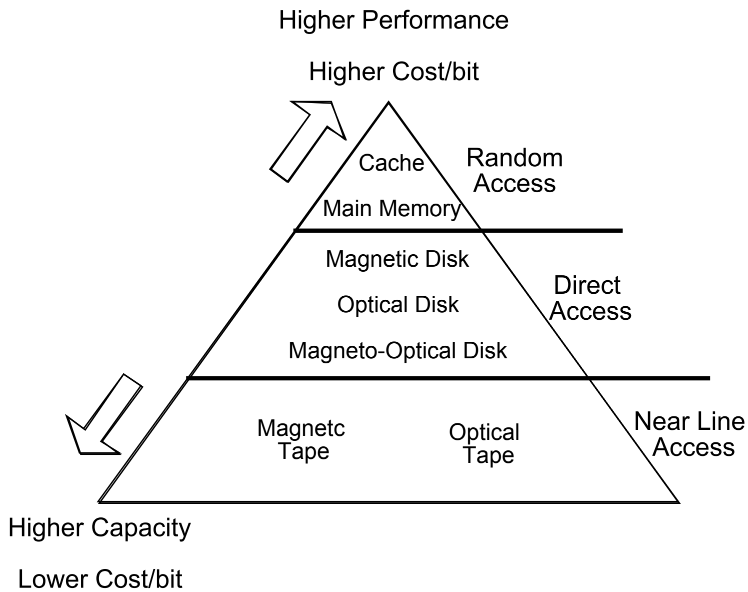

Figure 1.1: Memory hierarchy in existing computing architecture.

A. Primary Memory

Primary memories are currently based on solid-state storage technology. They are semiconductor transistors, either implemented as cache memory (local storage within the processing chip), called static read only memory (SRAM); or as main memory (add on chips installed on motherboard), called dynamic RAM (DRAM). Primary memories contain data that are critical for random access by CPU processing and are designed to have access times comparable to the microprocessor clock cycle, which is in the range of hundreds of megahertz to gigahertz. Due to the cost of semiconductor fabrication, primary memories are very expensive. Therefore, in spite of their speedy access times, storage capacity of these types of memories is limited, usually in the range of few kilobytes to hundreds of megabytes. Data stored in primary memories are volatile. Contents in the memory addresses will be lost when computer is rebooting.

B. Secondary Memory

These groups of memories are customary associated with the term, “data storage” instead of “memory”. They are designed to hold significantly more data (currently in excess of gigabytes) with lower cost per bit and slower access times (in the range of milliseconds) than those of primary memories. Due to the slower access speed, portions of stored software instruction codes are constantly swapped with primary memories to keep pace with microprocessor clock cycle time. As a result, secondary memories are designed to sustain many times of read and write operations. Although data can be hold more permanently, secondary memories are neither sufficient nor suitable for long-term archival storage purpose due to high cost of ownership and limited ability of long-term data preservation. Common storage devices of these types are hard disk drives (HDD), magneto-optical (MO) disks, and optical compact discs (CD).

C. Tertiary Memory

To supplement the shortcoming of secondary memories, tertiary memories are designed solely to handle mass data archival need with scarification of rather fast access time. These memories can store huge amounts of data well into terabytes range, but have data access time on the order of minutes to hours. Archival storages are not designed to require many write operations, and write-once, read-many (WORM) systems are adequate. Nor the designs are specified for random access and ease of interaction. The emphases of these groups of memories are on reliability, interconnection (server) capability, low cost of ownership, and long-term data perseverance. Presently, archival data storage systems require large installations based on magnetic and optical tapes, often operate off line. Despite having the lowest cost pr bit, archival storage is typically the most expensive single element of modern computer installations. Typical devices of these types are Magnetic Tapes Libraries and Optical Jukeboxes.

Figure 1.2 shows storage capacity versus access time for various commercial storage systems currently available. It also depicts the trade-off between short access times and high capacity among components of hierarchy memory systems.

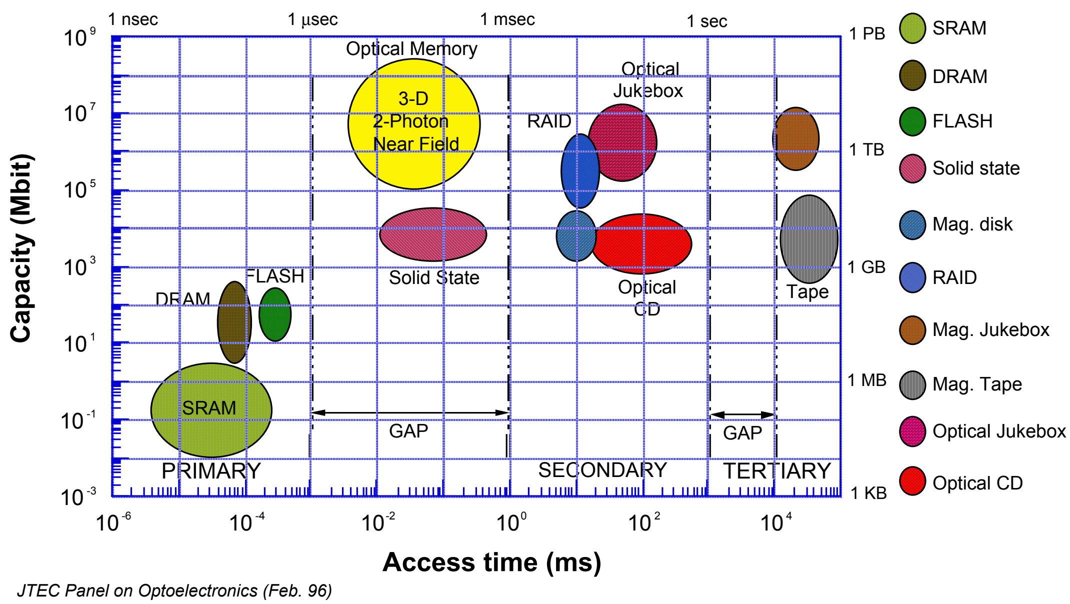

Figure 1.2: Comparison of capacity and random access time of computer memory systems. The general trend is that higher capacities are obtained at the expanse of longer access time.

1.3 Magnetic versus Optical System

Data is routinely stored as electrical charge in semiconductor chips, magnetic polarized domain in magnetic tapes and HDDs, optical modulation in CDs, or thermo magnetic domain switching in MO drives. However, the two most competitive form factors for mass archival data in current market are either in magnetic or optical systems.

In magnetic systems, areal density of data storage is governed by the size of a magnetic domain. To minimize the size of these domains, the magnetic heads need to be miniaturized and kept close to storage media (approximately 50 nm apart). Fortunately, due to the much simple magnetic induction head design, the magnetic heads are relatively easy to be minimized. The low inertia of these miniature heads in term allows the design for faster media rotation speed. Both factors permit the access times of magnetic systems to be shorter than that of optical disk systems by about one order of magnitude. The fragility of the magnetic head and the close proximity with the media, however, restrict magnetic media to be built in enclosed systems to avoid head clash, thus make them unsuitable for removable system. Nevertheless, there are some magnetic disk products such as, Iomega disks and Castlewood ORB disks, provide some transportability at the expanse of longer access times.

Optical systems, one the other hand, store and retrieve data by a focused laser beam. By using lens to focus the laser beam, the detection head can be built some distance away from media to avoid head crash. Due to the complexity of optical system designs, the readout head is built relatively bulky, thus penalize the effort to achieve access times that are comparable to those of magnetic systems. However, efforts to improve access times have been implemented by either with multi beam illumination- parallel detection approach (Kenwood Technologies), whereby a single laser beam is split into multiple beams through a diffraction grating and tracked by a detector array, or demonstrated by miniaturization of the readout head through optoelectronic integration techniques. To date, optical compact disk (CD) drive could record 700 megabyte of data or 80 minutes of audio on a 120 mm removable disc. Data can be written on a spinning media either once on recordable optical disk (CD-R) or many times on rewritable optical disk (CD-RW). Optical systems are like magnetic systems, insofar as they provide fast random access to any of the data recorded on the disk and their data rates and access times are on par with those of magnetic system. Optical systems, usually equipped with less expensive media, are however built more rugged, removable, portable, and interchangeable. They are ideal for mass data replication and possess long memory persistence for archival applications. In the past, optical systems have also provided higher storage capacity per disk than magnetic systems. However, improvement in new magneto-resistive readout heads and more efficient data coding scheme such as write-wide, read-narrow geometry, provide magnetic storage devices with low interference noise and high storage density. Thus, Magnetic systems have managed to increase areal storage density that is restricted by paramagnetic limit of magnetic in the past and diminished the advantage that have long been claimed by the optical systems. The storage density of magnetic hard disks is expected to increase at a rate not slower and possible faster than optical disk systems. Magnetic systems will therefore continue to maintain large market share in the foreseeable future. Nonetheless, the optical systems have certainly not lost their ground. In contrary, new innovation in both magnetic and optical systems will ensure the competition between both systems for years to come.

1.4 Race to Terabyte Storage Capacity

While the race between magnetic and optical systems has yet to be determined, the demand for terabyte data storage density has long been concluded. Figure 1.3 shows the general trend toward the need for high storage density and fast access time. The projected data need over the next 10 years will certainly exceed terabyte range. The race to terabyte storage capacity is essentially fueled by two mutually dependent factors: emerging of new applications and progression in technology innovation. New types of applications push a notch on technology demand to support the growing trend of storage capacity; new improvement in technology to meet storage demand will in term spur the creation of more new applications.

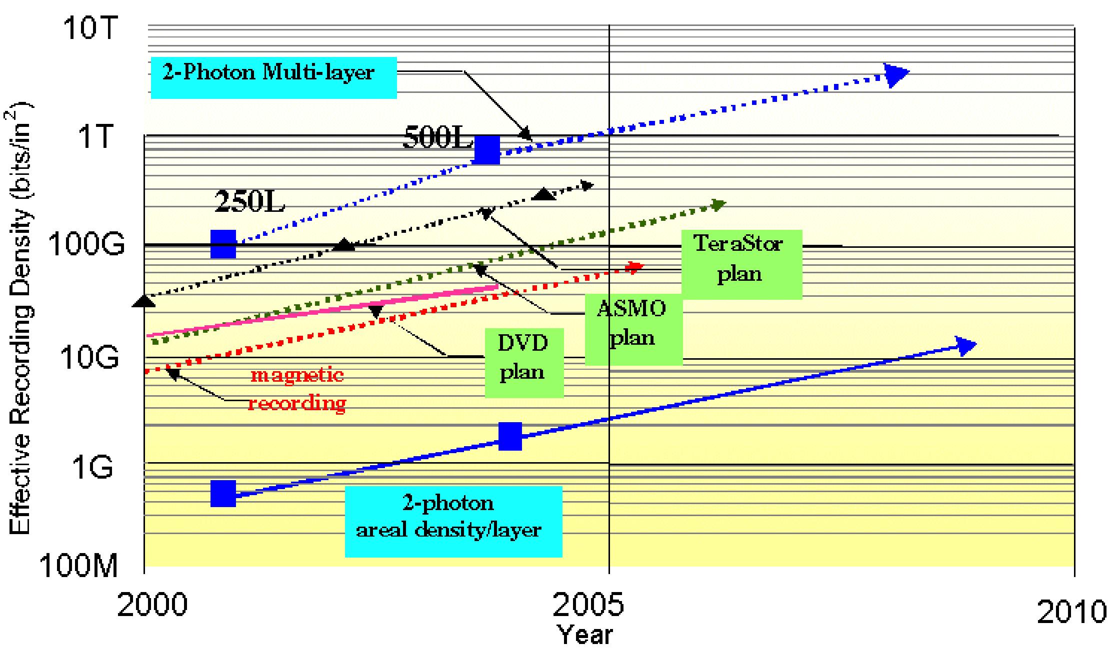

Figure 1.3: Possible roadmap for future data storage technologies.

Applications such as a two-hour long per disk video, call for digital versatile discs (DVD) standard. High definition television (HDTV) applications will need 15 GB storage capacities per movie. By the year 2005, phase change (PC) and MO manufacturers could produce 30-40 GB disks to replace VCR. Emerging storage applications, such as home multimedia application (10 GB), multimedia file servers (1 TB), high definition television and video disk recorder (HDTV/VDR) (100 GB), and massive storage applications (10 PB), will continue to push capacity requirements beyond 0.1 TB to 1 TB per disk. Beyond 2005, future applications will require affordable data storage systems capable of providing high capacity (in excess of 60 $Gbits/in^2$ effective areal density) and high data rates.

The race to terabyte storage capacity motivated by future application requirements will certainly boost the development of novel storage systems. Some of these innovative data storage techniques are near-field,[1] holography,[2,3] multilayer recording,[4,5] magnetic super resolution (MSR) recording[6,7] for MO, multi-value recording,[8] multi-wavelength reading,[9] partial response maximum likelihood (PRML) reading,[10] land and groove recording,[11] deep grove recording,[12] single carrier independent pit edge recording (SCIPER)[13] and radial partial response (RPR)-SCIPER recording,[14] pit pattern modulation, pit depth modulation,[15] two photon absorption multilayered disk,[16] cholesteric liquid crystal based multilayered disk,[17] 3-D recording,[18] and super resolution with photochromic mask layer.[19]

The road ahead is clouded but optimistic. No one can predict which novel techniques is the winner for future storage systems. However, Storage systems developed to meet future applications will certainly need to integrate advanced components including media, lasers, data sensors, actuators, micro-optics, and parallel optoelectronics signal processing, into cost-effective, robust packages.

1.5 Research Objective and Approach

The increasing reliance of today society on information services, such as Internet, E-commerce, B2B commerce, database systems, and multimedia, has fueled the ever-increasing demand for data storage. Current planar optical storage devices such as CD-ROM, WORM, CD-R, CD-RW, PD, MO, and DVD are insufficient to cope with the growing storage capacity requirements, which are expected to exceed the Terabyte level[20] by the year of 2010. Further, with access speeds on the order of 10 Mbits/sec current systems cannot provide the data transfer rates necessary for practical utilization of Terabyte storage systems. To satisfy the dual need for high density and fast access time, research in the area of optical data storage has begun focusing on alternative optical storage media. In contrast to current optical disk technologies that use far-field optics to read optically detectable data stored as a two dimensional arrangement of bits, these alternative media are capable of exploiting either the increased resolution associated with near-field optics or the three dimensional (3-D) potential of free space optics.

With near-field technology, such as solid immersion lens (SIL), near-field scanning optical microscopy (NSOM), and near-field arrays of vertical-cavity surface-emitting lasers (VCSELs), features as small as 10 nm in diameter can be read and write on an advanced optical disk.[21,22,23,24] The reduction in feature size has the potential to increase storage densities to 10^4 bits/μm^2. One drawback is that removable disks might not possible. To achieve near-field resolution the spacing between the optical disk and the read head is limited to the order of $\lambda/4$ or approximately 200 nm for near IR operation. This extremely close proximity may be prohibitive for removable disk storage systems.

Alternatively, volumetric storage methods increase storage capacity by stacking data three-dimensionally. Based on optical diffraction limitations, these 3-D optical memory systems have theoretical storage capacities approaching 10^{12} bits/cm^3. Further, the incorporation of page oriented pre-processing units designed to interface 3-D optical memories to existing electronic host systems, should allow data transfer rates on the order of hundreds of Mbits/sec.[25,26] Thus, archival storage systems based on 3-D optical memories should be capable of reasonable user access time while providing storage capacities significantly larger than the existing optical disk technologies.

First proposed in 1960, volumetric optical data storage has however proven extremely difficult to achieve.[27,28,29,30] Currently, holographic data storage,[31,32,33] multilayer disk technology,[34,35] and 3-D bit oriented methods that use femtosecond lasers are the leading technologies.[36] All three approaches promise to provide storage density hundreds of times denser and access speeds faster than current optical disk media. However, they are not without technological barriers. Holography faces significant materials quality and stability issues. Absorption and multi interface reflections may inhibit read and write operations to the lower layers of multilayer disks. Bit oriented 3-D memories can require expensive lasers and optics and fail to provide high access speeds.

Rare earth (RE) doped integrated optical devices have recently generated great deal of interest due to their board applications in fiber lasers, fiber amplifiers, optical communications, optical sensing, high resolution spectroscopy, and 3-D display.[37,38] Furthermore, RE atoms emit light with a very sharp linewidth associated with specific inner 4f shell transitions. A large variety of emission wavelengths are available, covering the UV, visible, and IR, with such atoms as praseodymium, europium, holmium, thulium, erbium, etc.[39,40,41,42] It is therefore a viable option to create a 3-D, high density, and page-oriented memory device based on optical emission from rare-earth-doped semiconductors. In fact, RE based optical storage researches have been gaining momentum in area, such as spectral hole burning, photon echo, electron trapping, and even holography with RE doped storage medium.[43,44,45,46] However, methods such as those require low temperature set-up, difficult manufactured storage mediums, expensive broad range tunable lasers, and radical shift from present bit-by-bit strategies. Therefore, there is need to find simple and conventional approach to make RE based optical storage.

1.6 Novel Erbium doped Gallium Nitride Nonlinear Optical Storage System

A. Objective

In this research we propose a concept for a high density, page-oriented memory using optical upconversion emission from Erbium (Er) rare-earth-doped Gallium Nitride (GaN) wide bandgap semiconductor (WBGS). The implementation of this proposed concept should include array of capabilities that is available in the Nanoelectronics Laboratory: non-optical recording technique with focused ion beam (FIB) implantation or milling, rare-earth liquid alloy ion sources (LAIS), epitaxial growth of GaN structures by MBE, readout optical system design for two-step two-frequency (TSTF) upconversion, and visible to infrared (IR) optical characterization.

B. Concept

B-I. Planar Storage Structure

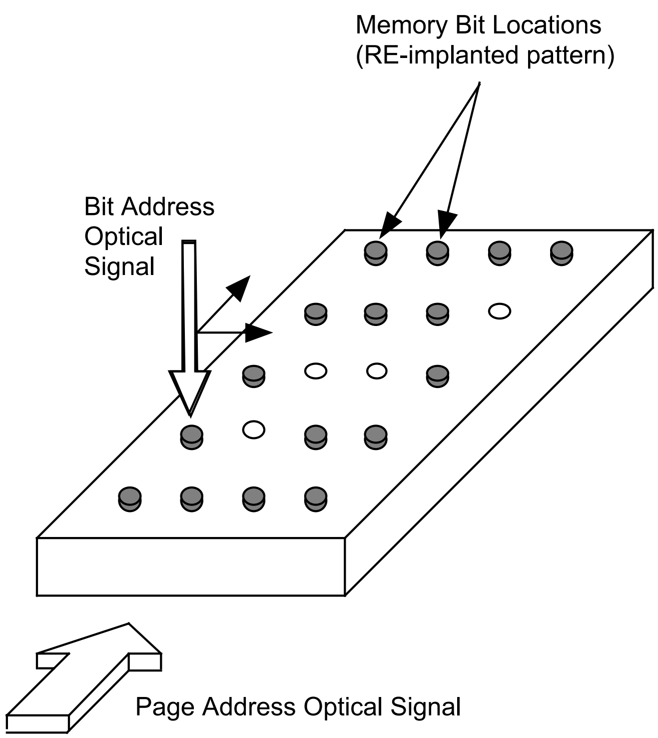

Figure 1.4: Two-dimensional, page-addressed archival memory utilizing two-photon absorption in rare earth ions.

Planar storage structure will be based on conventional CD format, where logical '1' and '0' are represented by the presence and absence of rare earths induce upconversion luminescence respectively. As illustrated in Figure 1.4, one approach is to store information by implanting a closely spaced pattern of single RE ions into an optically transparent wide band-gap semiconductor. Data bits would consist of pattern of implanted locations as logic '1' and unimplanted locations as logic '0'. This could be accomplished by FIB implantation with spacing as small as 10 to 50 nm (depending on species, energy, and substrate). In principle, this could result in an area bit density of 10^{10} to 10^{12} bits/cm^2. Alternative approach to achieve similar data bit recording effect could be attained by FIB milling technique. Surface of RE in-situ doped film would be strategically removed by FIB milling procedure to mimic unimplanted location as logic '0', while leave the rest of unmolested locations as logic '1'.

In the storage media the read operation could take advantage of the upconversion phenomenon in RE ions. Upconversion involves the absorption of two photons of same or different energies producing the emission of a third photon of energy higher than that of either of the incident photons. Only the location doped with RE ions would emit incoherent light when excited by IR laser, which could then be detected by a photodiode or other photodetector. Blue and green emission from Er and Pr in various hosts has been obtained under red and IR two-photon excitation.

Areal density can be increased either by recording sub-micron features that can only be retrieved by near field detection or by frequency multiplexing with codoping several RE ion species at single location, where each ion species would emit photoluminescence with distinct wavelength.

B-II. Volumetric Storage-Multilayer Structure

Volumetric storage system can be constructed simply by stacking multiple planar storage pages to form a three-dimensional memory. A conceptual operation of such a device is depicted in Figure 1.5. Data bits in each layer of the storage would be accessed by dynamically channeling optical beam to the desired page in the stack. Detecting incoherent upconversion signal will be much easier than detecting a reflected coherent optical beam, since incoherent beam would not create constructive interference noise when more layers are added to the structure. By detecting the incoherent upconversion emission, interference could be prevented from obscuring the real data signal thus

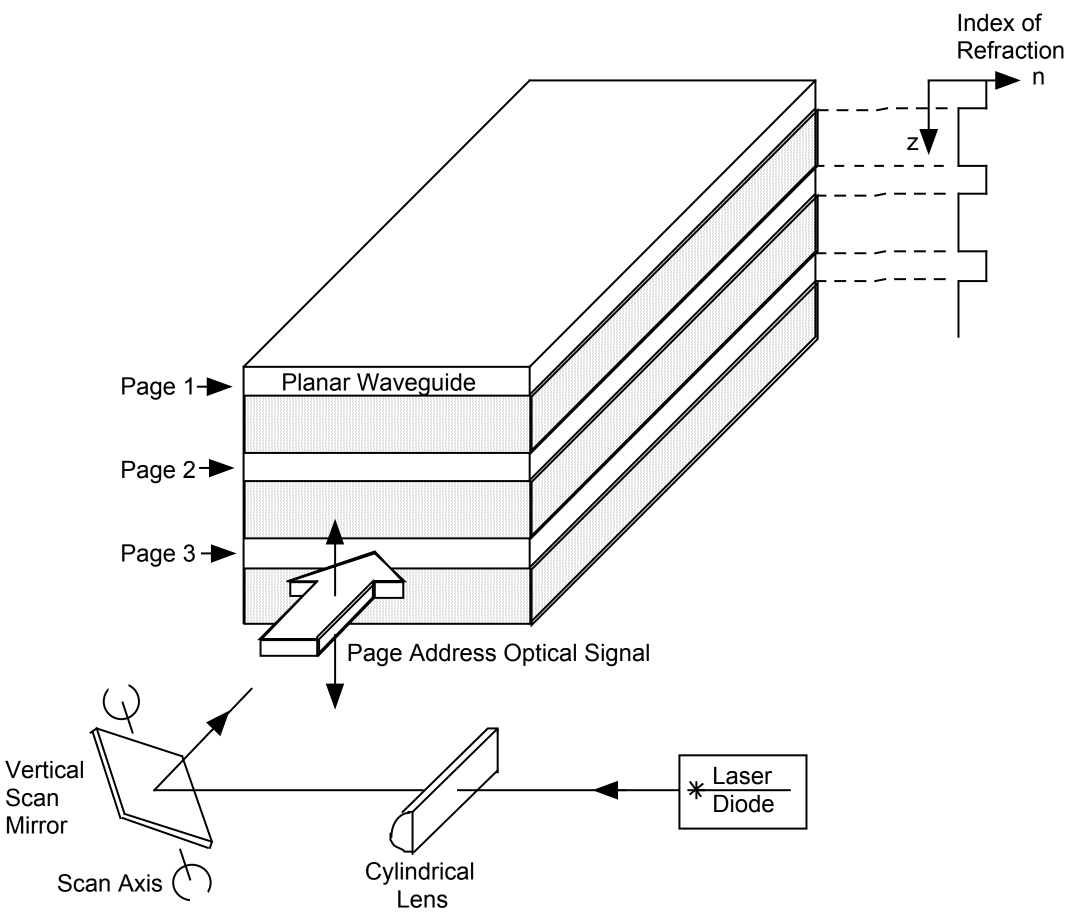

Figure 1.5: Three-dimensional archival memory using a multi - layered wide band-gap semiconductor (GaN/AlN) structure with alternating index of refraction.

increase the SNR. The enhanced SNR should allow stacking more layers into single structure and thereby increasing the effective storage capacity.

To fully take advantage of volumetric storage and enhance the overall system performance, the TSTF upconversion readout process could be implemented. In the TSTF upconversion readout process, two optical beams would be employed for accessing the 3-D data bit storage. One optical beam would serve as address beam and the other as data beam. Only at the location where both beams intersect, would the TSTF upconversion take place. This approach could greatly reduce attenuation loss when optical beams are needed to penetrate deep inside the volume.

To further improve SNR level, this 3-D memory storage could be built with multi-layered waveguide-like structure with alternating index of refraction and low optical loss. An interesting material candidate to accomplish this structure would be the GaN/AlN system. Both GaN and AlN are transparent to the three (two input and one output) optical signals involved in the read operation. GaN with the smaller bandgap and larger refractive index would serve as the waveguide material, while AlN would serve as the optically confining layer. Furthermore, Er implanted GaN can produce strong single-photon TSTF upconversion luminescence by two intersecting optical beams at room temperature.

C. Research Plan

The objective of our research is to demonstrate the feasibility of developing an optical storage system based on RE dopants. The whole research work is divided into three phases: basic RE materials research, FIB technology associated write-process evaluation, and optical read system development. In the first phase, initial studies will be done on basic materials research to develop the suitable RE based storage medium. Efforts will be focused on Er doped GaN films grown by MBE. In the second phase, samples written with both FIB implantation and milling approaches are evaluated to determine the best recording conditions. Investigation on Er LAIS implantation ariel sizes, energies, doses, and anneal time and temperature, will determine the best conditions for writing page oriented data using FIB implantation induced damage on the GaN film. Comparison study on optimized FIB milling condition will also be conducted. In the third phase, initial optical readout system for stepwise upconversion process is being developed. The feasibility of page oriented reading of RE storage medium is demonstrated with CCD camera.

1.5 References

[1] S. Hosaka, T. Shintani, M. Miyamoto, A. Hirotsune, M. Terao, M. Yoshida, K. Fujita, and S. Kammer, Jpn. J. Appl. Phys. **35**, 443 (1996).

[2] D. Psaltis, X. An, G. W. Burr, and F. H. Mok, Tech. Dig. ISOM/Optical Data Storage, JTuC1-1, 100 (1996).

[3] D. Lande, J. F. Heanue, M. C. Bashaw, and L. Hesselink, Tech. Digest ISOM/ODS'96, JTuC3-1, 106 (1996).

[4] T. Yashuhira, Y. Mitsuhashi, T. Morikawa, and J. Shimada, Appl. Opt. **16**, 2532 (1977).

[5] K. A. Rubin, H. J. Rosen, T. McDaniel, and W. Tang, Tech Dig. ISON/ODS'96, OMB1-1, 10 (1996).

[6] A. Takahashi, Y. Murakami, J. Hirokane, J. Nakayama, Y. Kurata, and H. Yamaoka, Jpn. J. Appl. Phys. **36**, 200 (1997).

[7] K. Torazawa, S. Sumi, S. Yonezawa, N. Suzuki, Y. Tanaka, A. Takahashi, Y. Murakami, and N. Ohta, Jpn. J. Appl. Phys. **36**, 591 (1997).

[8] H. Takao, K. Shimazaki, N. Ohta, M. Yoshihiro, N. Nagai, and S. Imai, Jpn. J. Appl. Phys. **36**, 414 (1997).

[9] K. Shimazaki, H. Takao, N. Ohta, K. Nakagawa, and A. Itoh, Tech. Dig. ODS'97, MC4, 20 (1997).

[10] T. Narahara, K. Aratani, A. Fukumoto, and S. Masuhara, Jpn. J. Appl. Phys. **36**, 549 (1997).

[11] K. Narita, T. Kawano, and H. Takeshima, Jpn. J. Appl. Phys. **36**, 495 (1997).

[12] S. Morita, M. Nishiyama, and T. Ueda, Jpn. J. Appl. Phys. **36**, 444 (1997).

[13] J. P. de Kock, S. Kobayashi, T. Ishimoto, H. Yamatsu, and H. Ooki, Jpn. J. Appl. Phys. **35**, 437 (1997).

[14] S. Kobayashi, T. Horigome, T. Ishimoto, and H. Yamatsu, Tech. Dig. ODS'97, TuB3, 42 (1997).

[15] B. V. Johnson, G. A. McDermott, M. P. Oneill, C. Piertrzyk, T. Shafaat, S. Spielman, D. K. Warland, and T. L. Wong, Tech. Dig. ODS'97, TuB4, 44 (1997).

[16] I. Cokgor, F. B. McCormick, A. S. Dvornikov, M. M. Wang, N. Kim, K. Cobvlentz, S C. Esner, and P. M. Rentzepis, Tech. Dig. ODS'97, TuC5, 54 (1997).

[17] W. Schlichting, S. Faris, B. Fan, J. Haag, Z. Lu, S. Kane, L. Li, T. Milster, and H. Luo, Jpn. J. Appl. Phys. **36**, 587 (1997).

[18] E. N. Glezer, M. Milosavljevic, L. Huang, R. J. Finlay, T. H. Her, J. P. Callan, and E. Mazur, Tech. Dig. ISOM/ODS'96, OWB2, 227 (1996).

[19] T. Tsujioka, M. Kume, Y. Horikawa, A. Ishikawa, and M. Irie, Jpn. J. Appl. Phys. **36**, 526 (1997).

[20] S. C. Esener, JTEC Panel On Optoelectronics, Chapter 3, 1996.

[21] E. Betzig, J. K. Trautman, R. Wolfe, and E. M. Gyorgy, P. L. Finn, M. H. Kryder, and C.-H. Chang, Appl. Phys. Lett. **61** (2), 142 (1992).

[22] B. D. Terris, H. J. Mamin, and D. Rugar, Appl. Phys. Lett. **68** (2), 141 (1996).

[23] S. M. Manfield and G. S. Kino, Appl. Phys. Lett. **57**, 2615 (1990).

[24] K. Goto, Jpn. J. Appl. Phys. **37**, 2274 (1998).

[25] M. E. Marhic, Optics Lett. **16** (16), 1272 (1991).

[26] S. Hunter, F. Kiamilev, S. Esener, D. A. Parthenopoulos, and P. M. Rentzepis, Appl. Opt. **29** (14), 2058 (1990).

[27] J. H. Strickler and W. W. Webb, Optics Lett. **16** (22), 1780 (1991).

[28] D. Day and M. Gu, Appl. Opt. **37** (26), 6299 (1998).

[29] H. E. Pudavar, M. P. Joshi, and P. N. Prasad, Appl. Phys. Lett. **74** (9), 1338 (1999).

[30] T. Nikolajsen, P. M. Johansen, X. Yue, D. Kip and E. Kratzig, Appl. Phys. Lett. **74** (26), 4037 (1999).

[31] P. van Heerden, Appl. Opt. **2**, 393 (1963).

[32] G. T. Sincerbox, Optical Materials **4**, 370 (1995).

[33] L. Hesselink, S. S. Orlov, A. Liu, A. Akella, D. Lande, and R. R. Neurgaonkar, Science **282**, 1185 (1998).

[34] K. Baba, R. Yamada, S. Nakao, and M. Miyagi, Electronics Letters **28** (7), 6676 (1992).

[35] J. R. Wullert-II and P. J. Delfyett, IEEE Photonics Technology Letters **6** (9), 1133 (1994).

[36] J. Qiu, K. Miura, H. Inouye, J. Nishii, and K. Hirao, Nuclear Instruments and Methods in Physics Research B **141**, 699 (1998).

[37] E. Downing, L. Hesselink, J. Ralston, and R. Macfarlane, Science **273**, 1185 (1996).

[38] F. Goutaland, Y. Ouerdane, A. Boukenter, and G. Monnom, Journal of Alloys and Compounds **275-277**, 276-278 (1998).

[39] M. Dejneka, E. Snitzer, and R. E. Riman, Journal of Luminescence **65**, 227 (1998).

[40] J. M. Zavada and Dahua Zhang, Solid-State Electronics **38** (7), 1285 (1995).

[41] I. F. Elder and M. J. P. Payne, Optics Communications **145**, 329 (1998).

[42] E. B. Mejia, A. N. Starodumov, and Yu. O. Barmenkov, Appl. Phys. Lett. **74** (11), 1540 (1999).

[43] S. Jutamulia, G. M. Storti, J. Lindmayer, and W. Seiderman, Appl. Opt. **30** (20), 2879 (1991).

[44] S. Kroll and P. Tidlund, Appl. Opt. **32** (35), 7233 (1993).

[45] E. S. Maniloff, S. B. Altner, S. Bernet, F. R. Graf, A. Renn, and U. P. Wild, Appl. Opt. **34**, 4140 (1995).

[46] B. Plagemann, F. R. Graf, S. B. Altner, A. Renn, and U. P. Wild, Appl. Phys. B **66**, 67 (1998).

Chapter 2
Optical Data Storage Technology

2.1 Characteristics of Optical Storage Systems

Optical storage systems consist of basic components such as: the drive (laser, light steering optical set, active servo control, moving drive/stage mechanism), read head (focus and track sensing, and read out photodetector), and optical data storage medium. Optical storage systems are based on the principle that data can be optically modulated and stored into media optically or non-optically. Scanning a laser beam on media and detecting optical signal can later retrieve these data. General characteristics of optical systems are, data detection is usually accomplished by scanning a focused laser beam on a moving medium, the ability to focus laser beam and place the detector head some distance away from the media surface, no direct contact between detector head and media surface for non-damaging optical readout, optical storage media are made to withstand considerable physical damage and cheap, and storage systems usually compliment with "mastering" techniques for mass replication of prerecorded media in low cost.

Figure 2.1 and Figure 2.2 show typical components of CD drive, one of the most common available optical storage systems. Information can be retrieved optically from a spinning disc. A diffraction-limited lens is used to focus a laser beam to a small spot on

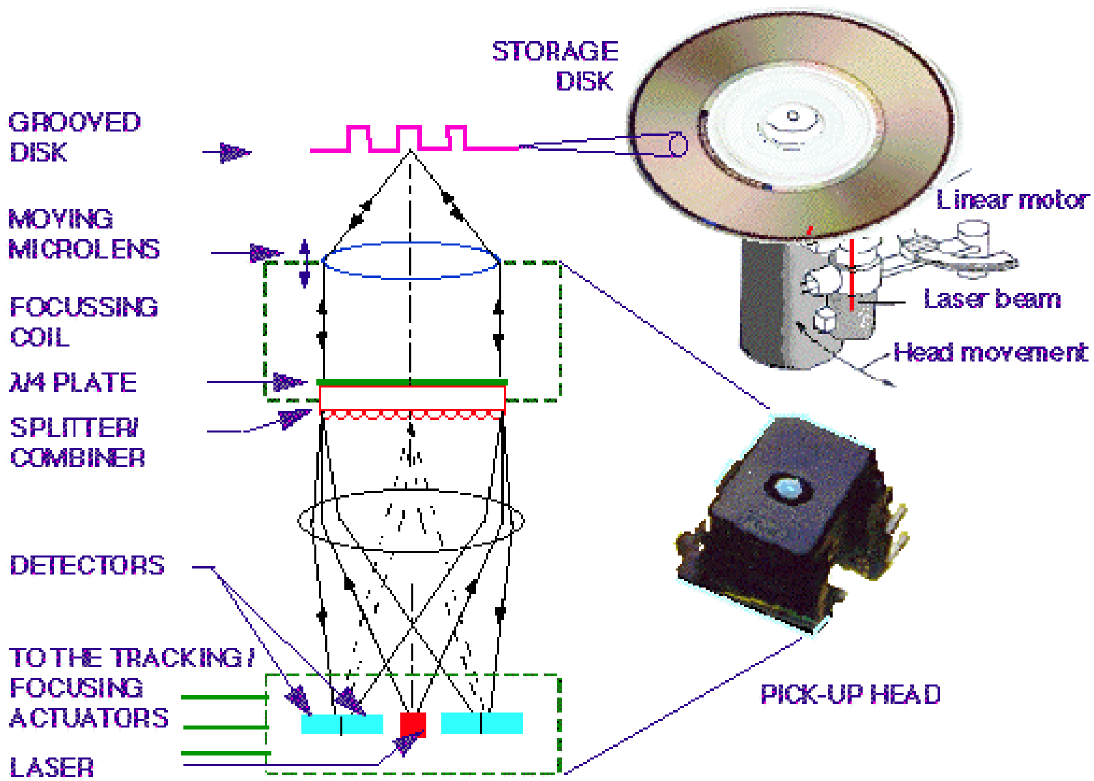

Figure 2.1: Major components of a typical optical disk system.

the record surface, where data are recorded as pits. Laser beam reflected from flat surface has different intensity than that from the pits. The reflected laser beam is collected by the same lens, passes through the beamsplitter, and impinges upon a detector, which generates a photocurrent proportional to the total radiant flux on its surface.

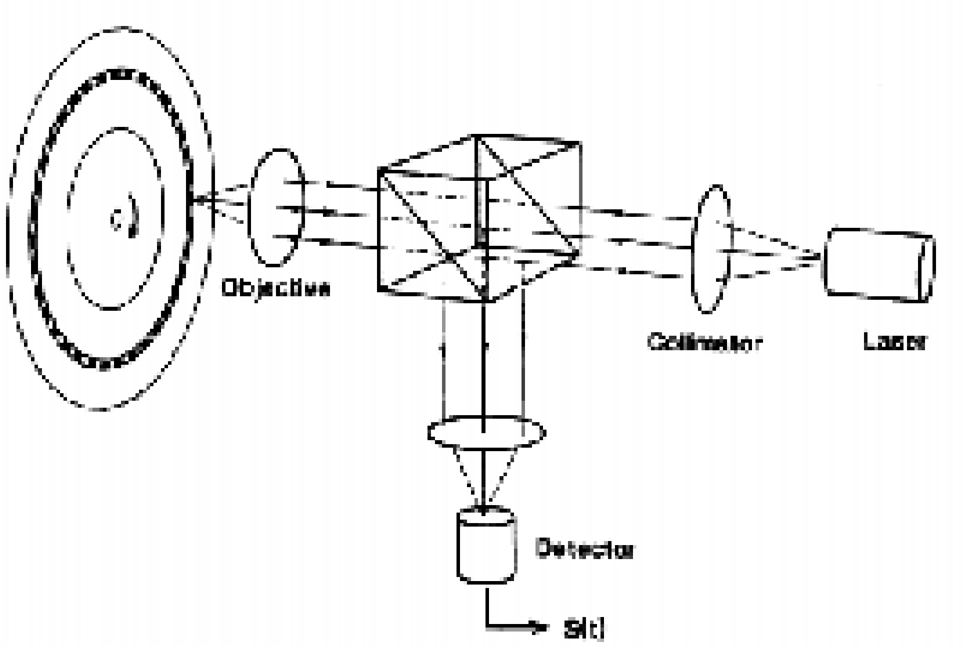

Figure 2.2: Schematic diagram of basic configuration of optical disk system. Laser from semiconductor diode is collimated by lens and focused through objective lens. The reflected light is directed at the beamsplitter toward the detector.

2.2 Optical Signal Modulations

Light as electromagnetic wave can be subscribed with four qualities, intensity/amplitude, phase, polarization/E-field direction, and frequency/wavelength. Binary information is recorded on the optical system media in such a way that one of these four qualities is modulated into two distinct states representing the logic '1' and logic '0' respectively. By scanning the media with an optical beam and detecting the optical modulation (reflection, absorption, transmission, refraction, emission) recover this information.

A. Intensity Modulation

Intensity or amplitude-modulated media store information by changing the reflectivity of the media. Recording process usually consists of focusing a laser beam onto the media to alter their physical state with sufficient level of power density, and thus changing the reflectivity of the media. For example, laser beam is used to ablate the thin tellurium film and create physical holes in WORM media. The reflectivity of smooth surface is higher than the holes. The physical hole could not be reverted back to smooth surface after the bit is written. Another example is to induce transitions between the crystalline and amorphous states of chalcogenide films with high power short pulse laser. The reflectivity of chalcogenide films in crystalline state is at least four times that of amorphous state. To record in the amorphous state, the film is heated to approximately melting temperature and then rapidly quenched into room temperature. To record in the crystalline state, then the film is heated to above the glass transition temperature and maintained at this temperature for a sufficiently long time. Transformation into the amorphous state is by nature faster than transformation into the crystalline state. Chalcogenide films can be used as rewritable media since transition between the crystalline and amorphous states is usually reversible.

B. Phase Modulation

In phase modulated recording, data are stored as pits with a depth of the order of $\lambda/4$, which is pressed onto a polymeric substrate. Data is then read out either in transmission or in reflection. The reflected light or transmitted light is diffractively scattered by the pit pattern recorded on the surface. Since, the phase of the light reflected from the pit is different from the phase of the light reflected from the surrounding area, the interference between the zero and first diffracted order will produce an intensity signal that vary with the pit structure on the disk. By detecting the intensity of the reflected light, the information stored on the disk is retrieved.

C. Polarization Modulation

Polarization modulation is based on the principle of polar magneto-optic Kerr effect. Typical material for polarization modulation is an amorphous ferromagnetic alloy of rare earth and transition metal (RE-TM). To record a spot, RE-TM material is heated by a laser beam to above a critical temperature and allowed to cool in the presence of an applied magnetic field. The magnetization (magnetic domain) in the heated region will orient in the direction of the applied magnetic field. This applied magnetic field has no effect on the material in the absence of the laser beam. When linearly polarized light is reflected from a perpendicularly polarized magnetic domain, the polarization of the reflected light is rotated. By detecting the rotation of polarization field, stored information can be retrieved.

D. Frequency Modulation

Frequency modulated recording stores information in the frequency domain. An example is to modify the absorption spectra of a dye material by burning holes (wavelengths saturation) in the broad absorption band with a narrow spectral width wavelength tunable laser. In this way information is actually stored as a string of bits in the frequency domain, represented by holes in the broad absorption spectra of the material.

2.3 Optical Storage Media[1]

Materials with optical qualities that can be easily modulated are idea media for optical storage. Thus, information can be optically modulated, encoded, stored, and later retrieved without penalty of losing original contents. Below are brief introductions of some basic storage properties of commonly used optical storage media.

A. Photographic Film

Photographic or silver halide film is generally made out of a layer of photographic emulsion (uniformly distributed tiny photosensitive silver halide grains in gelatin) on transparent acetate film or glass plate. When expose to light, silver halide grains that absorb sufficient optical energy are immediately transformed to silver atoms. Grains that have not been exposed or that have not absorbed enough optical energy remain unchanged. During chemical development process, the unexposed silver halide gains are removed, leaving only the opaque metallic silver particles in the gelatin. The more the optical energy absorbed, the higher the density of these opaque metallic silver particles formed. Thus, the transmittance of the developed film depends on the amount of optical energy absorbed. Silver halide emulsion can be used to produce phase and amplitude modulation.

B. Dichromated Gelatin

Dichromated Gelatin is formed by incorporating light sensitive ammonium dichromate ($(NH_4)_2Cr_2O_7$) into gelatin film. The mechanism of photochemical process is not well understood, however, it is generally accepted that optical energy is absorbed by Cr^{6+} ion, which then reduced to Cr^{3+} ions. Regions of gelatin molecular that are exposed to more light create more cross-linking. When immersed in water, and rapidly dehydrated by exposure to alcohol, the more cross-linking regions swell less. Different strains are thus produced between regions of maximum and minimum swelling. Due to the strains, localized index refraction has been effectively modified with respect to the amount of optical energy absorbed.

C. Photopolymer

Photopolymer soft film contains monomers with incorporated photosensitizers. Under light exposure, partial polymerization of monomers occurs. Polymerization is a process by which two or more molecules of monomer congregate and forms larger molecule of polymer. The composition of polymer is the same as the original monomer but with molecular weight that is an integral multiple of that of monomer. During and after optical exposure, light monomer molecules diffuse to low concentration area while the heavy polymer molecules remain still. After photopolymerization process is complete, uniform post exposure by fluorescent light is utilized to increase diffraction efficiency and desensitize the photosensitizers. The redistribution of monomers produces the variations of polymer concentration, which effectively modulate the local refractive index.

D. Photoresist

Photoresist is an organic photosensitive material that is commonly used in photolithography process in semiconductor fabrication. They are two types of photoresists, negative and positive. Negative photoresist becomes insoluble in a solvent after light exposure. The unexposed areas are washed away leaving the negative image of the pattern. On the other hand, the positive photoresist becomes soluble in the solvent after light exposure and leave behind positive image of the pattern after developing. An image or holographic interference pattern is then recorded as a surface relief pattern on the photoresist layer through aluminum coating and mass duplication of holograms via embossing.

E. Thermoplastic Film

Thermoplastic device, also known as photoplastic device, composes of top layer of photoconducting material (poly-n-vinyl carbazole sensitized with trinitrofluorenone), followed by a layer of a thermoplastic film, and a coat of transparent conducting layer (tin oxide or indium oxide) on a glass subtract. Before optical exposure, voltage is applied between the thermoplastic and photoconducting layers. Charging-optical exposure-recharging process then create an electrical field pattern. Thermoplastic is later molded into shape of the electrical field pattern by laser pulse heating the layer. At the end, this process allows the phase of the light beam passing through the layer to be modulated.

F. Photorefractive Materials

Photorefractive materials are crystals that contain electron traps. Electron traps are caused by intrinsic defects and residual impurities. When photorefractive materials are exposed to light, electrons from trap are excited and freed to conduction band. Under applied or internal electrical field, free electrons in conduction band migrate to regions of low intensity light and become trap once more. Migration of free electrons continues until the buildup of space charge cancels out the electrical field. The result is the redistribution of electrons charge that modifies the refractive index of the materials. This effect is also referred as linear electrooptic effect. One of the well-known photorefractive crystals that used for holographic storage is lithium niobate ($LiNbO_3$). Fe_2O_3 could be incorporated during $LiNbO_3$ crystal growth to enhance the sensitivity of electrooptic effect. Initially Fe^{2+} and Fe^{3+} ions are evenly distributed throughout $LiNbO_3$ crystal. When Fe^{2+} is exposed to light, an electron is excited to conduction band and Fe^{2+} change to Fe^{3+}. Freely moving electron eventually get trap again by Fe^{3+} in low light intensity regions and Fe^{3+} change back to Fe^{2+}. The redistribution of Fe^{2+} and Fe^{3+} gives rise to the local variation of refractive index modulated by light.

G. Photochromic Materials

Photochromic materials are usually inorganic insulators[2] or wide bandgap semiconductors (WBGS). There are two distinct stable states or traps, A and B, between conduction and valence bands. A and B states are sometime referred as color centers, since they are related to absorption light of λ_1 and λ_2 respectively. The materials absorb initially only light of λ_1, but not λ_2. Transition from stable state A to B occurs when light of λ_1 is absorbed. After the transition, materials shift to absorb light of λ_2 and no longer possible to further absorb light of λ_1. However, when the materials are exposed to λ_2, the process reverts the transition from stable state B to state A and the light absorption band switches vice versa. The reversal process may also occur even in the dark after storing the data for sometime or by heating the materials. Optical data can be recorded with λ_1 and read out with λ_2 with photochromic materials. However, the disadvantage of this mechanism is that while reading the stored information, data are inevitably erases simultaneously.

H. Electron Trapping Materials[3,4]

Electron trapping (ET) materials are alkaline-earth chalcogenides doped with two or three rare earth dopants. They are essentially stimulated phosphors. Quantex Corporation originally developed them as infrared sensors. ET materials are very similar to photochromics in the sense that they both have two reversible stable states of A and B, which correspond to absorption band of λ_1 and λ_2 respectively. However the data readout methods for ET materials is via the detection of the stimulated emission of λ_3 instead of the absorption of reading light of λ_2 by photochromics. Examples of ET materials are Eu or Sm doped SrS, Eu doped KCl, and $Ca_xSr_{1-x}S$:Eu,Ce,Sm thin films.

I. Two-Photon Absorption Materials

Two-photon absorption phenomenon is a nonlinear optical process, also known as photon gating, which means using a photon to control the behavior of another photon. These materials have been applied for three-dimensional optical storage. Two write beams are required to record data and a read beam to stimulate emission. Instead of single photon absorption, two photon absorption materials necessitate two photons for transition from ground state to upper level excited state and also another pair of photons to stimulate the excited state to return to the ground state. These two photons could have the same wavelength, but photons with different wavelengths are preferred. Example of a two-photon absorption material is spirobenzopyran. The write process begins with simultaneously absorption of photons at 532 nm and 1064 nm. Molecule of spirobenzopyran is thus excited from S_1 state to S_2 state, and then relaxes nonradiately to S_3 stable state. To read the data, pair of photons at 1064 nm is absorbed to excite the molecule from S_3 to S_4 state. When excited molecule relaxes radiately back to S_3 stable state, a stimulated emission of about 700 nm is observed. In this mechanism, the written data can be read without being erased.

J. Bacteriorhodopsin

Bacteriorhodopsin, a biologic photochromic material, is a light-harvesting protein in the purple membrane of a microorganism called Halobacterium halobium. The bacteriorhodopsin film can be made either by drying out isolated purple membrane patches onto a glass substrate or embedding these patches in a polymer. Bacteriorhodopsin function like a light-driven proton pump and is a key agent for halobacterial photosynthesis (a process that converts light energy into chemical energy). There are two distinct stable photochromic states in bacteriorhodopsin, namely state B and M. Bacteriorhodopsin is initially in state B. State B of bacteriorhodopsin will change to state J upon absorbing light of 570 nm. Followed by relaxation to the states K and L, bacteriorhodopsin settles firmly in state M by releasing a proton. Although, state M is a stable state, bacteriorhodopsin can be transformed back to state B by recapturing a photon upon absorbing light of 412 nm. State M can also be reversed to state B simply by a thermal process. By using lasers at 570 and 412 nm respectively to stimulate the state transitions, bacteriorhodopsin films can be used for optical storage system. Alternatively, the state transitions can also be stimulated with simultaneous absorption of two photons at 1140 nm and two photons at 820 nm.

K. Persistent Spectral Hole Burning Materials

Persistent spectral hole burning (PSHB) or photochemical hole burning (PHB) materials are materials with photosensitive atoms or molecules (absorbers) embedded in a host matrix, which have broadened inhomogeneous absorption band comprised of a large number of narrow absorption lines. Free atoms or molecules have narrow absorption lines. When these atoms or molecules (impurities) are embedded in a host matrix, their narrow homogeneous absorption lines are generally broadened and give rise to a broad continuous inhomogeneous optical absorption band. This broadening of inhomogeneous absorption line is caused by local structure variations in the host, which lead to variations in the energy levels of the free atoms or molecules. The absorption spectral width of an individual absorber is referred to as the homogeneous linewidth and the adsorption spectral width of a collection of broadened inhomogeneous absorption center is referred to as the inhomogeneous linewidth. The ratio of the inhomogeneous linewidth to homogeneous linewidth can be 10^3 at low temperature. When PSHB materials are illuminated by a tunable-wavelength, narrow-bandwidth laser beam, excited absorbers whose physical position and homogeneous spectrum match with the laser frequency will undergo photon transition to excited state. After the excited state is populated, the corresponding absorption spectrum is bleached out, so that a spectral hole (sharp dip) near the laser recording frequency appears in the broad inhomogeneous absorption band. This frequency-modulated information can be accessed in PSHB materials through either frequency-domain spectral hole burning or time-domain spectral holography. In frequency domain, each burned spectral hole could be registered as single bit stored. The storage density is therefore governed by the ratio of the inhomogeneous and homogeneous linewidth. In time domain, interference between coherence reference pulse and time delay, temporally modulated coherence data pulse is Fourier transformed into frequency-modulated information. Storage density in time domain is identical to that in frequency domain. However, data rate in time domain, determined by inhomogeneous linewidth, is significantly increased than that in frequency domain.

PSHB media can be organics, inorganics, RE-doped metal halides, RE-doped oxide crystals, RE-doped glasses, and dispersed photosensitive microparticle materials. They can be grouped into four categories: proton transfer group, donor-acceptor group,[5] mixed crystal[6] or glass matrix group,[7,8,9] and nanocrystal group[10,11,12]. PSHB materials that belong to proton transfer group encompass, chlorine dyes in polyvinylbutyral (PVB), phthalocyanine type organic materials in polyethylene, and prophine/polyethyelene mixtures. Examples of donor-acceptor group are TZT-halomethane in poly-methylmethacrylate (PMMA), meso-phenyl-tetrabenzoporphyrinato-zinc-aromatic cyanide (Zn-PTBP-AC) in PMMA, and zinc-tetraphenyl-benzoporphyrin-chloroform in PMMA or PVB polymer. Mixed crystal or glass matrix group includes, Sm in SrFCl, Sm^{2+} in $SrFCl_{0.5}Br_{0.5}$, Sm in sol-gel silicate glasses, Sm in fluorite-type crystals, Eu^{3+} in alumina, Pr^{3+} in YalO, and Cr^{3+} in SrTiO. In nanocrystal group, PSHB is created with semiconductor microcrystal or quantum dots in a host, such as nanometer sized particles of CdSe or CuCL in glass or crystal matrix, CuBr and CuI quantum dots in glass, and CdS quantum dots in polyvinylpyrrolidone polymer. The big disadvantage of storing information with PSHB materials is that these materials must be kept at very low temperature (< 100 K).

L. Magneto-Optic Materials

Magneto-optic (MO) materials are ferromagnetic materials that exhibit strong thermo-magnetic domain switching phenomenon. They are typical media for polarization modulated storage systems. When a small region in MO thin films is irradiated by a focused laser beam in the presence of magnetic field, its magnetic moments in the heated area will aligned themselves in the same direction of the applied magnetic field. By restricting the direction of applied magnetic field in up or down polarity, binary information can be stored in MO materials as upward and downward magnetization. At temperature below Curie point (T_c), the MO medium is resistant to changes in magnetization. The reverse magnetic field required to reduce the magnetization of the recording medium is called coercivity. The coercivity of MO film at room temperature is quit high and generally falls to zero at T_c. It may not necessary to raise the temperature to T_c in order to switch the magnetization, since at temperature of about 150 °C; the coercivity is decreased by a factor of three from that at room temperature. Thus, binary data can be written in the presence of applied magnetizing field coincident with the laser heating pulse that raises the temperature of the heated spot to 150 °C (which is lower than the Curie point). Once MO film is allowed to cool in the presence of magnetic filed, only the spot heated above 150 °C acquires the magnetization direction of the external filed. Detection of domain structure (data retrieval) of MO thin films is accomplished by observing the Kerr or Faraday magneto-optic effects with linearly polarized laser beam. Linearly polarized laser beam will undergo a small rotation through the Kerr or Faraday effect. By analyzing whether the polarization of the laser beam is rotated to the left or right, the upward or downward polarity of magnetization can be determined. In reflective readout, polarization of laser beam is rotated through the Kerr effect. This Kerr rotation is a sensitive function of the incidence angle, even though the Kerr rotation angle seldom exceeds 1°. In the transmissive Faraday effect, the rotation angle is proportional to the film thickness. In principle, the intensity modulation can even be obtained by applying an analyzer. Some commonly used MO thin films are rare earth transition metals (RE-TM) amorphous alloys, PtCo, MnBi, TbFeCo, TbFeCoAl, and GdFeCo alloys.

M. Phase-Change Materials

Phase change (PC) materials (include some chalcogenide materials) usually have two reversible switching states, amorphous and crystalline states while in solid phase. In crystalline state, the constituent atoms of PC materials are in a periodically repeated arrangement, whereas in amorphous state, the atoms are in a random pattern. PC materials are opaque in crystalline state but transparent in amorphous state. The reflectivity of the crystalline state can be four times that of the amorphous state. Heating PC thin films with short laser irradiation pulse induces the reversible phase transitions between the crystalline and amorphous states. The underlying process of phase transition induced by laser heating on PC films is very much the same process on chalcogenide films. Some examples of PC thin films are TeSeSn, InSb, GaSb, GeTeSb, and InSbTe alloys. PC thin films are currently being implemented in CD-RW discs.

2.4 Architectures of Optical Storage Systems

Optical data can be stored in either planar or volumetric dimension. Only planar optical storage systems are currently available commercially and have gained acceptance in consumer market. Limited by far-field diffraction limit, data capacity of current planar storage systems is fast approaching the theoretical limit. Several steps have been taken to remedy the short fall of current planar system designs. Minor capacity enhancement can however be achieved through using short wavelength blue laser sources, increase lens numerical aperture (NA), land and groove recording, efficient coding schemes, and read head miniaturization. The long-term solutions will have to relay on more drastic innovative designs. In the next five years, proposed double sided and multiple data layer digital versatile disc (DVD) disks will emerge from the market as first generation of commercial volumetric optical storage systems. Near-field design such as flying head solid immersion lens, which attempt to overcome the far-field recording diffraction limit by placing read head just a few hundred nanometer above the spinning media, would surely not far behind from becoming consumer products. With certain that the demand for data capacity continues to rise, full fledge novel optical systems like holography, two-photon absorption, and frequency modulated PSHB will have the opportunity to test their viability in commercial market. Diffraction limit, impose on current far-field planar optical systems, has not deterred the development and continuality usage of optical storage. It has in fact served as catalyst for ingenious innovation for new technological possibilities. Many more novel optical system designs are certainly expected to emerge in the future.

2.4.1 Planar Storage

Planar storage systems include optical disk, magnetic-optical, and phase change systems. There are two types of planar storage: far- and near-field. Optical disks are the most widely used far-field planar storage systems in the market. Optical disk drives use lasers to write to and read from their media. Information can be recorded optically or pre-molded into storage disc, but data are always retrieved optically. Optical disks come in various disk diameters, including 2.5 inch, 3.5 inch, 120 mm, 130 mm, 12 inch, and 14 inch. Common denominator of optical disks is optical compact disk. Planar storage that relay on far field detection suffers from optical diffraction limit, which place a cap on maximum areal storage density. On the other hand, advanced planar storage like near-field and probe storage do not suffer the same limitation. These near-field techniques are one of the answers for future high-density optical planar storage systems.

A. Compact Disk[13,14,15,16]

Philips and Sony first introduced compact disk (CD) in 1980 to replace laserdisc (LD). Basic CD physical parameters are 120 mm in diameter, 1.2 mm thick with 4 layers composed of polycarbonate substrate, aluminum reflector, protective lacquer and ink label. Digital data are recorded as pits (0.6 μm width x 0.9 to 3.3 μm length). Track to track distance is about 1.6 μm. CDs come with many standards. The popular types are read only CDs, such as audio CD and compact disc read only memory (CD-ROM); write once read many CD, such as CD recordable (CD-R); and erasable CD such as CD rewritable (CD-RW). Other CD formats include CD-DA, CD-ROM XA, CD-I, CD-

Digital, CD-Bridge, CD-Extra, photo CD, and video CD. Initially, not all CD-ROM drives can read various CD disc formats. Third generation "MultiRead" CD-ROM drives were specifically created in early 1997 to support all possible CD formats.

A-I. Read Only CD[17]

CD-ROM and Audio CD are by far the most common CDs in the market. CD-ROM can hold 650 MB of data and operate much like a 74-minute audio CD. At the factory, lasers are used to create a master CD-ROM disc, and then a mold is made from the master disc. Plastic is injected into the mold, and the data pattern is pressed into the disc. CD-ROM discs are polymer with high reflectivity metallic (usually aluminum) coating. CD-ROM with data transfer rate of 150 kBytes/sec is designated as having 1X read speed. Current newest CD-ROM drive has 48X read speed. CD-ROMs are typically used to distribute software applications, large databases and documents that required only periodic access.

A-II. Recordable CD[18]

Recording rate is always slower than reading rate. Multiread CD-RW drives are used to write both CD-R and CD-RW discs and are usually designated with three data speed rating. Newest CD-RW drive has 10X write, 4X rewrite, and 32X read speeds to date. Theoretically, CD-R disc can hold up to 700 MB of data or 80 minute of audio. However, overhead associated with various CD recording formats prevents data storage from achieving maximum capacity. Phase change materials or chalcogenide alloys are commonly used for recordable media. Recordable CDs are popular for short-term data storage.

B. Digital Versatile Disc[19]

Digital versatile disc (DVD) is a next generation of optical disk designed to replace CD-ROM. DVD is a lot like a CD-ROM physically, except its laser beam has shorter wavelength than that of CD-ROM (650/635 nm compare to 780 nm for CD-ROM). Thus, data can be recorded with smaller indentations to increase storage capacity. There are several versions of DVD. DVD-ROM is read only version and can hold from 4.7 GB single side format to 17 GB double layer double side format. A 4.7 GB DVD-ROM can hold 135 minutes of top quality video with 6-track stereo and the future 17 GB disk should hold 200 hours of multimedia products and movies. DVD R is write-once only version and can hold 3.9 GB per side. DVD-RAM, DVD-RW, and DVD+RW are the erasable version, and are tentatively specified to hold 2.6 GB per side. Newest DVD drives in the market can read both DVD and CD disc formats. DVDs have slowly flocked into market, most prevalently in replacing VCRs for movie titles. To prevent bootleg copies, DVD movies are made into region codes. DVD drive in one region code cannot read DVD movies made from another region codes. Current newly available PC version of the DVD drives are DVD-ROM drive with 2X DVD-ROM and 20X CD-ROM read speeds; and DVD-RAM drive with 1.38 GB maximum storage capacity.

While optical disks like CD and DVD offer reasonable high-capacity storage (form 650 MB to 17 GB), optical disk drives are not nearly as fast as hard disk drives. Access times average 30 to 120 ms, compared with average access times of 8 to 15 ms for hard disks.

C. Phase Change Dual Functions Drive[20,21,22]

Phase-change Dual disk (PD) is a rewritable optical disk standard from Panasonic introduced in 1995 that incorporates phase-change technology. PD cartridges are 130 mm (5 ¼ inches) and can hold up to 650MB storage capacity. The medium can be rewritten to approximately 500,000 times. Current PD 650 MB rewritable optical disk drives also come with readable function for CD/CD-ROM at 8X speed. The average seek time is 89 ms (90 ms for CD-ROM) and maximum transfer rate at 1141 kbits/sec (1200 kbits/sec for 8X CD-ROM). Future PD will provide up to 5.2 GB storage capacities. Unlike magnetic disk media, a high-intensity laser pulse is used to change the bits on the surface of the PD media from a natural crystalline reflective state to an amorphous dull state, which does not reflect light. A low-intensity laser pulse is then used to read the data in the amorphous state while a medium-intensity laser pulse is used to restore the crystalline structure. Besides Panasonic's PD drive, the phase-change technology is also used by CD-RW, and DVD-RAM drives. Nevertheless, PD and CD phase change formats are not compatible with each other. CD-DOM drives could not read PD discs, even though PD drives can read CD discs. There are not many vendors pushing PD drives at the moment; only Panasonic, Plasmon and Toray carry the products.

D. Magneto-Optic Disk[23,24,25]

MO disk was introduced as rewritable optical storage system long before CD-RW is made possible. MO recording is based on polar Kerr effect to achieve optical contrast between magnetic domains with up and down polarity. MOs are not as common as CDs due to their extra cost associated with producing complicated storage architecture. 3.5-inch MO disks can store data up to 230 MD. The 130 mm (5 ¼ inch) format come with 650 MB, 1.3 GB, 2.6 GB, and 5.2 GB capacities. The 5 ¼ inch MO drives support both WORM and rewritable disks. With average seek time of 39 ms and maximum transfer rate at 4.6 MB/s, data rate of MO disk is generally faster than CD. Future super MO will offer storage capacity of 2 GB single side disk and 4 GB double side disk. Current generation of commercially available MO disks are based exclusively on terbium-iron-cobalt [$Tb_x(Fe_yCo_{1-y})_{1-x}$] RE-TM amorphous alloys for MO active layer. Major shortcoming for MO is that the birefringence of the plastic materials that protect and support the magneto-optic thin film increases, as the wavelength of the recording and readout laser is shifted towards to the blue for increased storage density. This parasitic birefringence increases background noise and significantly reduces the available signal-to-noise ratio (SNR) during readout.

E. Near-Field[26,27,28,29]

Near-field optical recording includes any technology that retrieves information through evanescent wave detection. Consider advanced planar optical data storage, near-field storage seeks to increase areal density by overcomes the far-field diffraction limit. Near-field scanning optical microscope (NSOM), solid immersion lens (SIL), and arrays of vertical-cavity surface-emitting lasers (VCSEL) represent some of these near-field technologies.

E-I. Near-Field Scanning Optical Microscope[30,31]

Near-field scanning optical microscopy (NSOM) requires probe (read head) to be placed very near (about 50 nm above) the media to avoid optical diffraction limit. Spots as small as 40 nm in diameter can be resolved in favor of very slow scan speed. In concept, NSOM could provide ultra high areal densities on the order of 100 Gbits/in^2. However, since the probe has to be put at close proximity over the medium, it is a great challenge to prevent head crashes and support removable media. The practical storage area (capacity/device) is also restricted by slow scan speed. Assuming a scan area of 1 cm^2, 30 nm effective spot sizes yields merely a total capacity of 10 GB. One of the original NSOM recording techniques was through the use of a tapered fiber as the probe.[32] The tip of a fiber is smaller than the wavelength of the recording light. Positioning the tip within 10 nm above the MO medium, bits as small as 60 nm have been recorded and read out. Nevertheless, the tapered fiber approach suffers from very low optical throughput, slow scan speed, and not being portable. Research on area such as, using parallel access and MEMS technology, has been on going to resolve current NSOM teething problems. Considering high density offered by this approach, NSOM is expected to have a potential market for applications in the future.

E-II. Solid Immersion Lens[33,34]

This near-field recording architecture actually composed of two pieces of elements: flying head and solid immersion lens (SIL).[35,36] Flying head is a modified version of the hard disk storage flying read/write head. It maintains close proximity distance over a rapidly spinning disc without crashing by floating on a cushion of air above the surface. SIL is the optical lens elements in the bottom of the flying head that is closest to the media. SIL must be held within 100 nm or less from the surface of the recording media in order to focus the evanescent wave from underneath the lens surface. By refracting the rays at the lens sphere surface and by having an increased index of refraction (up to n = 2) within the lens, SIL can reduce the actual beam spot size. SILs with equivalent NA of up to 1.8 have been fabricated. Using a 780 nm laser, spot size on the order of 320 nm has been written. This spot size corresponds to storage density on the order of 3 Gbits/in^2. Data rates up to 3 Mbits/sec and possible up to 15 Mbits/sec can be sustained with the flying head. Currently, TeraStor Corporation is in the process of developing the commercial version of SIL system.

E-III. Arrays of vertical-Cavity Surface-Emitting Lasers[37]

Kenya Goto of Tokai University (Shizuoka, Japan) envisions a near-field optical storage system based on arrays of vertical-cavity surface-emitting lasers (VCSEL). By placing VCSEL very close to an optical disk surface with a lubricating fluid in between, array of laser beams could be coupled to the medium surface through a 10 nm hole etched by photolithography into a single thin silicon crystal. Such a near-field array system would operate like a magnetic hard drive and might not have portability. The spacing of the parallel lines of bits on the disk will be on the order of 10 nm compare to the 1 μm spacing of the VCSEL. In order to read all the bits, the VCSEL will have to be set at an angle to the direction of disk motion, similar to VCR. This design will allow locating a given bit by the timing of the light pulse. The array design permits extremely high memory-readout rates. If each VCSEL operates at 1 Mhz, the total array can read out data at 10 Gbits/sec. Assuming a 1-μm minimum diameter per array VCSEL with 100 x 100 arrays, 2 TB (Tbits/in^2) storage densities per 120 mm disk can be achieved.

F. Probe Storage

Probe storage employ a variety of modulation techniques including topographic (mechanical), charge, magnetic, conductivity, and optical modulation. They have been used with large variety of materials including organic, ferro-electric, magneto-optic, magnetic, and phase change media. Examples of these techniques are scanning tunneling microscope (STM), field emission probe (FEP), atomic force microscope (AFM), and near-field scanning optical microscope (NSOM).

F-I. Scanning Tunneling Microscope[38]

Scanning tunneling microscope (STM) detects the tunneling current that occurs across the gap between two conductors that are held very close together (on the order of angstroms). With current flow, cluster of atoms (10-20 nm size bits, giving a data density of over 1 Tbits/in^2) are deposited onto a substrate. Since the height of the probe tip must be held very constant or else it will lose the tunneling current or crash into the substrate, scanning speed is very slow. Data rates as fast as 100 kbits/sec have been demonstrated.[39] Although phase change materials (by altering the electrical conductivity) have been developed for erasable disc, they suffer from fatigue and slow recording times.[40]

F-II. Atomic Force Microscope[41]

Atomic force microscope (AFM) employs a cantilevered tip to scan across a sample. Features on the surface that cause deflections of the tip can be optically detected by monitoring the reflected laser signal from the tip with a split photodiode detector. Information can be recorded in ROM, WORM and erasable media. Inexpensive ROM discs could be produced by "Mastering" technique with e-beam lithography.[42] Features as small as 50 nm have been successfully replicated in photo-polymer materials. WORM recording may be achieved with thermo-mechanical process, where a pulse laser is used to focus, heat, and cause the tip to sink into the polymer substrate to create a pit (100 nm size bits, giving a data density of over 30 Gbits/in^2). The recording speed was 200 kbits/sec and readout speed was 1.25 Mbits/sec. Erasable disc could be manufactured with charge trapping materials such as nitride-oxide-semiconductor (NOS) layers[43] or phase change materials.[44] The smallest bit recorded on erasable disc is on the order of 75 nm giving a recording density of over 100 Gbits/in^2. Readout rate was 30 kbits/sec, but will be possible up to 10 Mbits/sec. The major hindrance for AFM storage is tip wear. Since tip is usually in contact with the surface while probing, it is slowly worn down as it drags across the sample.

2.4.2 Volumetric Storage[45]

Volumetric storage explores the advantage of three-dimension (3-D) structure of the media, stacked multiple layers of storage media, or third dimension property of the media. The potential impact of volumetric storage on the storage capacity can be much grater than any improvement that can be done with planar storage. Volumetric storage is assumed to provide the potential of realizing disks with 100 GB to 1 TB capacities by 2005. Volumetric storage can generally be grouped into multilayer optical disk, fluorescent multilayer disc, two photon absorption 3-D optical disk, femtosecond pulse laser induce bit oriented volumetric disk, holography, and PSHB.

A. Multilayer Optical Disks[46]

Multilayer optical disks include stacked multiple layers of CD, DVD, PC, or MO disks. It is a natural extension of present planar optical disk systems with a potential to increase the storage capacity without significantly affecting the production cost. Multilayer disk requires dynamic focusing lens for data access through the volume. This recording approach not only increases storage capacity by adding additional storage layers, but also relaxes constraints in other dimensions. For example, a multilayer disk system may afford to use larger laser spot size, lower numerical aperture optics and simple low cost servo systems and yet achieves higher data capacity than planar disk system. . However, there are also limitations. These limitations include higher laser power level determined by the medium transparency, aberrations and inter-layer crosstalk issues of accessing volumetric storage, extra costs associated with focusing and tracking in three dimensions, and more complex signal processing and error correction schemes essential for smaller signal level detection. IBM has demonstrated multilayer disk of 4 to 16 layers with single optical head. The numbers of layers were limited by interlayer crosstalk considerations and the capability of the dynamic focusing lens addressing the data in 3-D. On the other hand, Matsushita is experimenting with four-layer DVD-RAM by using more transparent recording layers in PC medium with some success. There is also multilayer MO disk medium that consists of two active TbFeCo MO layers, one modified by the existence of an additional PtCo layer. Two lasers of different power and wavelength are used to selectively record thermo-magnetically onto each layer due to the slight differences in characteristics of the two layers.

B. Fluorescent Multilayer Disc

Developed by Constellation 3D (C3D), fluorescent multilayer disc (FMD) is essentially a stacked layers of CD discs. Fluorescent materials are embedded in the pits and grooves of each layer of the media. Information is stored and retrieved based on the principles of fluorescence, instead of optical reflection as currently used by CDs and DVDs. Detecting incoherent fluorescent signal will be much easier than detecting a reflected coherent laser beam, since reflected coherent laser light will increase constructive interference noise when more layers are added to the disc. By detecting the incoherent fluorescent emission, interference will not play a part to obscure the real signal, thus increase the SNR. The enhanced SNR allows stacking more layers into single disc and increases the effective storage capacity per disk. Currently, C3D claims that FMDs are backward compatible with existing CD and DVD technology. Designed in standard DVD format (120 mm in diameter and thickness), the first generation of FMD will store up to 140 GB in 10 layers, with 1 TB version follows suit in near future.

C. Two photon Absorption Three-Dimensional Optical Disk

Recording bits in a volume by using two-photon absorption has been pioneered by Call/Recall, Inc.[47] Information is written to a spot in the volume of a molded organic polymer only at the location where two laser beams intersect temporally and spatially.[48,49,50] The recorded bits are then retrieved by fluorescence emission with single laser. So far multiple layer ROM disk with portable readout unit has been demonstrated with no crosstalk between layers that were spaced as closed as 30 μm. The spot size is limited by optical diffraction limit and the responsivity of the readout detector. This approach promises low-cost thousand-layers removable disk with ultra high effective areal density (1-100 Tbits/in^2) and high rate of parallel data accessing capability. The approach, however, is challenged by surface quality and volumetric homogeneity of the storage media and the high cost of short-pulse high-intensity lasers required for two-photon recording. Moreover, materials with high fidelity that can withstand fatigue of frequent writing and erasing are yet to be found. Although only small (1.5 inch diameter) disks have been demonstrated so far, two-photon recording appears to be potential contender for future removable ultra-high capacity optical disk storage.

D. 3-D Bit-by-Bit Recording[51,52,53]

Another 3-D storage approach is based on bit-by-bit recording into transparent thick medium with low-cost high-power femtosecond lasers. These femtosecond lasers can generate large changes in optical properties in such a short time that heat energy cannot spread to the surrounding material. In such, very small dots with significant refractivity change were created as data bits. Low power laser is then focused at a given depth within the recording medium to retrieve the information. With such high power fluxes, the recording medium is not limited to photorefractive materials but can be any stable transparent materials like glass. Research in ERATO (Kyoto, Japan) has demonstrated a 10^{13} bits/cm^3 storage capacity system. A 120-fs Ti:sapphire laser focused through a microscope objective produced dot as small as 400 nm diameter at 0.4 μm spacing. Theoretically, this would allow surface densities of 10^5 bits/μm^2 for 1 cm thick media, or 10^3 bits/μm^2 for 100 layers.

E. Holography[54,55,56]

Holographic is a distributive information storage system. If a portion of the holographic storage media is damaged, all stored information suffers from partial degradation instead of catastrophic total loss of some data. There has been continued research in this field since the early 1960s.[57] To record volumetric holograms, a laser is split into coherent object and reference beams. Data are spatially encoded into object beam as pages of 2-D light pattern by a spatial light modulator (SLM). Reference beam is then either directed at a particular angle (angular multiplexing), spatially phase modulated (phase code multiplexing), or wavelength selected (wavelength multiplexing) to serve as the proper page address.[58,59,60] Interference grating (hologram) created by intersecting the reference with object beam is then captured as a pattern of varying refractivity in the storage medium. The original page image can be reconstructed by illuminating the hologram with reference beam. Holographic storage allows for parallel read-write operations, thus has the potential of being fast access, mass data storage system. Photorefractive crystals (PRC) and photo-polymers are the typical materials for both non-moving and volumetric disk. Using PRCs such as, lithium niobate ($LiNbO_3$),[61,62] 10,000 images have been successfully stored and retrieved.[63] This corresponds to effective areal densities in excess of 64 Gbits/in^2. The main drawback of PRCs is the high cost of materials, the decrease in diffraction efficiency with increasing number of multiplexed holograms and read-out cycles, and the relatively small and slow changes in the index of refraction. Nevertheless, enhancement such as, using recording schedules to improve the uniformity of the recorded data, fixing procedures to permanently store data in PRCs, and new recording geometries to minimize crosstalk, has been made to improve competitiveness of holographic storage devices. Moreover, photorefractive polymers that exhibit large index of refraction changes under very large electric fields have been demonstrated recently. Polymers available from DuPont and Polaroid can be used as holographic ROM storage. However, improvement on reducing shrinkage is needed to prevent the polymer from contraction after recording. Polymer shrinkage results in a shift in readout wavelength over time increase crosstalk, and loss of resolution. Corporations such as, Holoplex, Inc., Optitek Corp., IBM, Rockwell International, Lucent, and Polaroid are actively pursuing research in holography.

F. Persistent Spectral Hole Burning[64,65,66]

Persistent spectral hole burning (PSHB) is a frequency-domain optical storage device.[67,68] In such device, a spectral hole is burned at particular wavelengths and constitutes as logic '1' and with the normal unburned region designated as logic '0'. As frequency-domain storage, PSHB allows for a greatly increased random-access capability over the magnetic and optical disk devices. It is possible to achieve 10^{12} bits/cm^2 of information density. To use PSHB storage system, the temperature must usually be kept at near liquid helium temperatures in order to achieve narrower widths and to keep the hole persist indefinitely. However, spectral diffusion frequently leads to the boarding of the spectral holes and eventual loss of information. Viable memory materials for PSHB should be capable of hole-reversibility for erasable device and fast irradiation time needed to write a hole. However, when the irradiation time is on the order of tens of nanoseconds, the burnt holes are shallow, which requires intense light for reading and may cause photochemical damage to the materials. Alternatively, using high SNR detector to detect small signals from shallow hole in the future may solve this problem. The dilemma is that if the material is good for fast hole-burning formation, then the reading beam will probably also induce hole burning in the material. On the other hand, to make the material with efficient fast reading speed, then most likely during the writing process, the hole formation will require higher power lasers or longer writing times. The power of the laser may also affect the temperature of the system, which could result in loss of information at unacceptably short times. Various systems based on PSHB recording such as, long-term photon echo phenomenon (LTSPE),[69] point-wise scanning, holography, time domain holography,[70] and polarization photon-gated PSHB have been proposed. Templex Technology Corp. is currently in the effort of commercializing a rare earth based optical Dynamic RAM (ODRAM), a PSHB based storage system. ODRAM is designed to provide the capacity of magnetic hard drives with data speed intermediate between hard drives and semiconductor RAM.

2.5 References

[1] F.T.S. Yu and S. Jutamulia (eds), **Optical Storage And Retrieval: Memory, Neural Netwoks, and Fractals** , Marcel Dekker, New York, 1996.

[2] T. Tsujioka, M. Kume, and M. Irie, Jpn. J. Appl. Phys. **35**, 4353 (1996).

[3] S. Jutamulia, G. M. Storti, J. Lindmayer, and W. Seiderman, Appl. Opt. **29** (32), 4806 (1990).

[4] S. Jutamulia, G. M. Storti, J. Lindmayer, and W. Seiderman, Appl. Opt. **30** (14), 1786 (1991).

[5] M. Tian, T. Chang, J. Zhang, H. Wang, K. Dou, B. Luo, S. Huang, and J. Yu, J. Luminescence **64**, 131 (1995).

[6] J. Zhang, S. Huang, and J. Yu, J. Luminescence **53**, 51 (1993).

[7] K. Hirao, S. Todoroski, D. H. Cho, and N. Soga, Opt. Lett. **18** (9), 1586 (1993).

[8] D. H. Cho, K. Nirao, and N. Soga, Non Cryst. Solids **189**, 181 (1995).

[9] M. Nogami, Y. Abe, K. Hirao, and D. H. CHo, Appl. Phys. Lett. **66** (22), 2952 (115).

[10] Y. Matsumoto, L. G. Zimin, K. Naoe, S. Okamoto, T. Arai, Mat. Sci Eng. **B27**, L5 (1994).

[11] Y. Matsumoto, T. Kawazoe, T. Yamamoto, Phys. Rev. B **52** (7), 4688 (1995).

[12] Y. Matsumoto, K. Kawabata, and T. Kawazue, Phys Rev. B **52** (11), 7834 (1995).

[13] G. Bouwhuis, J. Braat, A. Huijser, J. Pasman, G. Van Rosmalen, and K. S. Immink, **Principles of Optical Disc Systems**, Adam Hilger, Bristol, 1985.

[14] N. Tamaru, Appl. Opt. **32** (35), 7243 (1993).

[15] T. Maeda, A. Saito, H. Sugiyama, Shinichi Arai, and K. Shigematsu, Appl. Opt. **34** (22), 4965 (1995).

[16] R. E. Gerber and M. Mansuripur, Appl. Opt. **35** (35), 7000 (1996).

[17] B. Techranchi and D. G. Howe, Appl. Opt. 35 (29), 5831 (1996).

[18] A. B. Marchant, **Optical Recording: A Technical Overview,** Addison-Wesley, Massachusetts, 1990.

[19] D. J. Parker, http://www.emediapro.net/EM1999/parker1.html, 1999.

[20] M. C. Morilla, J. Solis, and C. N. Afonso, Jpn. J. Appl. Phys. **36**, 1015 (1997).

[21] L. Men, F. Jiang, and F. Gan, Mater. Sci. Eng. **B47**, 18 (1997).

[22] Internet, http://www.imagingmagazine.com/db_area/archs/1996/April/4_1232.htm, 1996.

[23] M. Mansuripur, **The Physical Principles of Magneto-Optical Recording**, Cambridge University Press, Landon, 1995.

[24] T. W. McDaniel and R. H. Victora (eds), **Handbook of Magneto-Optical Data Recording: Materials, Subsystems, Techniques,** Noyes Publications, Westwood, 1997.

[25] R. E. Gerber and M. Mansuripur, Appl. Opt. **34**, 4780 (1995).

[26] B. D. Terris, H. J. Mami, and D. Rugar, Appl. Phys. Lett. **68**, 141 (1996).

[27] Y Martin, S. Rishton, and H. K. Wickramasinghe, Appl. Phys. Lett. **71**, 1 (1997).

[28] A. Sakai, H. Yamada, M. Fujita, and T. Baba, Jpn. J. Appl. Phys. **37**, 517 (1998).

[29] K. Song, J. Bae, K. Cho, S. Yim, and S. Park, Appl. Phys. Lett. **73**, 2260 (1998).

[30] E. Betzig, J. K. Trautman, J. S. Weiner, and R. L. Kotelak, Science. **251**, 1468 (1991).

[31] J. Tominaga, T. Nakano, and N. Atoda, Appl. Phys. Lett. **73**, 2078 (1998).

[32] E. Betzig, J. K. Trautman, R. Wolfe, E. M. Gyorgy, P. L. Finn, M. H. Kryder, and C. H. Chang, Appl. Phys. Lett. **61** (2), 142 (1992).

[33] S. M. Mansfield and G. S. Kino, Appl. Phys. Lett. **57**, 2615 (1990).

[34] S. M. Mansfield, W. R. Studentmund, G. S. Kino, and K. Osato, Optics Lett. **18**, 305 (1993).

[35] B. D. Terris, H. J. Mami, D. Rugar, W. R. Studenmund, and G. S. Kino, Appl. Phys. Lett. **65** (4**)**, 388 (1994).

[36] I. Ichimura, S. Hayashi, and G. S. Kino, Appl. Opt. **36**, 4339 (1997).

[37] K. Goto, Jpn. J. Appl. Phys. **37**, 2274 (1998).

[38] D. M. Eigler and E. K. Schweizer, Nature **344**, 524 (1990).

[39] H. J. Mamin, B. D. Terris, L. S. Fan, S. Hoen, R. C Barret, and D. Rugar, IBM J. Res. Develp. **39**, 681 (1995).

[40] A. Sato and Y. Tsukamoto, Nature **363**, 431 (1993).

[41] T. C. Reiley, L. S. Fan, and H. J. Mamin, Microelectronic Engineering **27**, 495 (1995).

[42] B. D. Terris, H. J. Mamin, M. E. Best, J. A. Logan, D. Rugar, and S. A. Rishton, Appl. Phys. Lett. **69**, 4262 (1996).

[43] I. Fujiwara, S. Kojima, and J. Seto, Jpn. J. Appl. Phys. **35**, 2764 (1996).

[44] H. Kato and T Tohda, Appl. Phys. Lett. **66**, 2961 (1995).

[45] M. E. Marhic, Opt. Lett. **16** (16), 1272 (1991).

[46] K. Baba, R. Yamada, S. Nakao, and M. Miyagi, Electronics Letters **28** (7), 676 (1992).

[47] S. Hunter, Kiamelev, S. Esener, D. A. Parthenopoulos, and P. M. Rentzepis, Appl. Opt. **29**, 2058 (1990).

[48] Z. Chen, D. Govender, R. Gross, and R. Birge, BioSystems **35**, 145 (1995).

[49] A. S. Dvornikov and P. M. Rentzepis, Opics Communications **136**, 1 (1997).

[50] H. Sun, S. Matsuo, and H. Misawa, Appl. Phys. Lett. **74**, 786 (1999).

[51] K. Davis, K. Miura, N. Sugimoto, and K. Hirao, Opt. Lett. **21**, 1729 (1996).

[52] E. N. Glezer, M. Milosavljevic, L. Huang, R. J. Finlay, T. Her, J. P. Callan, and E. Mazur, Opt. Lett. **21**, 2023 (1996).

[53] J. Qiu, K. Miura, H. Inouye, and K. Hirao, Nucl. Instr. and Meth. In Phys. Res. B **141**, 699 (1998).

[54] D. Psaltis and F. Mok, Scientific American **November** Issue, 70 (1995).

[55] J. H. Hong, I. McMichael, T Y. Chang, W. Christian, and E. G. Paek, Optical Engineering **34**, 2193 (1995).

[56] M. A. Neifeld and W. Chou, Appl. Opt. **36**, 514 (1997).

[57] L. Solymar and D. J. Cooke, **Volume Holography and Volume Gratings**, Academic Press, London, 1981.

[58] H. S. Li and D. Psaltis, Appl. Opt. **33** (17), 3764 (1994)

[59] J. H. Zhai, Y. Ruan, and Z. G. Li, Optics Communications **118**, 499 (1995).

[60] T. Tanaka and S. Kawata, J. Opt. Soc. Am. A **13** (5), 935 (1996).

[61] J. Liu, J. Xu, G. Zhang, and S. Liu, Appl. Opt. **34** (22), 4972 (1995).

[62] J. Amin, B. Dussardier, T. Schweizer, and M. Hempsted, J. Luminescence **69**, 17 (1996).

[63] F. Mok and H. M. Stoll, Proc. SPIE **1701**, 312 (1992).

[64] W. E. Moerner and M. D. Levenson, J. Opt. Soc. Am. B **2** (6), 915 (1985).

[65] Y. P. Wang, D. P. Landau, R. S. Meltzer, R. M. Macfarlance, J. Opt. Soc. B **9**, 946 (1992).

[66] L. Zhao, X. Zhang, Y. Qin, Z. Lu, Y. Nie, D. Wang, M. Hu, and L. Hu, J. Opt. Soc. Am. B **14** (7), 1591 (1997).

[67] W. E. Moerner (ed), **Persistent Hole Burning: Science and Applications**, Springer, Berlin, 1987.

[68] O. Slid and K. Haller (eds), **Zero Phonon Lines and Spectral Hole Burning in Spectroscopy and Photochemistry**, Springer-Verlag, new York, 1988.

[69] N. Akhmediev, J. Luminescence **66** & **67**, 74 (1996).

[70] X. A. Shen, A. Nguyen, J. W. Perry, D. L. Huestis, and R. Kachru, Science **278**, 96 (1997).

Chapter 3
Rare Earth Emission

3.1 Rare Earth[1,2]

The rare earth (RE) elements (or rare earth metals) include two groups of elements: the lanthanides with atomic number 57 through 71, and the actinides with atomic number 89 through 103. Those elements with atomic numbers of 93 and above are also referred as transuranium elements. The Lanthanide series, named in the order of atomic number, are lanthanum (La), cerium (Ce), praseodymium (Pr), neodymium (Nd), promethium (Pm), samarium (Sm), europium (Eu), gadolinium (Gd), terbium (Tb), dysprosium (Dy), holmium (Ho), erbium (Er), thulium (Tm), ytterbium (Yb), and lutetium (Lu). Yttrium (Y) [atomic no. 39] is often included in the lanthanide series. The Actinide series are, in order of increasing atomic number, actinium (Ac), thorium (Th), protactinium (Pa), uranium (U), neptunium (Np), plutonium (Pu), americium (Am), curium (Cm), berkelium (Bk), californium (Cf), einsteinium (Es), fermium (Fm), mendelevium (Md), nobelium (No), and lawrencium (Lw). Only the first four elements in the actinide series have been found in nature in abundance while the rests are synthesized.

The RE elements are not so rare. Cerium is present at a level of 46 ppm in the earth's crust. Oxides of the RE elements are often simply called REs, and are found in minerals that are actually more abundant than those of some other metals, such as those in the platinum group. The principal source of REs is the mineral monazite. Some other rare minerals that also contain small amounts of REs include cerite, gadolinite, and samarskite. Most RE compounds are strongly paramagnetic. An alloy composed of iron and of RE metals, called misch metal, is pyrophoric. When scratched it gives off sparks capable of igniting flammable gases. It is used in cigarette lighters, miners' safety lamps, and automatic gas-lighting devices. Misch metal is also used in making aluminum and magnesium alloys and some types of steel. Eu is used as a phosphor activator in a color television tube to provide the red color seen by the viewer. The vast majority of RE-doped fibers have been doped with lanthanide elements like Er. There are many more known lasers with lanthanides as the active element than with actinides.

The most common form of RE elements is the ionic form, in particular the trivalent state $(Ln)^{3+}$. Neutral lanthanide elements have the atomic form of (Xe) $4f^{N}6s^{2}$ or (Xe) $4f^{N-1}5d6s^{2}$, where (Xe) represents a Xenon core. The ionization of the lanthanides involves the removal of the two loosely bound 6s electrons, and then of either a 4f or a 5d electron. Thus, the trivalent RE ions, on which most active RE-doped devices are based, have the electrostatic shielding of the 4f electrons by the $5s^{2}5p^{6}$ shells. This shielding constitutes something akin to a metal sphere, is responsible for the atomic like properties of the lanthanides when present in a solid host such as a crystal or glass.

J. Becquerel first observed the optical spectra of REs in the 1900s. He noticed sharp absorption lines in the spectrum of RE salts when they were cooled to low temperatures (less than 100 K). The optical behavior of lanthanide elements is influenced by their very particular atomic structure. The average radius of the 4f shell slowly decreases with increasing atomic number along the lanthanide series. This so-called lanthanide contraction is about 10 % from the beginning to the end of the lanthanide series. The average radius of the 4f shell is about 0.7 times the Bohr radius. The shielding of the 4f electron shell from its environment by the outermost 5s and 5p electrons is responsible for the REs' rich optical spectrum and for the many laser transitions that have been observed.

3.2 Nonlinear Optical Theory in Rare Earth[3,4]

Linearity or nonlinearity is not a property of the light itself, but a property of the optical medium. Nonlinear changes in the optical properties of a medium appear only when high intensity light wave propagates through the material or when one or more light waves interact with one another in the medium. There is no nonlinear behavior when light travels in free space. Media that display nonlinear behavior are commonly referred as nonlinear optical materials. Examples of nonlinear phenomena are, change of the refractive index with respect to light intensity, violation of superposition principle, frequency shift when light passing through nonlinear materials, and photon interactions. There are two general categories of optical nonlinearity: extrinsic and intrinsic. Extrinsic nonlinearity is a change of optical properties of the medium, resulted from absorption, or emission of light. The history of exposure as well as the instantaneous intensity of the light determines this type of nonlinear optical behavior. Intrinsic nonlinear optical phenomena are violations of the principle of superposition, arising from nonlinear response of the individual molecule or unit cell to the fields of two or more light waves. In either type, the nonlinear optical properties of the medium depend on light intensity. These nonlinear optical effects include, Kerr and Pockels effect, second-harmonic scattering, rectification, sum- or difference-frequency generation, third-harmonic scattering, Raman scattering, Brillouin scattering, inverse Raman effect, inverse Faraday effect, two-photon absorption, intensity-dependent refraction, induced opacity, induced reflectivity, and breakdown of gases.

A. Upconversion[5,6,7]

Nonlinear optical process of rare earths can arise as a consequence of 4f-4f ion-ion interactions. This kind of nonlinear process is referred as upconversion.[8,9,10,11,12] Upconversion basically denotes an energy transfer effect between RE ions, where energy is being transferred to an excited ion thereby promoting it to an even higher energy state. The resulting emission has higher energy than the pumping light. Thus, this is often the prefer method for converting infrared (IR) laser to visible light. Upconversion processes include those in which more than one photon is absorbed or emitted simultaneously by group of ions and those in which two or more ions cooperative combine to absorb and emit a single photon. There are many possible mechanisms that give rise to upconversion with widely different conversion efficiencies. The following are some of the common upconversion processes:

A-I. Resonant or Nonresonant Energy Transfer

Resonant transfer is the simplest upconversion process where energy is transferred from an excited ion to nearby ion in its ground state, without gain or loss of energy as a whole on the two-ion system. Nonresonant transfer is similar to resonant transfer, except it involves photon or phonon to make up the difference in energies between initial and final ionic states.

A-II. Stepwise Upconversion

This process is also known as two-step absorption or simply as upconversion. Energy is first transferred to an ion in its ground state and elevates it to an excited state. Further energy transfer resulting in the promotion of excited ion to an even higher excited state. Subsequence energy transfer could be of the same or different frequency. When ion is excited by two photons of different energy, the process is referred as two-step two-frequency upconversion (TSTF).

A-III. Addition de Photons par Transfers d'Energie

Addition de Photons par Transfers d'Energie (APTE) effect or upconversion by energy transfer usually involves more than one types of ions. In this process, ions A transfer successively their excitation energy to another ion B. This allows excited ion B to lift up to and emit from a higher energy level.

A-IV. Cooperative Sensitization

This process involves energy transfer of two or more ions that are so closely coupled together as if they act as a single constitute. In codopant system, two species of ions, A and B, are in a host. Ion B has a higher excited state than that of ion A and has no energy state that is at the same level as the excited state of ion A. When two ions A transfer simultaneously their excitation energy to ion B, the combined energy transfer will elevate ion B to a level that is higher than the excited energy level of ion A. Emission then occurs from the real excited level of ion B.

A-V. Cooperative Luminescence

In cooperative luminescence, two coupled excited ions in the same excited state simultaneously decay to their respective ground states and emit a single photon with twice the energy of the single ion excited state. This process is very similar to cooperative sensitization, except for lucking the real emitting level of second ion specie.

A-VI. Second Harmonic Generation

This process is also known as frequency doubling where the frequency of the irradiated light wave is double without any absorption transition takes place. The energy states of rare earth ions play no role in this process.

A-VII. Two-Photon Absorption

In two-photon absorption process, two photons are simultaneously absorbed without relying on any real intermediary energy level at all. Ion is excited to an energy level that is higher than any single photon can provide. The excited ion decays from this excited energy level with emission of one single photon.

Figure 3.1 shows the corresponding energy schemes described above. The first three processes require real energy states, which are resonant with the incoming or outgoing radiation and are therefore more efficient than the latter three, which are allowed to take place on virtual energy states.

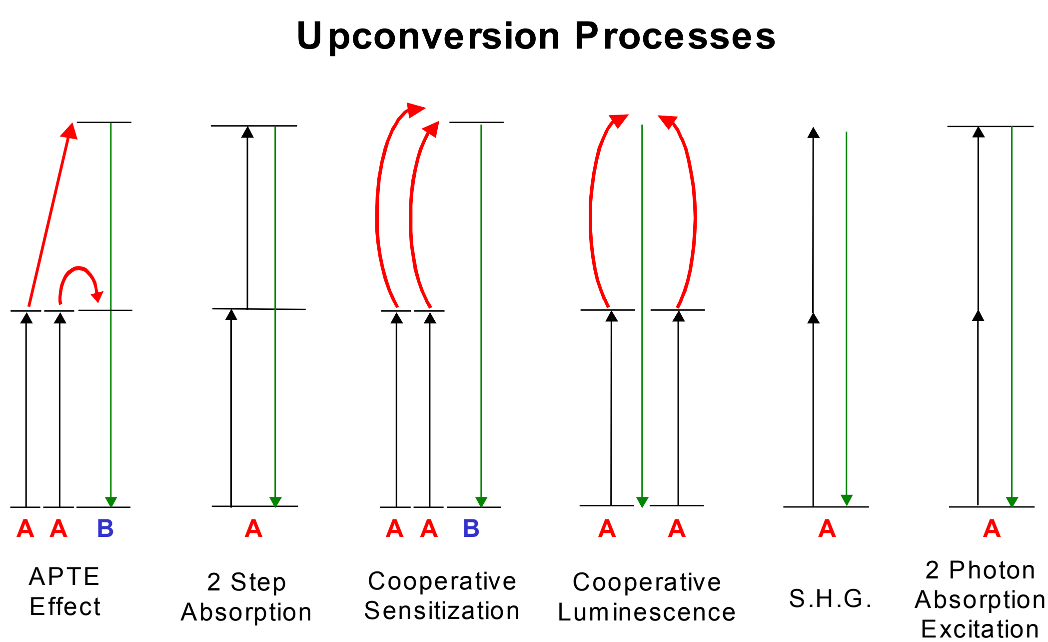

Figure 3.1: Upconversion Process: shown above is from the most efficient at left to the least efficient at right.

3.3 Two-Step Two-Frequency Upconversion of Pr doped ZBLAN Glass

Two-step two-frequency (TSTF) upconversion was demonstrated with Pr -doped ZBLAN ($53ZrF_4$-$20BaF_2$-$4LaF_3$-$3AlF_3$-20NaF) Glass[13] and other transparent oxyfluoride glass ceramics.[14] Bulk glass sample of ZBLAN transparent host doped with 0.55 wt % PrF_3 was used in this demonstration. ZBLAN is a heavy metal fluoride glass (HMFG) and is characterized by low (<500 cm^{-1}) phonon energies, a critical parameter leading to reduced nonradiative losses and increased upconversion efficiencies. Absorption/transmission band profiles for Pr-doped ZBLAN (ZBLAN:Pr) glass were determined from this sample with Perkin-Elmer UV/VIS/IR spectrophotometer. For a single laser excitation, Omnichrome model 532 air-cooled Ar laser at 488 nm wavelength was used to excite ZBLAN:Pr fluoride sample. Photoluminescence (PL) spectral had been collected via ARC 500 monochromator equipped with photomultiplier. Localized TSTF emission was obtained by using two SDL high power tunable diode lasers, the SDL-8630 at 840 nm and the SDL-TC30 at 1014 nm. Light emission at 605 and 636 nm was detected by Ocean Optics SD2000 miniature fiber optic spectrometer. The photoemission intensity and linewidth have been investigated as a function of laser pump wavelength and power.

The trivalent rare earth ions are well known for their ability to absorb IR energy and become excited to higher metastable quantum states. Their 4f electronic levels are well shielded from the ligand field in crystalline and vitreous hosts by the outer 5s and 5p

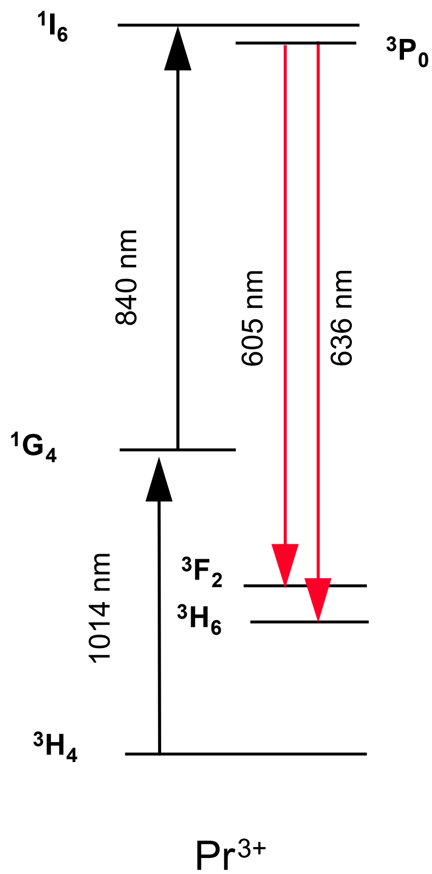

Figure 3.2: Energy level diagram of Pr^{3+} showing pumping and emission scheme of two-step two-frequency up conversion.

electrons, yielding long-lived metastable lifetime. The basic TSTF absorption process is shown in Figure 3.2 and schematic of the two pumped lasers intersect inside a bulk ZBLAN:Pr sample is shown in Figure 3.3. Red upconversion fluorescence emission in ZBLAN:Pr was obtained using excitation with two orthogonal laser beams at λ_1 = 1014 nm and λ_2 = 840 nm. 1014 nm laser excites Pr ion form the $^3H_4$ ground state to the $^1G_4$ first excited state, and 840 nm laser, subsequent transfers the population to upper energy level from $^1I_6$ to $^3P_1$ states. Very rapidly, nonradiative transition brings the population down to the $^3P_0$ metastable state. Excited

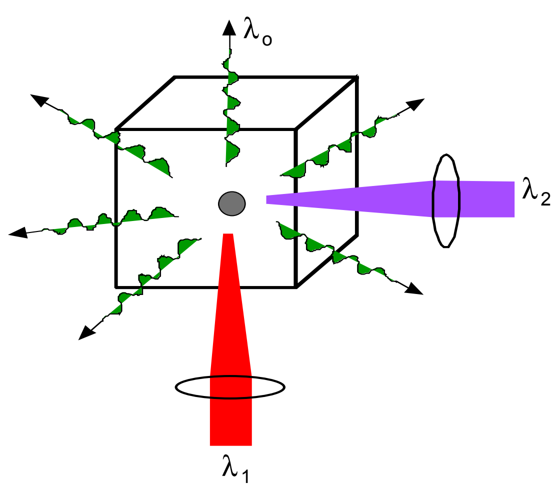

Figure 3.3: Schematic of the two pumped lasers intersect inside a bulk Pr-doped ZBLAN sample.

ions then return to the ground state through multi-phonon emission and visible light emission at 605 nm ($^3P_0$ to $^3H_6$) and 636 nm ($^3P_0$ to $^3F_2$).[15]

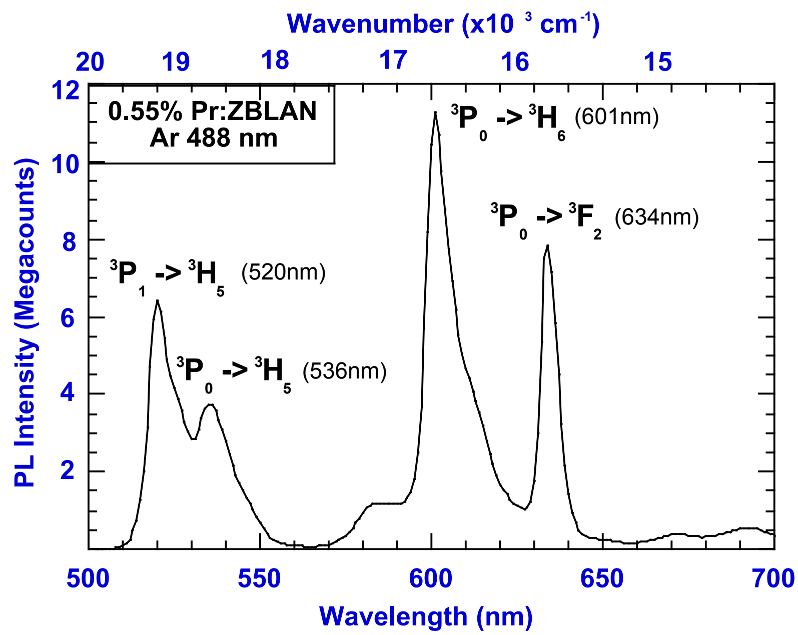

Figure 3.4: Photoluminescence spectra of Pr in ZBLAN glass pumped by 488 Ar laser. The PL spectral characteristics depend on the ground state absorption coefficient and the absorption cross section for photons from the optical pumping sources.

Figure 3.4 and Figure 3.5 show the PL spectral excited by 488 nm and TSTF absorption by 1014 nm and 840 nm respectively. Both spectrums show similar PL peaks at 605 and 636 nm correspond to transition energy level as shown in Figure 3.2. In addition, there is 489 nm blue transition occurred at TSTF absorption process. PL intensity is strong at 605 and 635 nm peaks, whereas 489 nm is the weakest of all PL peaks. The 489 nm blue transition terminates on thermally depopulated high lying levels of the ground multiplet, so emission occurs in the edge of emission band, avoiding three-level reabsorption losses. Thus, this transition is correspondingly inefficient.

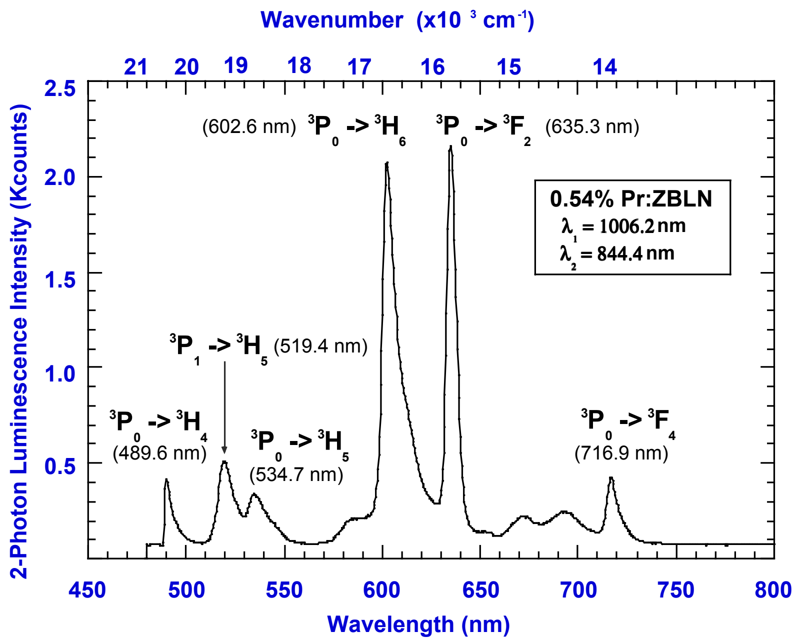

Figure 3.5: Emission spectra of Pr in ZBLAN glass excited by TSTF absorption with 1014 nm and 840 nm lasers. There is an addition weak transition at 489 nm peak not present at PL spectra.

The absorption cross-section and absorption coefficient at Figure 3.6 are derived from the absorption spectrum measured. Spectra shown in the figure is labeled with correspond ground state absorption (GSA) band transition. The 1014 nm pump beam is resonant with GSA band at 1010 nm and acts as an intermediate level for the two-step pumping process. The population of this multiple is then transferred by the excited state absorption (ESA) of the 840 nm pump beam. The transition is evidently extremely weak compared with the others shown in this range. In contrast to the weak GSA at 1014 nm, the ESA at 840 nm is extremely strong. Studies of the effect of pumped laser power on output intensity at 605 nm and 635 nm show a much increase in intensity by increase input power of 840 nm diode laser as compare to that of 1014 nm diode laser.

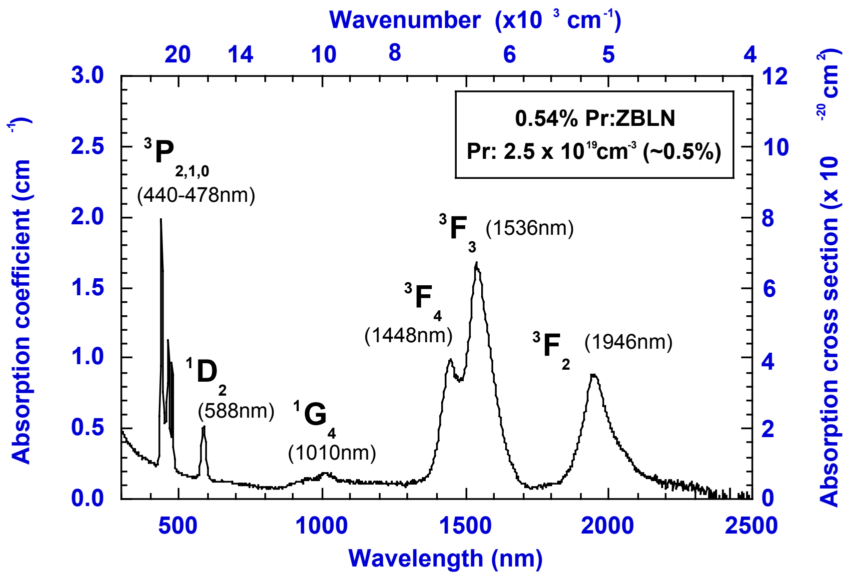

Figure 3.6: Absorption spectral for ground state absorption (GSA) band transition pumped with 1014 nm IR laser. 1014 nm pump beam is resonant with GSA band at 1010 nm and acts as an intermediate level for the two-step pumping process. The population of this multiple is then transferred by the excited state absorption (ESA) of the 840 nm pump beam.

The photoemission intensity and linewidth have been investigated as a function of laser

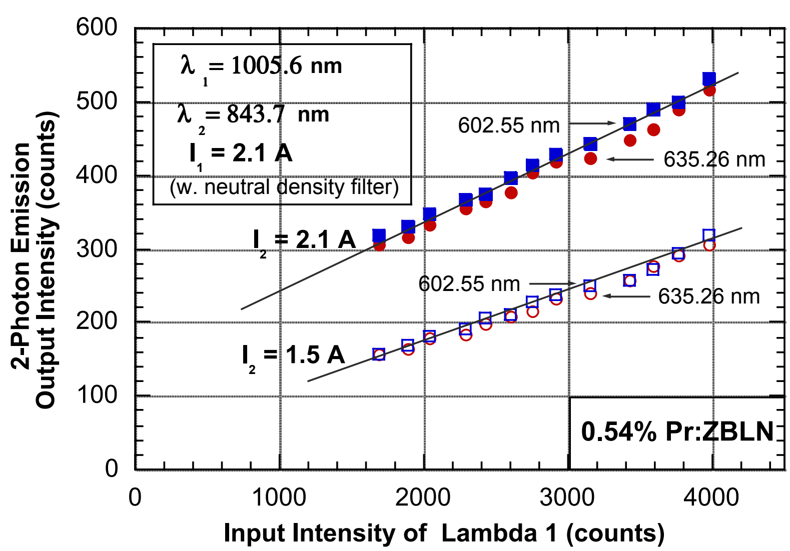

Figure 3.7: Upconversion emission intensity is linearly proportion to laser input power.

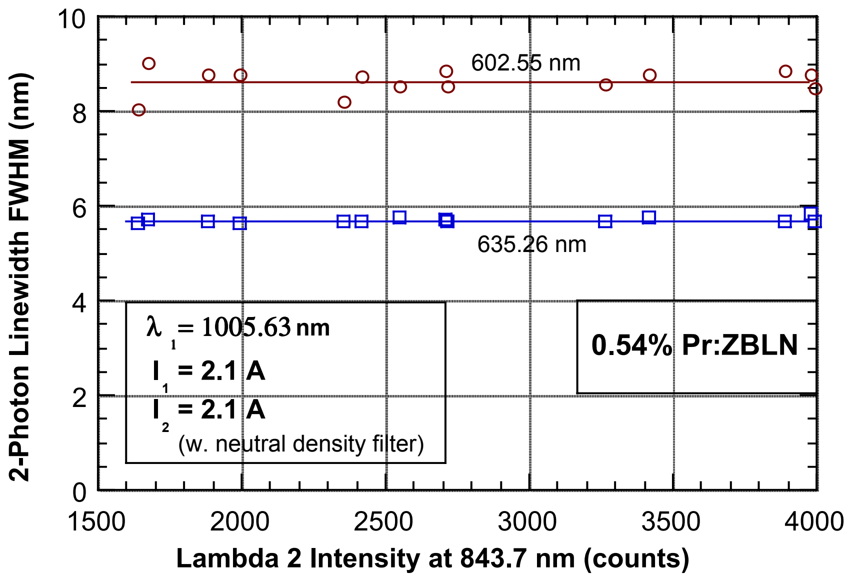

Figure 3.8: Linewidth of upconversion emission is relatively constant over a range of laser input power.

pump wavelength and power. The impact on pump laser power on the output intensity is shown in Figure 3.7. There exhibit a linear relationship between the pump power and output power. Where in Figure 3.8 shows the linewidth of upconversion emission versus the laser power. The full width at half maximum (FWHM) linewidth is roughly constant at about 8-9 nm for 605 nm peak and 5-6 nm wide for 635 nm peak.

This experiment demonstrates the TSTF upconversion emission from ZBLAN:Pr fluoride glass. The basic mechanism of TSTF excitation of the Pr ions through an intermediate energy level has relatively long lifetime. Because of this long lifetime, this "two-color" process is much more efficient than stepwise upconversion, which utilizes the absorption of two photons of the same energy through a virtual state that has a very short lifetime.

Figure 3.9 shows the photos of upconversion emission excited by the two pumped lasers intersect inside a bulk ZBLAN:Pr fluoride glass. Upconversion fluorescence emission in ZBLAN:Pr was obtained using excitation with two orthogonal laser beams at λ_1 = 1006 nm and λ_2 = 844 nm. TSTF upconversion emission beam diameter was measured at ~100 µm. Stepwise upconversion emission exited by each single laser at 1006 nm and 844 nm is represented by the two orthogonal lines, which are shown in the photo. Since this picture was not taken by IR camera, the two orthogonal lines shown in the photo are in fact the result of stepwise upconversion emission, and not the invisible IR laser beams. Intensity of TSTF upconvesion emission (represented by bright emission at the intersected spot) is much stronger than stepwise upconversion (represented by each orthogonal emission lines). This is the physical evident that TSTF is more efficient than stepwise upconversion process as predicted.

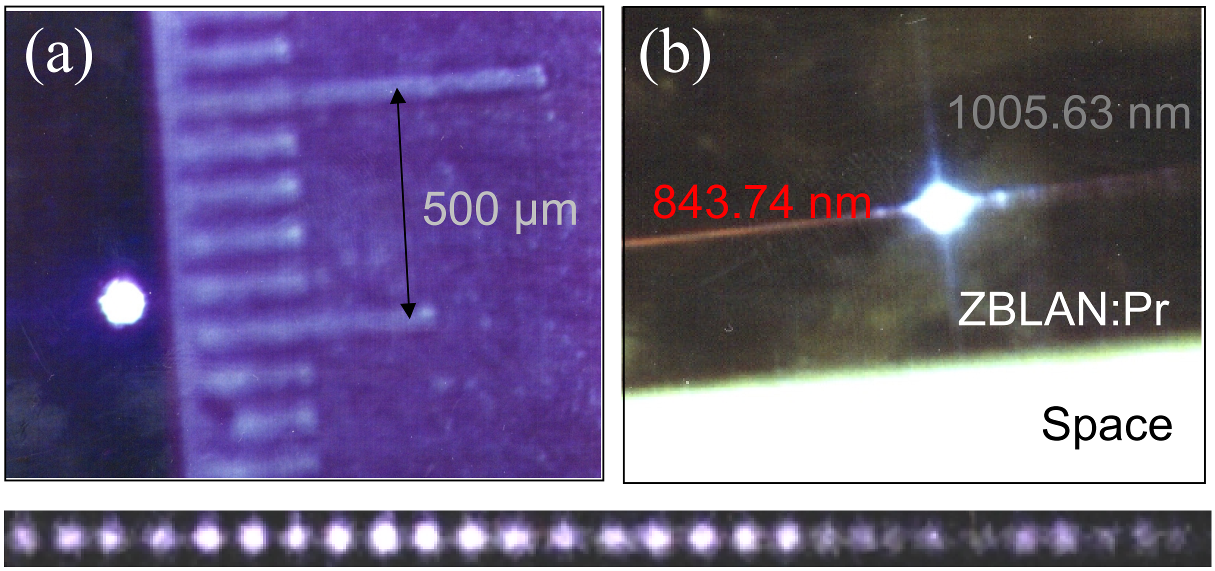

Figure 3.9: TSTF upconversion emission from ZBALN:Pr fluoride glass pumped by both 840 nm and 1000 nm tunable lasers.

(a) TSTF upconversion emission beam spot measured at ~100 µm in diameter.

(b) Upconversion emission pumped by each single laser is observed as two perpendicular lines intersect with each other to produce TSTF upconversion within ZBLAN:Pr glass. Emission due to TSTF is clearly much stronger than single stepwise upconversion.

3.4 References

[1] H. M. Crosswhite and H. Crosswhite (eds), **Spectra and Energy Levels of Rare Earth Ions in Crystals**, Interscience Publishers, New York, 1968.

[2] R. Reisfeld and C. K. Jørgensen (eds), **Lasers and Excited States of Rare Earths**, Springer-Verlag, New York, 1977.

[3] G. C. Baldwin, **An Introduction to Nonlinear Optics**, Plenum Press, New York, 1969.

[4] P. N. Butcher and D. Cotter (eds), **The Elements of Nonlinear Optics**, Cambridge University Press, Avon, 1990.

[5] B. Jezowska-Trzebiatowska, J. Legendziewicz, and W. Strek (eds), **Rare Earth Spectroscopy: Proceedings of The International Symposium on Rare Earths Spectroscopy, Wrocaw, Poland, September 10-5, 1984**, World Scientific Pub., Philadelphia, 1985.

[6] R. Scheps, **Upconversion Laser Processes**, Elsevier Science, Tarrytown, 1996.

[7] B. D. Bartolo (ed), **Nonlinear Spectroscopy of Solids: Advances and Applications**, Plenum Press, New York, 1994.

[8] F. Auzel, Proc. IEEE **61**, 758 (1973).

[9] F. Auzel, Phys. Rev. **B13**, 2809 (1976).

[10] F. Auzel, J. Lum. **31** & **32**, 759 (1984).

[11] F. Auzel, Elect. Lett. **29**, 337 (1993).

[12] F. Auzel, J. Lum. **60** & **61**, 101 (1994).

[13] E. Downing, L. Hesselink, J. Ralston, and R. Macfarlane, Science **273**, 1185 (1996).

[14] M. J. Dejneka, MRS Bulletin **23**, 57 (1998).

[15] R. G. Smart, D. C. Hanna, A. C. Tropper, S. T. Davey, S. F. Carter, and D. Szebesta, Elec. Lett., **27**, 1307 (1991).

Chapter 4
Experimental Procedures and Equipment Design

4.1 Experimental Setup

4.1.1 Molecular Beam Epitaxy

Molecular Beam Epitaxy (MBE) is used to growth our rare earth (RE) doped gallium nitride (GaN) samples. Thin layers on the heated substrate are grown by the beam-like molecules of several kinds of materials heated in the effusion cells under ultra-high-vacuum (UHV) chamber (about 10^{-10} Torr). The shutters in the front of the effusion cells control the formation of crystallization to develop an extremely abrupt transition layer as

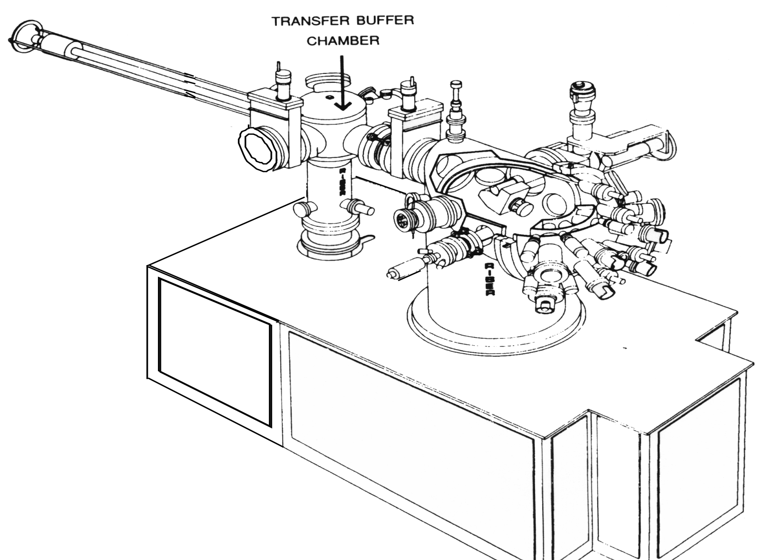

Figure 4.1: Schematic diagram of Riber MBE-32 system.

thin as several Angstroms. Figure 4.1 and Figure 4.2 show the Riber MBE-32 system with five major components: loadlock, growth chamber, gases cabinet, control electronics, and computer console. The growth chamber is retrofitted with sample manipulator holder, cell panel (contains both Knudsen effusion cells and high temperature gas injector for hosting solid source UHP materials), Stain Instruments 35 kV reflection high-energy electron diffraction (RHEED), Leybold residual gas analyzer (RGA), liquid nitrogen (N_2) gas cryoshrouds, and UHV cryopumps. Samples are inserted from loadlock and transferred to the growth chamber. Growth temperature as high as 1200 °C with pressure as low as 1.2×10^{-11} Torr could be sustained with this MBE system.

Figure 4.2: Photo of Riber MBE-32 system.

4.1.2 Focus Ion Beam

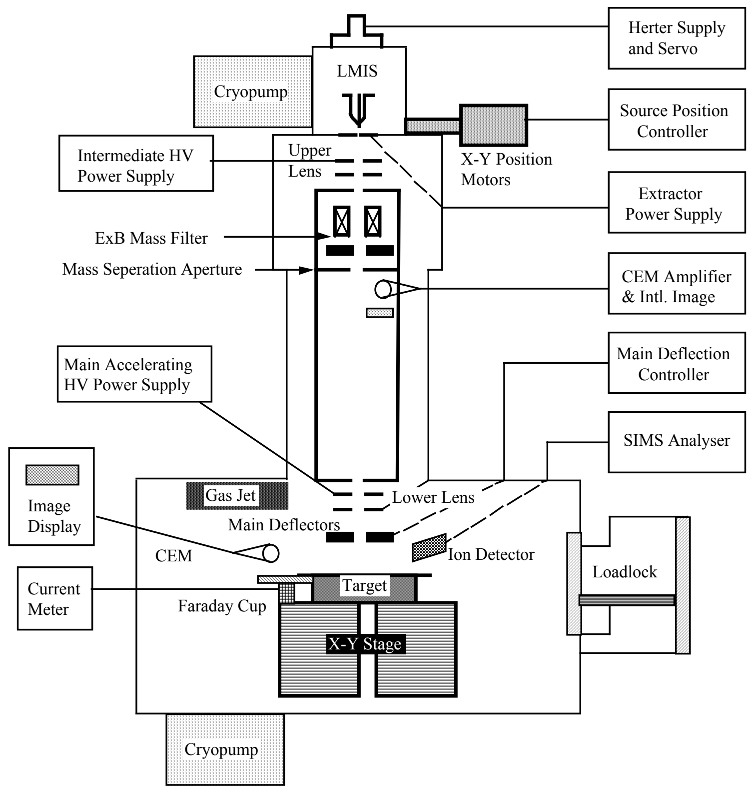

Figure 4.3: Schematic diagram of NanoFab-150 focused ion beam system.

Focused ion beam (FIB) is used for rare earth ion implantation into GaN thin films and for ion milling of sub-micron features on rare earth doped GaN samples. FIB technique is a maskless and resistless process. Region of substrate is scanned and implanted or milled by ion beam (usually Ga^+ ions or other liquid metal ion sources) without incurring damages to other areas of the sample. There are two types of FIB systems being utilized, the MicroBeam NanoFab 150 FIB system, with schematic diagram shown in Figure 4.3 for ion implantation process and FEI FIB 200 TEM system for Ga^+ ion beam micromachining.

A. MicroBeam NanoFab 150 FIB System

The MicroBeam 150 FIB system is a 150 kV two electrostatic lens system which incorporates an E×B mass separator with a sensitivity of m/Δm = 50. Retrofit with differentially pumped chamber and column at base pressure of about 10^{-7} Torr, and SIMS analyzer for sample composite structural analysis, this FIB system is capable of high-energy implantation (above 200 keV), liquid ion source specie selection, and laser interferometer aid precision stage movement in sub micron range. Ion sources for this system are usually in the form of liquid metal ion sources (LMIS) or liquid alloy ion source (LAIS). Primary ion species in use are but not limited to, Ga, Si, Au, Be, In, As, B, Er, Pr, and Tm. This FIB system is capable of both high-energy ion implantation and ion milling processes. A photo of this system is shown in Figure 4.4.

Figure 4.4: Photo of MicroBeam NanoFab 150 system.

B. FEI FIB 200 TEM System

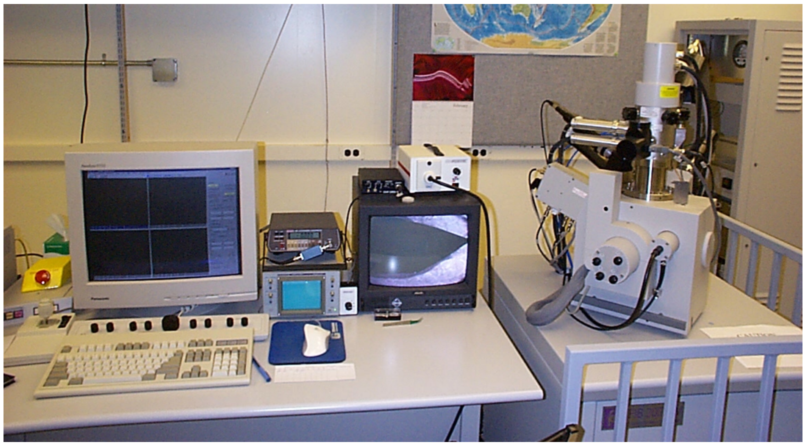

Figure 4.5: Photo of FEI FIB 200 TEM system.

The FEI FIB 200 TEM system is equipped with high-resolution finely focused Ga^{+} ion beam with implantation energy ranged from 5 to 30 keV at base pressure of 10^{-7} Torr. It contains powerful two-lens column capable of emitting high current density ion beam. This ion column dramatically increases the beam resolution for nano fabrication, reduces the milling time for micromachining, and is capable of maintaining sharp imaging at high beam currents. FEI FIB 200 TEM system is idea for rapid, precise micromachining and deposition of sub-micron features on variety of substrates. It can also be used for SEM/TEM specimen cross-section preparation, high contrast imaging, grain structure analysis, high aspect ratio probe drilling, and fabrication of micro-electromechanic structures (MEMS). A photo of FEI FIB 200 TEM system is shown in Figure 4.5.

4.1.3 Optical Setup

The complete optical setup for data retrieval consists of active and passive components. The active components include ILX Lightwave LDC-3900 modular laser diode controller, two 500 mW continuous wave (CW) tunable diode lasers, the SDL 8630 GaAs/AlGaAs at 840 nm wavelength and SDL TC30 InGaAs/AlGaAs at 1000 nm wavelength, Newport programmable PMC-200-P2 motion controller, Melles Griot NanoBlock X-Y-Z axis flexure stage (with resolution up to 20 nm step size) with piezoelectrical feedback controller, 0.27 meter ISA SPEX-270M spectrometer equipped with Spectrum One, 1024 x 256 pixel liquid nitrogen (N_2) cooled Si-CCD detector array, Newport model 1830-C optical power meter with model 818-IR infrared detector, and Diagnostic Instruments Spot RT Color CCD digital camera. The passive components include laser beam optical steering set, Newport 401 two-axis large platform translation stage (13 mm maximum travel distance) controlled manually by two 860A-05 motorized

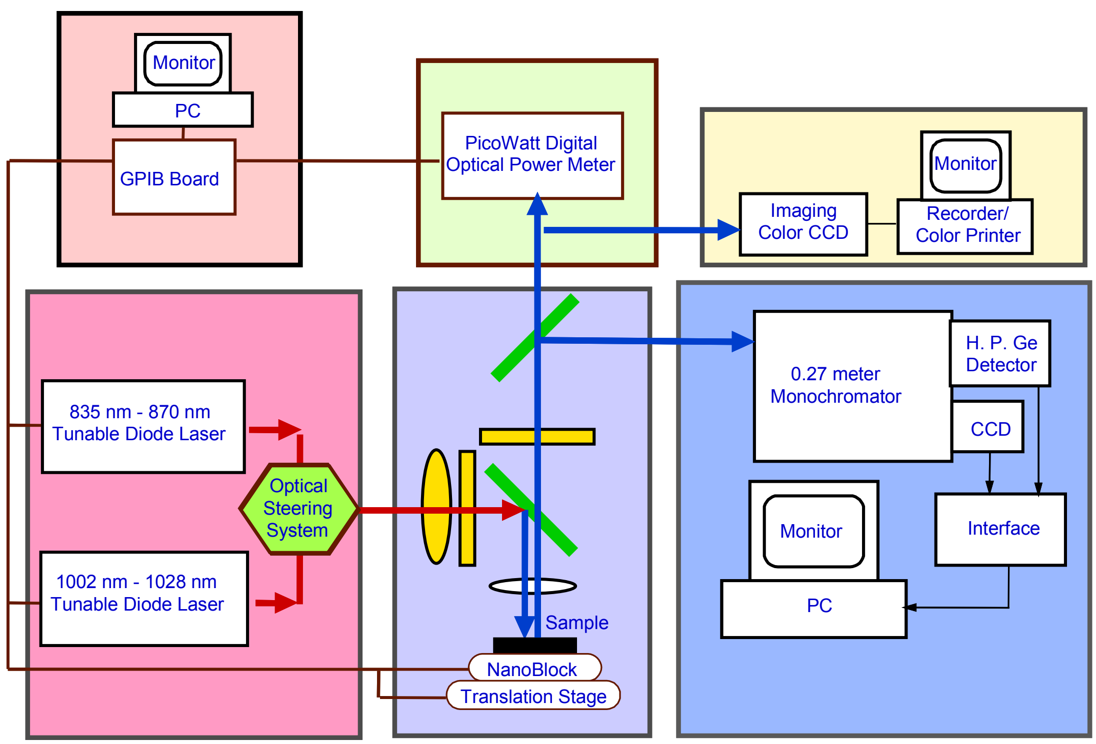

Figure 4.6: Schematic diagram of optical setup for TSTF, upconversion, luminescence, and imaging. This setup is adapted for GaN:Er optical memory storage experiment.

drives, and modified Nikon Eclipse E600-FN Physiostation optical microscope. Schematic diagram and photo of the experimental set up are shown in Figure 4.6 and in Figure 4.7 respectively.

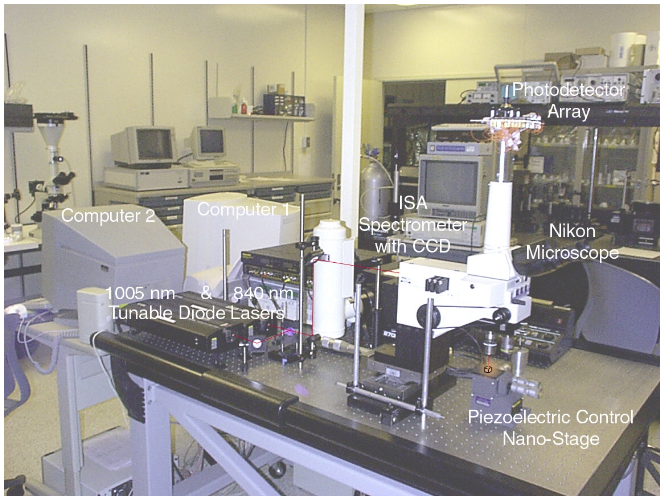

Figure 4.7: Photo of optical setup for upconversion optical memory storage based on GaN:Er.

4.1.4 LabVIEW Integration

Laboratory Virtual Instrument Engineering Workbench (LabVIEW), developed by National Instruments Corporation, is a graphical programming development environment based on the G programming language. This graphical programming language is written for instrumental control, data acquisition, data analysis, and data presentation. Due to the inherent intuitive graphical programming methodology, LabVIEW provides the flexibility of a powerful programming language without the associated difficulty and complexity of traditional test based programming languages. After acquired the data, raw measurements can be converted into polished results by using the powerful data analysis

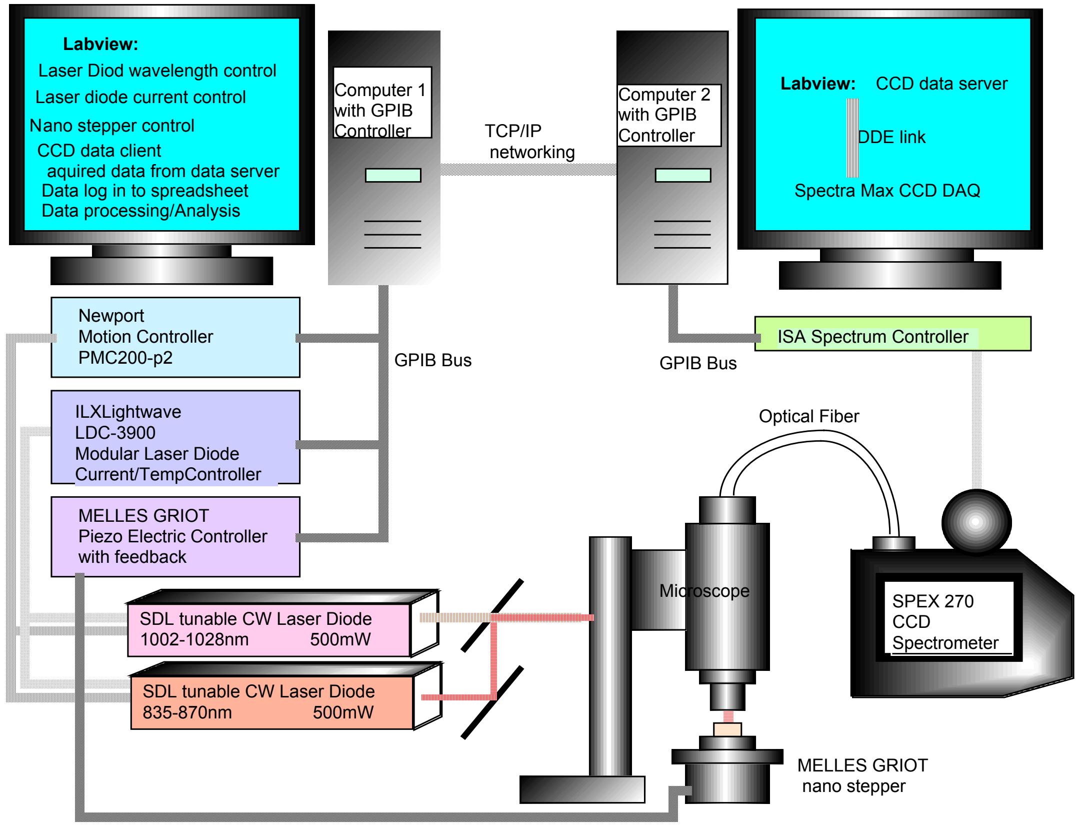

Figure 4.8: LabVIEW control configuration for optical memory characterization station.

and visualization capabilities of LabVIEW. In short, LabVIEW simplifies and reduces the development time of a complete system.

Thus, LabVIEW was chosen for our optical readout system for its ease of programming the control of instruments and flexibility of integrating various equipments from different vendors. Hardware communication within instruments such as, LDC-3900 modular laser diode controller, PMC-200-P2 motion controller, Melles Griot NanoBlock piezoelectric controller, and Newport optical power meter is carried over with the General Purpose Interface Bus (GPIB). To increase data acquisition rate and enhance overall performance, two computers (PCs) are deployed to facilitate the entire system. One PC is deployed for operating the SPEX-270M spectrometer and collecting spectrum measurement. The other PC is deployed for controlling the SDL laser output power, Melles Griot NanoBlock movement, as well as for data processing, analysis, and real-time graphical presentation. Data transfer between two PCs is done through TCP/IP networking. Figure 4.8 presents the schematic diagram of LabVIEW configuration for the optical system.

4.2 Storage Medium Preparation

Er doped GaN (GaN:Er) thin films were grown on p-Si (111) in the Riber MBE-32 system. Prior to insertion into MBE, all substrates received a surface-cleaning treatment. Si wafer was cleaned in acetone and methanol and dipped in 10% HF. Some silicone (Si) samples, however, were cleaned via standard RCA procedure. All substrates were immediately inserted into load lock and degassed at least 1 hour at T ~ 400 C. The substrates were then transferred to the growth chamber and outgassed at T > 800 C before commencing growth. Typical background pressures of the main chamber were in the low 10^{-10} Torr range. Solid source were employed to supply the Ga (7N purity), Al (6N), and Er (3N) fluxes, while the SVTA rf-plasma source was used to generate atomic nitrogen. Growth of the GaN:Er film proceeded at temperatures varying 650-950 °C for 3 hours with a variable Ga beam pressure of 7.0 x 10^{-7} to 1.2 x 10^{-5} Torr depending on the conditions examined. The Er cell temperature was also varied form 950-1200 °C depending on the experiment. The resulting GaN film growth rate was nominally 0.8 μm/hr. Occasionally, a GaN:Er film was annealed in situ at high vacuum after growth but was found to have negative effect on Er visible emission intensity. In summary, growth of GaN:Er on Si were depend and varied with four important growth parameter set: Ga, Er, N fluxes, and substrate temperature. These relationships are illustrated on Figure 4.9.

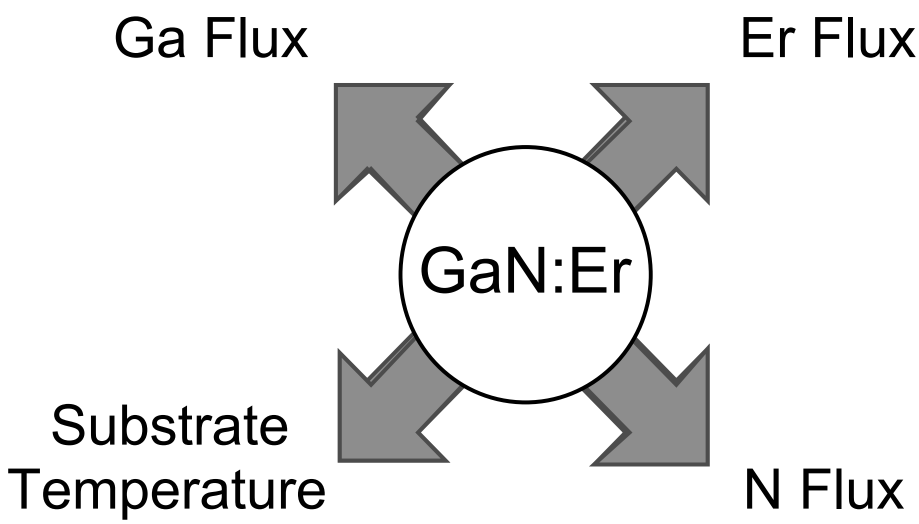

Figure 4.9: The dependency of MBE grown Er doped GaN film quality on the four growth parameter.

4.3 LAIS Fabrication

Ion sources for FIB technology are usually in the form of liquid metal ion sources (LMIS).[1,2] However, since Er has a high melting point (1529 °C) and a high vapor pressure at its melting point (≈1 Torr), it is unsuitable for an elemental LMIS. Therefore, Er ion source must be made in the form of erbium (Er)-nickel (Ni) liquid alloy ion source (LAIS) in order to lower the melting point and the vapor pressure. Figure 4.10 shows the phase diagram of the Er-Ni binary system[3] where a mixture of Er to Ni atomic percent ratio of 69:31 produces a eutectic binary alloy with a melting point of 765 °C.

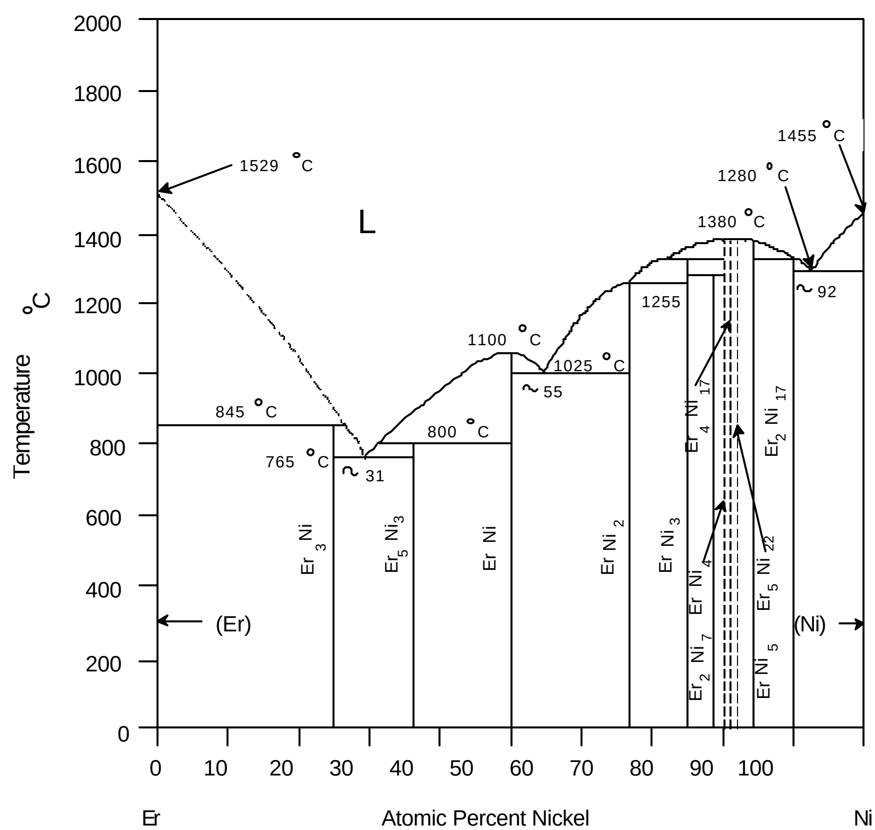

Figure 4.10: The phase diagram of the Er-Ni system.

First, a 250 μm diameter tungsten wire is twisted around an I.D. 0.125” Al_2O_3 tube in order to be fitted into the ion gun module of a MicroBeam 150 FIB system. Another tungsten wire is wrapped around the first wire which shanks to form a reservoir. The tip is mechanically polished and then electrochemically etched in a NaOH solution until the end radius is approximately 10 μm. The source is wetted with Er-Ni alloy in a separate vacuum system. The alloy was prepared by mixing erbium and nickel powders at Er to Ni atomic ratio of 69:31. The mixed powder was put into an Al_2O_3 crucible that can be heated to temperatures above 1800 °C by a tungsten filament. Before dipping the tip into the crucible, the crucible was heated to 1800 °C for two minutes to ensure proper mixing. After the alloy was in its molten state, the tip was dipped into the crucible for 30 seconds and than retracted. A puddle of the alloy should form on the reservoir. The source is tested in-situ by applying appropriate voltage and heating current to the source. After the preliminary test, the source is then transferred to a MicroBeam 150 FIB system. Figure 4.11 shows an SEM micrograph of an Er-Ni LAIS before and after being exposed to air for 12 hours. The heavy formation of oxides on the surface of the tip is observed.

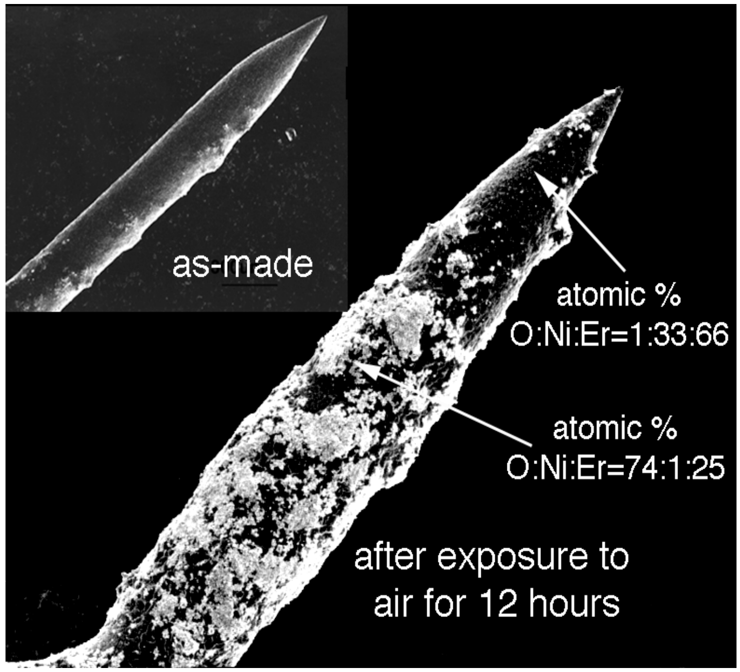

Figure 4.11: SEM microphotographs of an Er-Ni LAIS before and after 12 hours exposure to air.

4.4 Write Process – Focus Ion Beam

Data recording is implemented with FIB technology. This non-optical write mechanism is a proven and well-developed lithographic technique used in current semiconductor industry. Furthermore, FIB technology could be easily modified and adapted cost-effectively for future mass mastering process. In our research, writing process with FIB was implemented with two approaches: ion implantation and ion milling.

With ion implantation approach, Er ion source in the form of LAIS was prepared for FIB. These Er ions were then implanted into undoped GaN thin film grown on sapphire or Si substrates. Thermal annealing process is required to activate the optical properties of implanted Er ions. Upconversion emission was stimulated with IR lasers, where implanted regions that could emit are designated as logic ‘1’ and unimplanted regions that could not emit are designated as logic ‘0’.

With ion milling approach, sub-micron patterns were micro machined on MBE grown in-situ GaN:Er film on Si substrate. Upon IR laser stimulation, regions, where GaN:Er film was completely removed, do not emit and serve as logic ‘0’; while the reminder unaltered regions that emit upconversion luminescence serve as logic ‘1’.

4.4.1 Focus Ion Beam Implantation

To demonstrate RE optical memory concept based on upconversion emission of RE ions, closely spaced patterns as small as 0.5 μm size of Er ions were implanted by FIB into GaN films grown on sapphire or Si. Er-Ni LAIS was fabricated for implanting Er into GaN with MicroBeam NanoFab-150 FIB system.[4] The MicroBeam 150 FIB system is a 150 kV two-lens system which incorporates an E×B mass separator with a sensitivity of $m/\Delta m = 50$. The Er-Ni source was positioned at 3.5 mm upstream of a Wehnelt electrode, which has an aperture of 3 mm in diameter. The extractor electrode was positioned 25 mm downstream of the Wehnelt electrode, which has an aperture of 1.85 mm in diameter. The extractor voltage V_E is applied between the extractor electrode and the source. The Wehnelt electrode was biased at positive 1.1 kV relative to the source. An automatic source stabilization software program to maintain steady emission adjusted the Wehnelt electrode voltage. The Er^{2+} ion beam was accelerated to 200 keV energy with doses ranging from 1 x 10^{12} atoms/cm^2 to 1 x 10^{17} atoms/cm^2. GaN films used for Er incorporation were grown by molecular beam epitaxy (MBE), hydride vapor phase epitaxy (HVPE), and metalorganic chemical vapor deposition (MOCVD). After implantation, samples were either annealed with rapid thermal annealing (RTA) condition for 60 seconds, or in a furnace at 1100 °C from 100 seconds to an hour in N_2 gas. Figure 4.12 shows the optical picture taken under optical microscope of typical Er

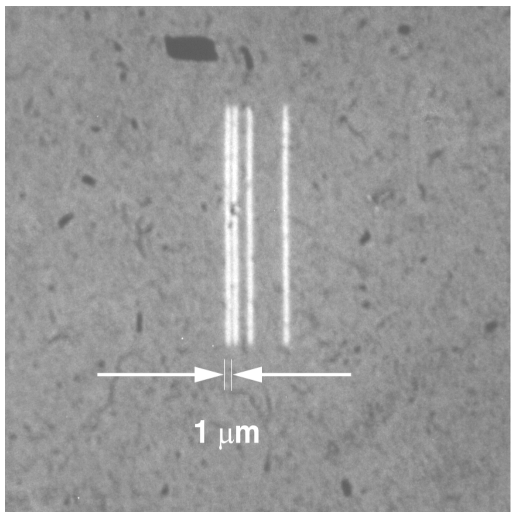

Figure 4.12: 1 μm wide Er lines on GaN patterned by FIB direct write. Picture is taken under optical microscope with brightfield-reflected light technique. Due to the index of refraction change induced by FIB implantation, Er lines appear brighter than surface.

lines patterned by FIB direct write on GaN. The lines are 1 μm wide by 30 μm long.

4.4.2 Focus Ion Beam Milling

RE optical memory concept based on upconversion emission of RE ions can also be demonstrated with FIB milling approach. This is accomplished with micro milling of closely spaced nanometer features in GaN:Er films grown on Si substrate. FIB milling technique is performed with the FEI FIB 200 TEM system with Ga^+ ion source. The beam dwell time was set steady at 0.2 μs while the beam spot overlap was held constant at 50%. The ion energy was fixed at 30 keV, whereas the beam current was controlled at the range from 100 pA to 5 nA to fabricate different sizes of feature. All patterns were micro-milled at normal incident. There are two common types of patterns being fabricated: positive and negative bit patterns. To generate positive bits, large box was milled out and left with remnant of square pattern array with equal distance spacing as shown in Figure 4.13. Square pattern of various size from 0.2 μm^2 to 4 μm^2 were fabricated. To create negative bits, arrays of circular holes with identical diameter size were drilled and arranged in box formation as shown in Figure 4.14. The circular diameter, which ranged from 0.4 μm to 4 μm were fabricated.

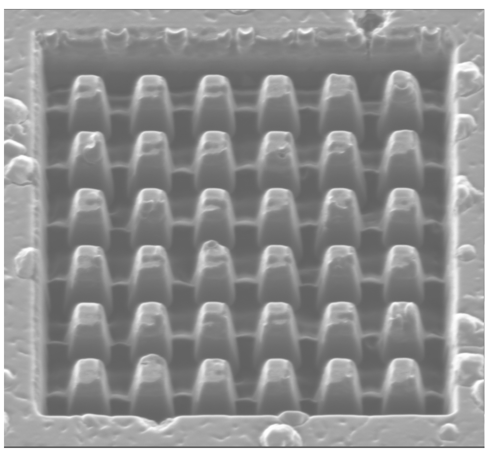

Figure 4.13: Positive bit pattern, where square box was milled out and left out array of cube structures. Each cube has area dimension of 1 x 1 μm^2 and is spaced at 1μm distance with neighboring cubes.

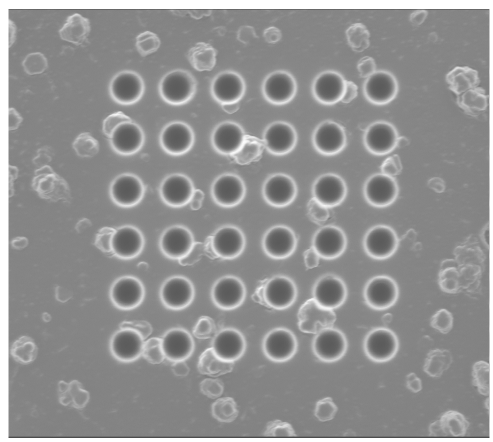

Figure 4.14: Negative bit pattern, where circular holes with constant diameter were drilled away and left out array of circular holes. Each circular is 1 μm in diameter and is spaced at 1μm apart from neighboring circles.

4.5 Read Process

Both in-situ doped and FIB implanted GaN:Er type films can be excited with visible luminescent emission. Photoluminescence is achieved with either 325 nm helium-cadmium (HeCd) metal vapor laser or argon (Ar) ion laser. Stepwise upconversion is excited with either 840 nm or 1000 nm tunable IR diode laser. When GaN:Er films are collinearly pumped by both IR lasers (840 nm and 1000 nm), TSTF upconversion emission can also be achieved. Although TSTF upconversion is possible with two folds increase in output intensity, most of the data readout is carried out with stepwise upconversion excited by 1000 nm IR laser in order to simplify the optical read process.

Modified optical microscope, which is capable of luminescence and reflection detection, is utilized to steer the input laser beam to the bit location and simultaneously to read the incoherent upconversion emission signal. Both 10X and 40X objectives are installed with the microscope. Depend on the detection scheme; a 40X objective is used to focus the laser beam into small diameter so that only one bit location is accessed sequentially at a time. 40X objective is used for sequential scanning readout process. While 10X objective is used to slightly expand the laser beam to envelop rows of bit arrays without lowering down power density below upconversion excitation threshold. 10X objective is needed for parallel read demonstration with CCD camera imaging.

4.5.1 Scanning Optical Serial Read Out

Upconversion spectra were obtained at room temperature by pumping the sample with two 500 mW CW tunable diode lasers, the SDL 8630 GaAs/AlGaAs at 840 nm wavelength and SDL TC30 InGaAs/AlGaAs at 1000 nm wavelength. Both lasers were coupled into collinear beams and focused to 2-μm diameter beam spot through a modified Nikon Eclipse E600-FN Physiostation microscope with CFI Super Flour 40X, 0.9 NA objective. Reflected laser beams and emission were simultaneously recaptured back to the same microscope and objective. Dichroic mirror installed inside the microscope, which reflects all wavelengths above 800 nm but transmits all wavelengths below 800 nm, was used to filter out both lasers and photoluminescence from upconversion emission. Emission was then coupled into optical fiber located on top of the microscope, and transmitted to a 0.27 meter ISA 270M spectrometer equipped with Spectrum One, 1024 x 256 pixel liquid N_2 cooled Si-CCD array detector. Spectra were acquired with SpectraMax software for spectrometer control and data acquisition. A grating of 300 grooves/mm blazed at 500 nm wavelength was selected for spectra collection.

Melles Griot NanoBlock X-Y-Z axis flexure stage with resolution up to 20 nm step size was used for spatial scanning. This translation stage provides both 4 mm of fine position adjustment with 50 nm resolution along each axis by differential micrometers, and high resolution 20 μm scanning range at 20 nm minimum step size by piezoelectric control drives. For added scanning range, Melles Griot NanoBlock was placed on top of Newport 401 two-axis large platform translation stage, which offers additional 13 mm travel distance by two 860A-05 motorized drives. Computer automation for spatial scanning was written with LabVIEW programming software to control both spectrometer and translation stage, and to construct spatial scanning profile by integrating spectra intensity while simultaneously recording the scan position in real time. Three types of patterns were fabricated for spatial scanning detection. Implanted patterns include (a) square pattern with 136 x 136 μm^2 and 50 x 50 μm^2 dimensions; (b) line patterns with 2 x 20 μm^2, 1 x 20 μm^2, and 0.5 x 20 μm^2 dimension, where spacing between lines ranging from 5 μm, 10 μm, and 15 μm wide; and (c) array pattern each at 2 x 3 μm^2 dimension with 7 μm spacing.

4.5.2 CCD Parallel Read Out

The feasibility of parallel reading is demonstrated with CCD digital camera. The above-mentioned serial readout optical setup has been slightly adjusted to adapt for this experiment. To simplify the read operation, instead of using two IR lasers, only one SDL TC30 InGaAs/AlGaAs laser at 1000 nm wavelength was used. Stepwise upconversion emission was monitored for simulating data retrieving process. Laser beam was directed and focused to 10-μm diameter beam spot through a modified Nikon Eclipse E600-FN Physiostation microscope with CFI Plain Flour 10X, 0.3 NA objective. Reflected laser beam was filtered out from incoherent upconversion emission through the same dichroic mirror. The optical fiber system originally placed on top of the microscope was replaced with Diagnostic Instruments Spot RT Color CCD digital camera. Instead of coupling the emission into optical fiber, the upconversion signal/image was captured by CCD digital camera in real time. Spot RT Color CCD digital camera is a reliable, high speed, and low noise camera. It is designed to capture high-resolution image for fluorescence, darkfield, and brightfield objects. The Kodak KAI-2092 interline scientific grade CCD sensor of this digital camera has inherently lower noise and greater dynamic range. The objective of this experiment is to study the effect of FIB milling on upconversion emission intensity, milling condition, micro-milled feature size, and to optimize the milling process.

4.5.3 Si-Detector Parallel Read Out

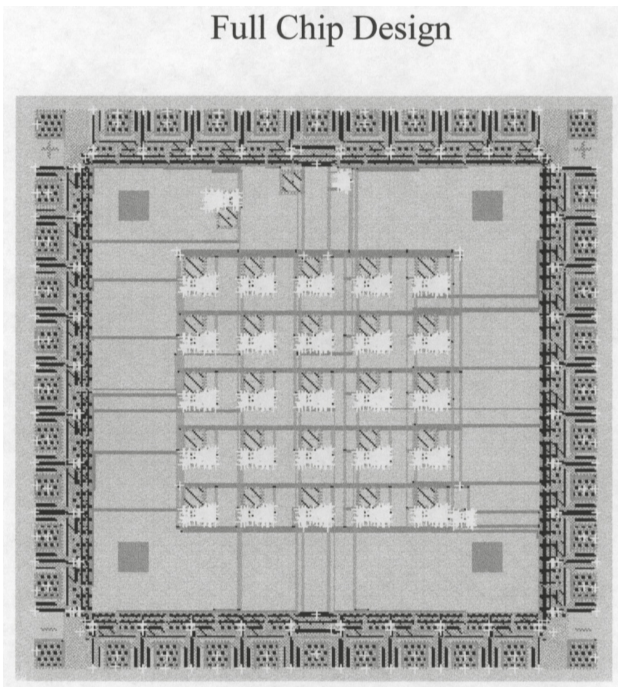

Figure 4.15: CMOS photoreceiver array with low threshold optical power level < 1 nW. This detector is capable of near-field sub-wavelength detection with spatial resolution of 50 -100 nm, current responsivity of 0.1 - 0.5 A/W, and minimum detectable optical power at ~ 100 fW.

Parallel read process through a page-oriented-access enabling optical memory read device is currently being developed by Dr Beytte's research group. Based on a photonic VLSI device technology, this optical read device uses a standard CMOS fabrication process to implement a 5 x 5 array of photodetectors, current amplifiers, and differential amplifiers with a tunable threshold power level. The initial design has been fabricated by the MOSIS CMOS fabrication service and initial testing has demonstrated digital logic voltage transitions for optical powers as low as 10 nWatts. The near term plans include determination of the minimum threshold power detectable by the photoreceivers, evaluation of performance uniformity across the 25-element array and building the optical system required to read an optical storage device based on Er doped GaN. Photo of this CMOS photoreceiver array is shown in Figure 4.15.

4.6 References

[1] J. Orloff, Rev. Sci. Instrum. **64**(5), 1105 (1993).

[2] J. Melngailis, J. Vac. Tech. B **5**(2), 469 (1987).

[3] T. B. Massalski (ed), **Binary Alloy Phase Diagrams** (ASM International), 1990.

[4] L. C. Chao and A. J. Steckl, J. Vac. Sci. Technol. B **17** (3), 1056 (1999).

Chapter 5
Experimental Results

The success of the incorporation of the rare earth (RE) element erbium (Er) into gallium nitride (GaN) by ion implantation[1,2,3] and during growth by hydride vapor phase epitaxy (HVPE),[4] metalorganic molecular beam epitaxy (MOMBE),[5] has made possible to design an optical storage device based on RE doped GaN semiconductor. In addition, room temperature visible emission from Er in GaN by photoluminescence (PL),[6,7] electroluminescence (EL),[8,9] and cathodoluminescence (CL)[10] have been achieved by solid source MBE in-situ doping or by ion implantation. Visible, room temperature emission by PL, EL, and/or CL of various other rare earth elements (Pr, Tm, Eu, and Dy) in GaN has also been observed.[11,12,13] This reveals that GaN is an excellent host for the incorporation of rare earth elements to produce visible light emission.

5.1 Er doped GaN based on Implantation Technology

Thermal annealing is necessary to activate the upconversion process after FIB implantation. Green upconversion emission, pumped by either single lasers or by two collinear laser beams, was observed. Emission spectra of implanted GaN films grown by MBE, HVPE, and MOCVD under same thermal annealing condition are identical.

Figure 5.1 shows the allowed energy levels of Er^{3+} ions and four possible upconversion processes, namely Ia, Ib, IIa, IIb. Er^{3+} ions can be excited by: (I) two photons of same energy; (II) two photons of different energy. Upconversion processes of Ia and Ib require only single laser source, whereas upconversion processes of IIa and IIb utilize two laser sources. In all four upconversion processes, the resulting emission at 522 nm is attributed to radiative transition from the $^2H_{11/2}$ excited state to the $^4I_{15/2}$ ground state, while 546 nm emission is due to the transition from $^4S_{3/2}$ to the ground state.

Type I upconversion consists of simple two-photon processes, which involve a single laser source. The upconversion process Ia, which uses 840 nm laser pumping, begins

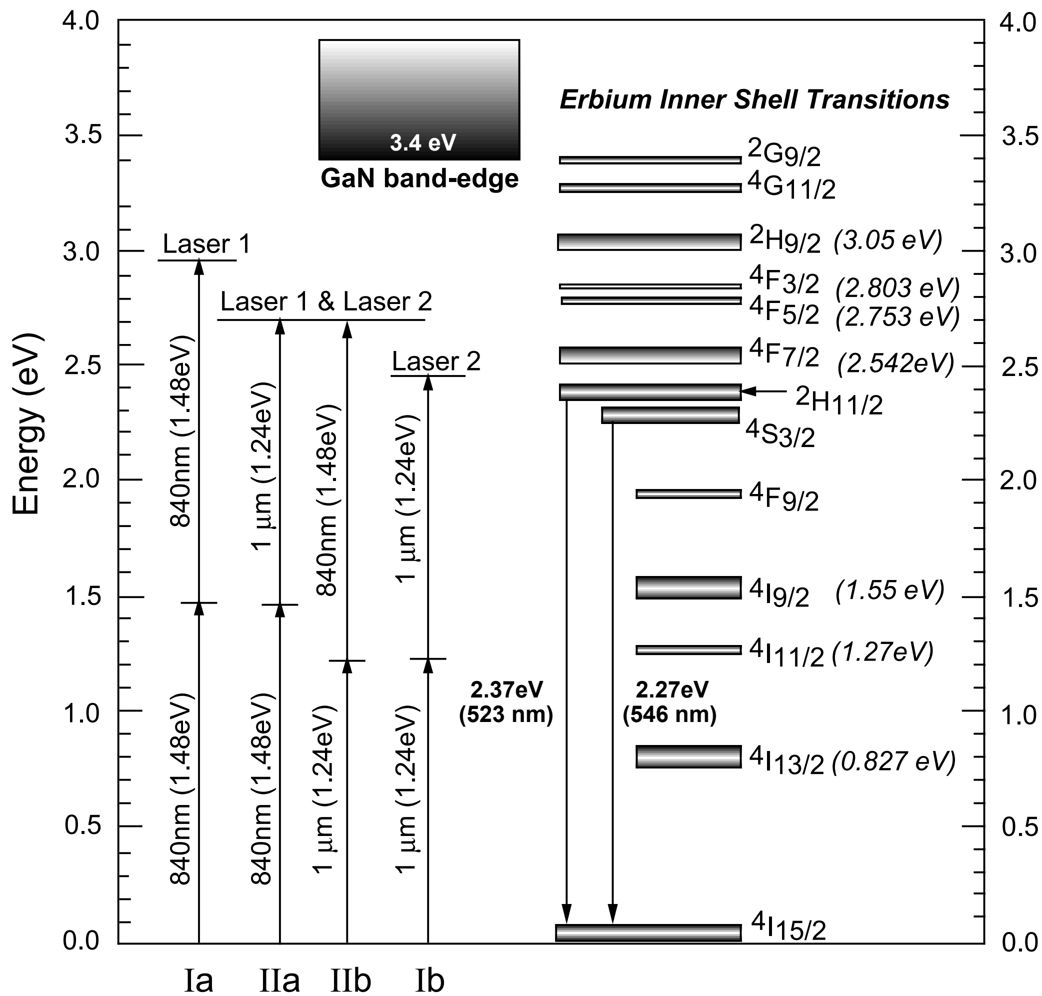

Figure 5.1: Er energy levels and upconversion processes for FIB implanted GaN.

with Er^{3+} ions being excited from the ground state to the intermediate $^4I_{9/2}$ state, and then to virtual states above the upper $^2H_{11/2}$ and $^4S_{3/2}$ states. In upconversion process Ib, Er^{3+} ions are excited by 1000 nm photons to the $^4I_{11/2}$ intermediate excited state, and then to upper excited states. Type II upconversion consists of the two-step, two-frequency (TSTF) upconversion process, wherein two lasers at different wavelengths are employed. In process IIa, Er^{3+} ions are excited by 840 nm photons from the ground state to the intermediate $^4I_{9/2}$ state, followed by excitation to upper states by 1000 nm photons. In process IIb the upconversion occurs in reverse sequence. Er^{3+} ions are excited from the ground state to the intermediate $^4I_{11/2}$ state by 1000 nm photons, followed by excitation to upper states by 840 nm photons. In all four processes, Er^{3+} ions, which are excited to upper states, eventually relax to $^2H_{11/2}$ and $^4S_{3/2}$ states with nonradiative transitions. From

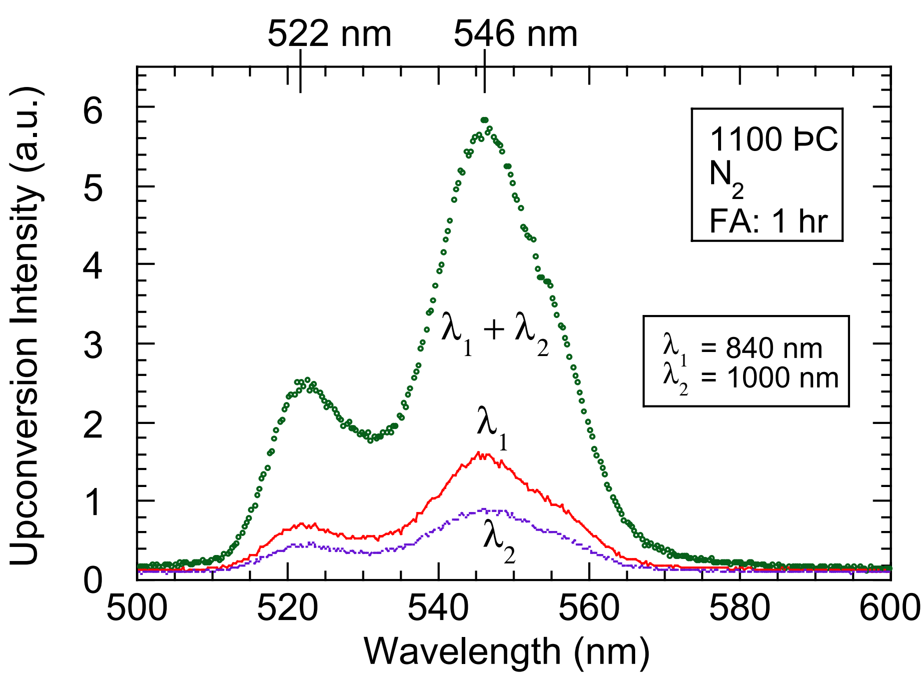

Figure 5.2: Upconversion spectra under single and double laser pumping from FIB implanted GaN:Er with 1 hour furnace annealing (FA) at 1100 °C in N_2.

these metastable states, excited ions gradually decay radiatively to the ground state with emission of green light.

Figure 5.2 contains typical upconversion spectra under single and double laser pumping from FIB Er-implanted GaN films grown on sapphire and annealed for 1 hour at ~ 1100 °C. Patterns were implanted on GaN films using 200 keV Er^{2+} beam with a target current of 100 pA. The pixel exposure time was 0.46 ms and the pixel size was 0.1 x 0.1 μm^2. This results in a dose of 1.4 x 10^{15} atoms/cm^2. Simulation of this condition using TRIM 95 calculates a projected range of ~38 nm and a peak concentration of ~3.7 x 10^{20} atoms/cm^3. All three spectra show peaks at 522 and 546 nm. The lowest intensity spectrum is obtained by pumping at 1000 nm. Using the 840 nm laser increases the upconversion by a factor of 2. A 5X increase in upconversion intensity is generated

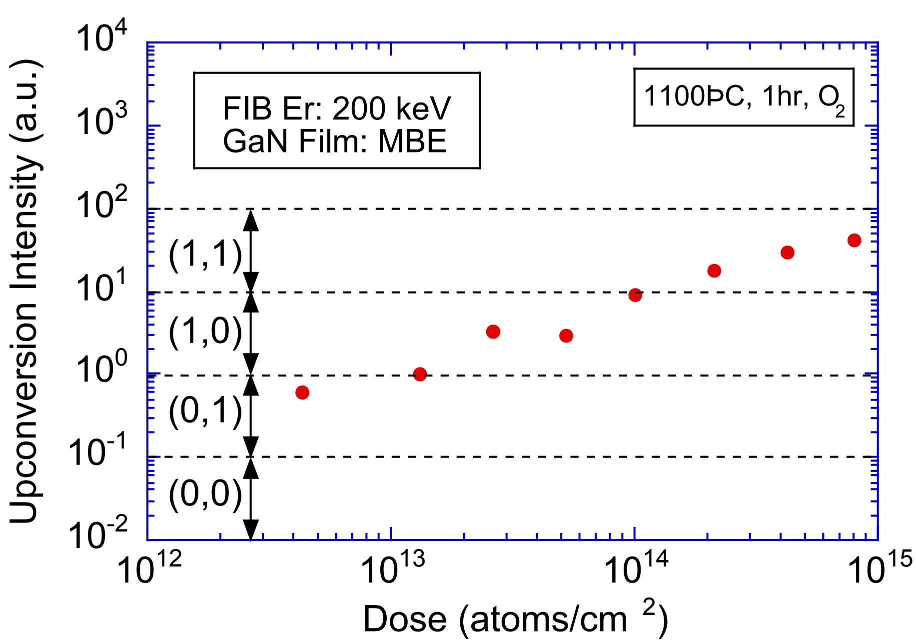

Figure 5.3: Multiple level storage capacity as a function of FIB Er dose into GaN.

when both lasers are used.

Figure 5.3 shows the upconversion intensity of FIB implanted GaN films at 546 nm as a function of the Er implanted dose from 4.3 x 10^{12} to 2.4 x $10^{16}/cm^2$. After FIB implantation, samples were annealed at 1100°C for 1 hour in oxygen. The upconversion intensity was measured in the center of the pattern. The upconversion intensity at 546 nm becomes discernable for a dose of ~ 4 x 10^{12} atoms/cm^2 and increases up to a dose of ~ 10^{15} atoms/cm^2. Further increase in Er dose results[30] in a decrease of the upconversion

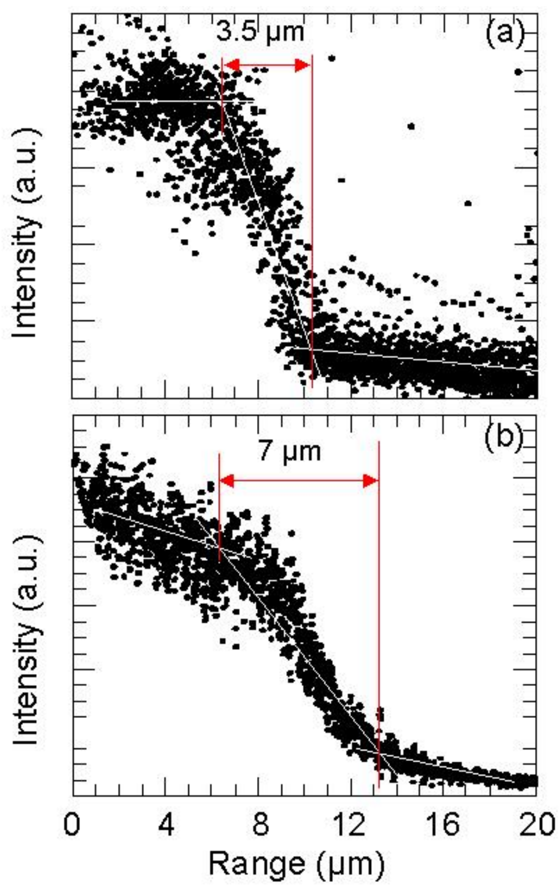

Figure 5.4: Upconversion intensity across the edge of FIB implanted GaN:Er samples. FIB dose: $10^{15}/cm^2$. Furnace annealing at 1100 ˚C for duration of: (a) 100 seconds; (b) 1 hour.

intensity. As suggested in Figure 5.3, upconversion intensity dependence on implanted Er dose can be used as a means to obtain "gray" scale levels to increase storage capacity. In this case, four levels of intensity gray scale have been demonstrated with one order of magnitude difference between each level.

Upconversion intensity increases with annealing time for FIB implanted GaN films. Although high upconversion intensity is a desired feature, there is an unintended issue. During annealing, thermal kinetic energy not only repairs the implantation damage, but also provides Er^{3+} ions with enough energy to diffuse away from the implanted area. Figure 5.4 shows this edge diffusion effect by measuring the upconversion intensity across the edge of regions implanted with a $10^{15}/cm^2$ Er dose. The two Er implanted GaN samples were furnace annealed at 1100 °C for 100 seconds and 1 hour, respectively. The presence of non-zero photon counts in the unimplanted region is primarily due to stray light and noise picked up by the detection system. The transition region between the implanted and unimplanted areas is a function of annealing time, increasing from 3.5 μm for the 100 second anneal to 7 μm after the 1 hour anneal. One must keep in mind that the laser beam diameter of ~ 2 μm determines the minimum transition region width measurable. Therefore, the diffusion length for the 100 seconds annealing time is probably smaller than 3 μm.

The first optical memory was fabricated with a 3 x 3 array of FIB Er-implanted regions. Each "bit" has a nominal area of 2 x 3 μm^2 with a center-to-center spacing of 10 μm. Er implantation conditions were 200 keV energy and dose of 1×10^{15} atoms/cm^2. The GaN sample was RTA annealed at 1100°C for 60 seconds in N_2. Figure 5.5a hows the optical reflection image of the array. An upconversion image produced with a single pump laser at 1000 nm is shown in Figure 5.5b. LabVIEW™ programming software was used to automate both spectrometer and NanoBlock translation stage operation for obtaining

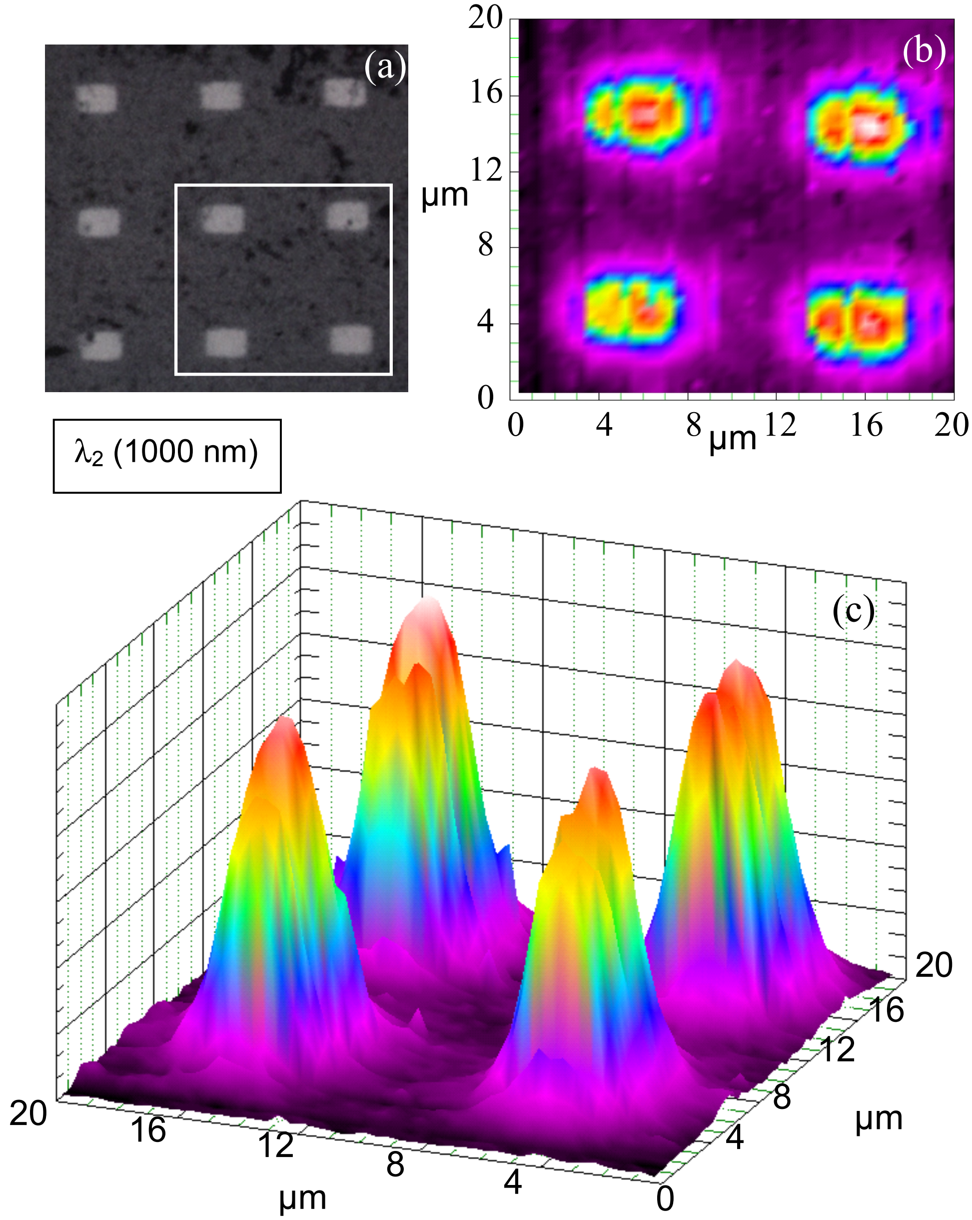

Figure 5.5: Optical memory stored information in FIB-implanted Er pattern: (a) reflected light image of 3 x 3 array – optical microscopy; (b) upconversion scanned image of 2 x 2 array – pumped with 1000 nm laser; (c) scanned intensity profile of 2 x 2 array – pumped with 1000 nm laser. Nominal bit area 2 x 3 μm^2, center to center spacing of 10 µm.

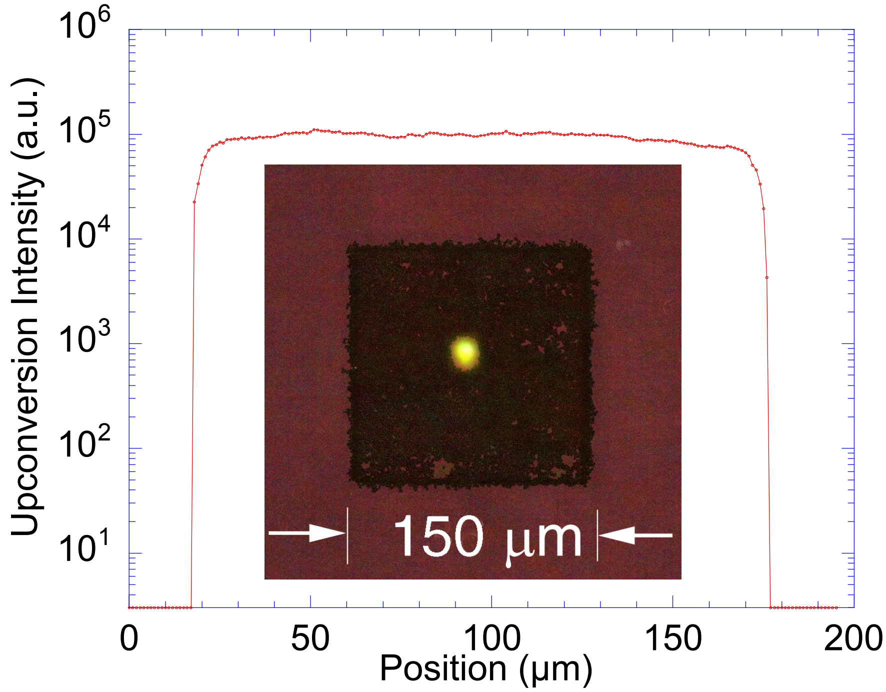

Figure 5.6: Upconversion signal from linear scan across FIB implanted GaN:Er region, pumped by both 840 and 1000 nm lasers.

The spatial scanning profile of the bit area was measured to be slightly larger than the nominal implanted 2 x 3 μm^2. This is not unexpected, taking into consideration the fact that the pump laser beam has a diameter larger than the implanted bit and that diffusion of the implanted Er occurs during annealing.

Single upconversion scanning profiles across square and rectangular implanted patterns are shown in Figure 5.6 and Figure 5.7. These patterns were implanted with Er at 1 x 10^{15} atoms/cm^2 and furnace annealed at 1100 °C for 1 hour. Collinear illumination was used for measuring the spatial scanning profiles. Figure 5.6 shows the line scan across a 150 x 150 μm^2 square pattern under dual laser pumping. The difference in intensity

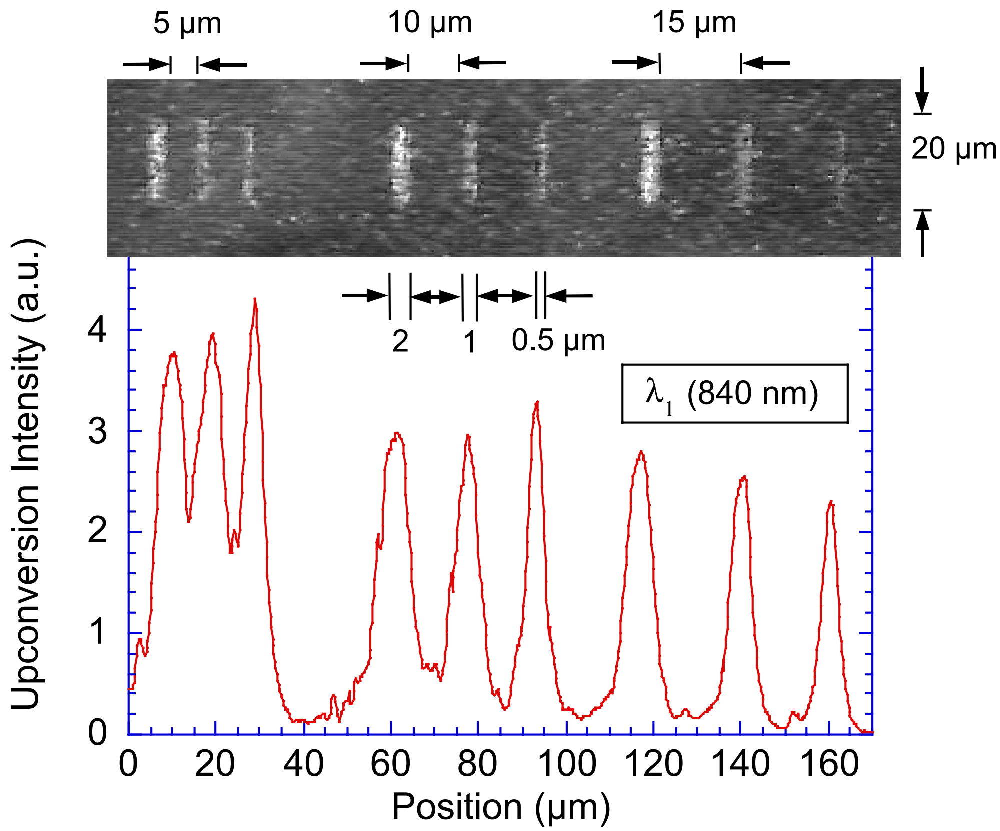

Figure 5.7: Upconversion signal from FIB Er-implanted rectangular pattern, pumped with 840 nm laser. Each set contains rectangles with nominal values of 2, 1, and 0.5 μm width at spacings of 5, 10, and 15 μm.

between the implanted and unimplanted area is about three order of magnitudes higher than the intensity fluctuation at implanted area. The width of the region over which diffusion has occurred at the edge of the pattern was measured to be ~10 μm.

To investigate the possibility of fabricating memory arrays with higher bit density, rectangular patterns with varying dimensions were implanted and evaluated. Figure 5.7 shows a cross section and spatial scanning profile for 3 sets of 3 line patterns. Each set of the line patterns consist of lines with dimension of 2 x 20 μm^2 on the left, 1 x 20 μm^2 on the middle, and 0.5 x 20 μm^2 on the right. The spacing between the lines in the line patterns is 5 μm wide for the left hand set, 10 μm wide for the middle set, and 15 μm wide for the right hand set. As expected, the broadening caused by 2 μm laser beams scan and diffusion effect due to thermal annealing have made the measured line width slightly larger than the implanted size.

5.2 Er doped GaN based on Milling Technology

Two common types of bit patterns, positive bits and negative bits, were fabricated with FIB milling technique. Positive bits are patterns where regions that do emit upconversion emission are defined as logic '1', while regions that don not emit upconversion emission are defined as logic '0' upon IR laser stimulation. To create a positive bits, GaN:Er film was selectively milled. Area where Er in-situ doped GaN layer is completely removed could not emit upconversion emission, whereas the remaining area that is not milled could emit upconversion luminescence. GaN:Er films were grown on Si substrate by MBE system. Typical film thickness ranges from 1 μm to 1.5 μm thick. To increase contrast between luminescent and non-luminescent regions, GaN:Er film at area that is designated for logic '0' was completely removed from Si substrate. Bit pattern fabrication was milled by FEI FIB 200 TEM system. This system is also capable of taking real time pictures during FIB milling process.

Figure 5-8 shows the real time picture of positive bit array, taken after the completion of FIB milling process. The logic-'1' bit is represented by boxy dots inside a big square pattern. These dots were fabricated by removing GaN:Er film between the bits. Each logic-‘1’ bit is located from its neighboring bits at distance that is equal to its size. Typical bit array pattern was fabricated with formation of six-by-six dots of logic-‘1’ bits.

Arrays of logic-‘1’ dots with dot size ranging from 4 x 4 μm^2 to 0.4 x 0.4 μm^2 were successfully fabricated with FIB milling technique. Condition for ion milling was set to be identical accepts for ion beam current. Adjustment of ion beam current is necessary for trade off between total milling time and bit size resolution. Large beam current is required for short total milling time, whereas small current beam is preferred for sub-micron feature. A series of positive bit patterns were milled by FIB system under same conditions. Ion beam energy was set at 30 keV and beam current at 5000 pA with 0.2 μs dwell time. The overlapping of beam spot is fixed at 50%. Figure 5.9 shows pictures of six by six logic-‘1’ bits with bit sizes ranging from 3 x 3 μm^2 to 1 x 1 μm^2. Bit patterns with bit sizes from 3 x 3 μm^2 to 0.4 x 0.4 μm^2 could retain decent box shape after milling at 5000 pA ion beam current. However, distortion becomes an issue when attempt to mill

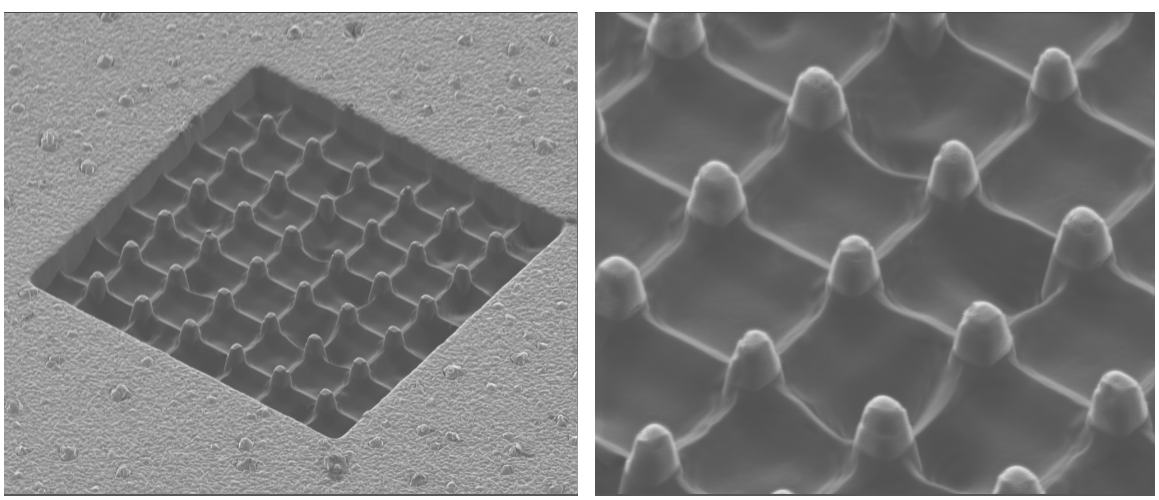

Figure 5.8: Typical positive bit pattern fabricated on GaN:Er film by FIB milling process. GaN layer was completely removed to form dots with box shape, which are defined as logic 1.

pattern with bit size smaller than 1 x 1 μm^2, as illustrated by 0.8 x 0.8 to 0.4 x 0.4 μm^2 logic-'1' bits. It is not feasible to fabricate sub-micron bits at 5000 pA beam current. Instead of fabricating logic-'1' bit with box shape, bits with pyramid and even cone shape were unintentionally produced. At the extreme, the result of fabrication of 0.4 x 0.4 μm^2 bits at 5000 pA was the remnant of Si substrate surface.

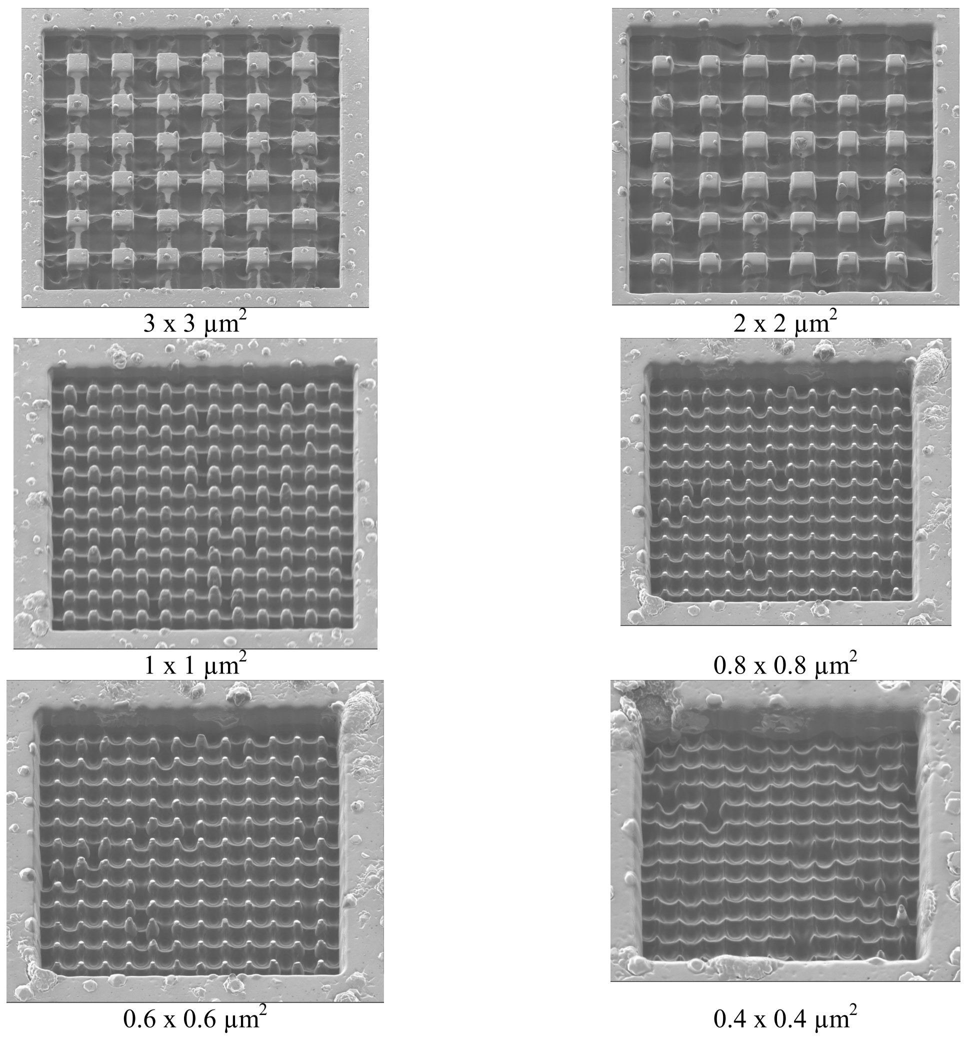

Figure 5.9: Positive bit patterns of GaN:Er film without ITO cap layer fabricated by FIB milling process. Patterns were milled at 30 keV ion beam energy, 0.2 μs dwell time, 50% overlapping beam spot, and 5000 pA beam current.

Smaller ion current is necessary to fabricate sub-micron bits. Figure 5.10 shows three pictures of positive bit array patterns at 1 x 1 μm^2 bit size. All patterns were fabricated under same fabrication condition except for beam current. Patterns were milled at 500 pA, 1000 pA, and 5000 pA respectively. These patterns were designed to have logic-‘1’ dots with box shape. At 500 pA beam current, resulted pattern retains dots with well-defined box shape. At beam current of 1000 pA, slight distortion is present at some bits, where bits with pyramid instead of box shape were fabricated. At 5000 pA beam current, acute distortion has led to bits fabricated with cone shape.

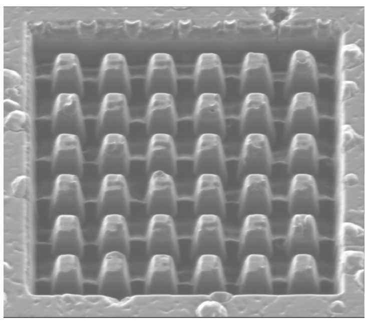

1.0 X 1.0 μm^2 at 500 pA

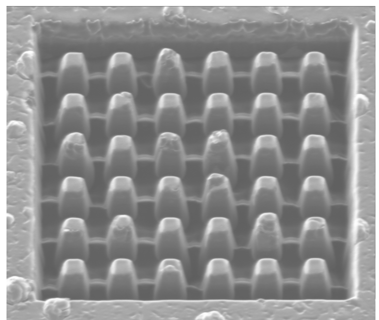

1.0 X 1.0 μm^2 at 1000 pA

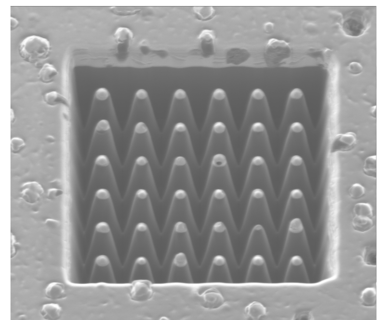

1.0 X 1.0 μm^2 at 5000 pA

Figure 5.10: Comparison of three identical patterns fabricated at different beam current. Smallest beam current maintains precision during milling process.

To enhance fabrication process, thin layer of indium tin oxide (ITO) was deposited on GaN:Er film prior to milling process. This enhancement allows ITO layer acting as protection layer to support sub-micron feature fabrication and as heatsink to prevent thermal damage caused by laser readout beam. Figure 5.11 shows the comparison of two patterns with 0.4 x 0.4 μm^2 bit size. Pattern on the left picture was fabricated on GaN:Er film with ITO cap and pattern on the right picture on the film without ITO layer. ITO cap with layer thickness from 0.1 to 0.2 mm was sputtered on GaN:Er film by sputtering machine prior to FIB milling of 0.4 x 0.4 μm^2 bit pattern array. Well defined box-shape bit structure in the square was successfully fabricated on GaN:Er film with ITO cap, whereas there is no recognizable structure remains in the square that was produced on the film without the ITO protection layer. ITO cap layer has helped minimize ion damage during FIB milling process. The extra shielding of ITO permits sub-micron feature to be fabricated.

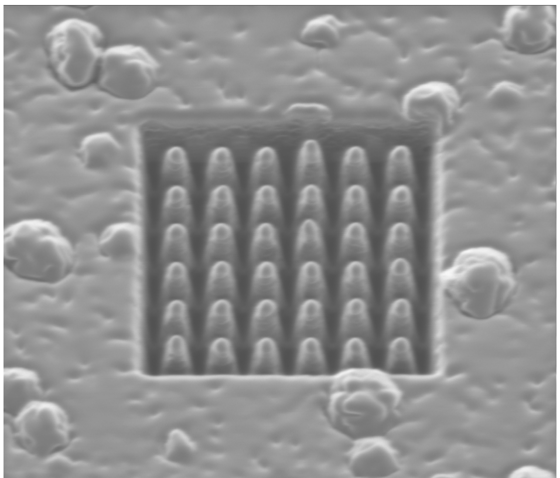

0.4 x 0.4 μm^2 with ITO cap at 100 pA

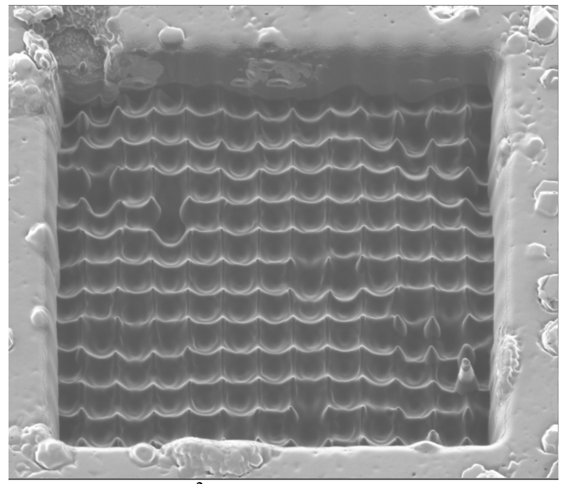

0.4 X 0.4 μm^2 without ITO cap at 5000 pA

Figure 5.11: ITO cap layer improves precision of ion milling process for sub-micron bit pattern on GaN:Er film.

Sub-micron bit size pattern was easily damaged by high intensity beam power of IR laser excitation source. Thermal heat generated by laser read beam could not effectively dissipate for bit with dimension smaller than 1 μm^2. Heat was trapped in GaN:Er film by high intensity laser pumping. The localized thermal heat could reach GaN melting point temperature and subsequently melt the logic-'1' bits. The result was bits were damaged during data readout cycle. After depositing thin layer of ITO cap on GaN:Er film, no thermal damaged has occurred during data retrieval process. ITO film has contributed to more efficient heat dissipation solution. Figure 5.12 shows the post laser readout picture of two bit pattern arrays with 0.8 x 0.8 μm^2 bit size. Pattern on the right was deposited wit ITO cap and pattern on the left was without. After several minutes of laser pumping by 1000 nm laser at 350 mW power, bits on the film without ITO cap layer were found to be seriously damaged by high intensity laser beam.

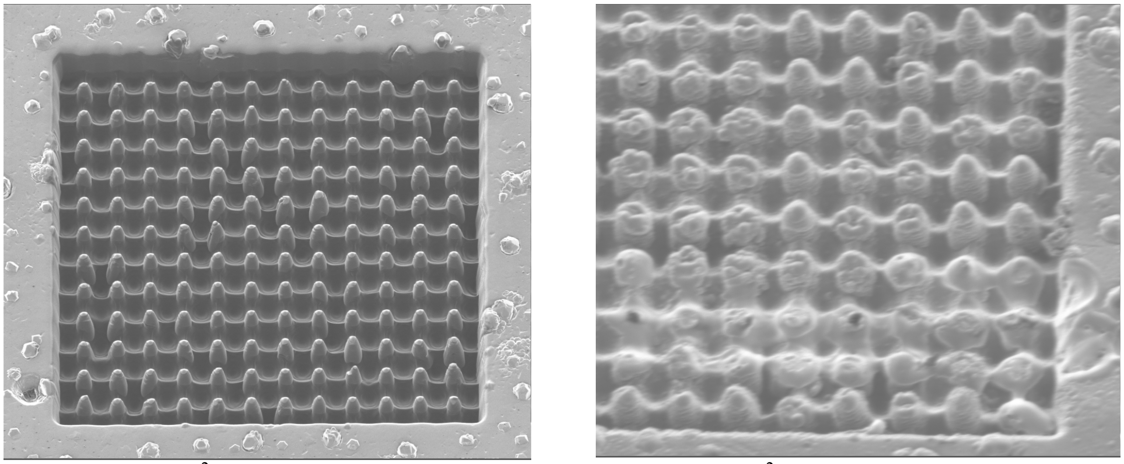

0.8 x 0.8 μm^2 with ITO no damage   0.8 x 0.8 μm^2 without ITO laser damage

Figure 5.12: Laser induced heat damage can be minimized or even prevented with thin layer of ITO cap. Heat dissipation is improved with ITO cap layer.

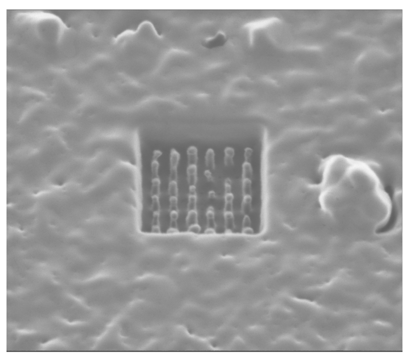

Figure 5.13: Film surface roughness is critical for fabricating small bit structure. In order to let bits be easily distinguished from surface morphology and avoid from unintentionally removed.

GaN:Er film with good surface morphology on GaN surface is critical for sub-micron fabrication. Figure 5.13 depicts that as the bit pattern is being made smaller, bits are indistinguishable from rough surface morphology of the film. Furthermore, fabricating bits on rough film surface could cause “missing bits” as shown in Figure 5.13. Therefore, fabricating pattern with bit size smaller than 0.4 x 0.4 μm^2 requires high quality GaN:Er film with relative even surface roughness.

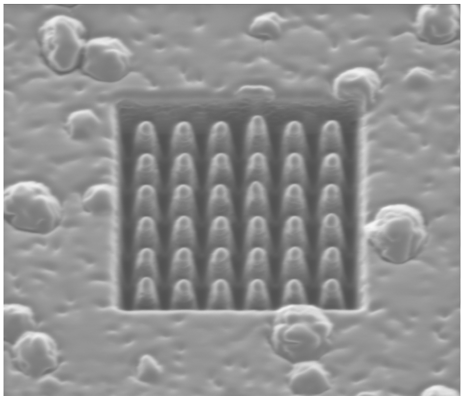

0.4 x 0.4 μm^2 at 100 pA

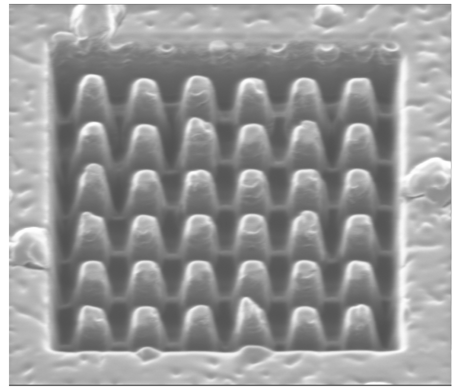

0.6 x 0.6 μm^2 at 300 pA

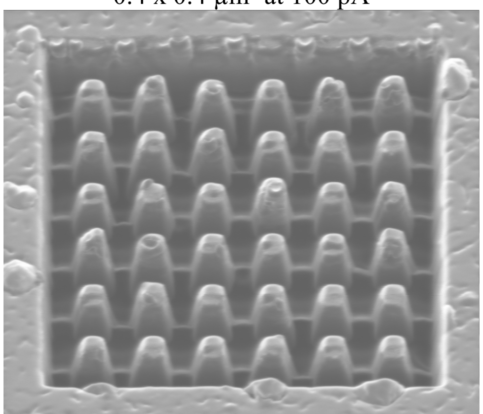

0.8 x 0.8 μm^2 at 500 pA

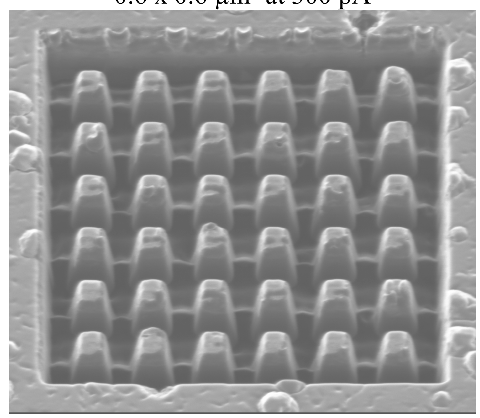

1.0 x 1.0 μm^2 at 500 pA

Figure 5.14: Positive bit patterns of GaN:Er film with ITO cap layer fabricated by FIB milling process under optimum condition. Patterns were milled at 30 keV ion beam energy, 0.2 μs dwell time, 50% overlapping beam spot with varying beam current.

Figure 5-14 shows a series of array bit pattern fabricated with GaN:Er film with ITO cap layer at optimized condition. Although bit patterns of all sizes could be fabricated with smallest beam current, higher beam current is sometime desired for faster milling time. Therefore balance between total milling time and beam current is optimized for each bit pattern size. As shown from the picture, well define 0.4 x 0.4 μm^2 bit pattern could be fabricated with beam current of 100 pA. To fabricate a 0.6 x 0.6 μm^2 bit pattern, higher beam current up to 300 pA can be applied. While bit pattern with size of 0.8 x 0.8 to 1 x 1 μm^2 and up could be satisfactorily milled with beam current up to 500 pA.

Negative bits are patterns with regions defined as logic '1' do not emit upconversion emission and regions defined as logic '0' do emit upconversion emission. It is defined just the opposite way to positive bits. Fabricating negative bit patterns with FIB milling is simpler than that of positive bit patterns. Negative bits is fabricated with circular holes drilled into GaN:Er film with FIB. These holes are designated as logic-'1' bits. Array of holes in negative bit pattern is arranged in similar formation of positive bit pattern. Figure 5.15 shows a series of negative bit patterns with hole-diameter ranging from 0.4 µm to 4 µm, which had been fabricated at optimized beam current. Each logic-'1' bits is spaced from its neighboring bits at a distance equal to its diameter. These negative bit patterns were fabricated with GaN:Er film with ITO cap layer. Patterns were micro-milled through 30 keV Ga^+ FIB at normal incidence. Beam dwell time was set at 0.2 µs, while the beam spot overlap was held constant at 50%. Beam current was changed from 300 pA to 5 µA. Constrains faced by negative bit milling process are the same as that of positive bit. Short total milling time is achieved with high beam current and sub-micron feature fabrication can only be accomplished with small beam current. Thin ITO cap layer deposited on GaN:Er film has certainly improved sub-micron fabrication process. Patterns with hole-diameter that is equal and larger than 1.4 µm could be fabricated with beam current up to 5 µA. For negative bits with smaller hole-diameters, 1 µA is a maximum current for bits with 1.0 to 1.2 µm in hole-diameter, 500 pA for 0.8 µm, 300 pA for 0.6 µm, and 30 pA for 0.4 µm.

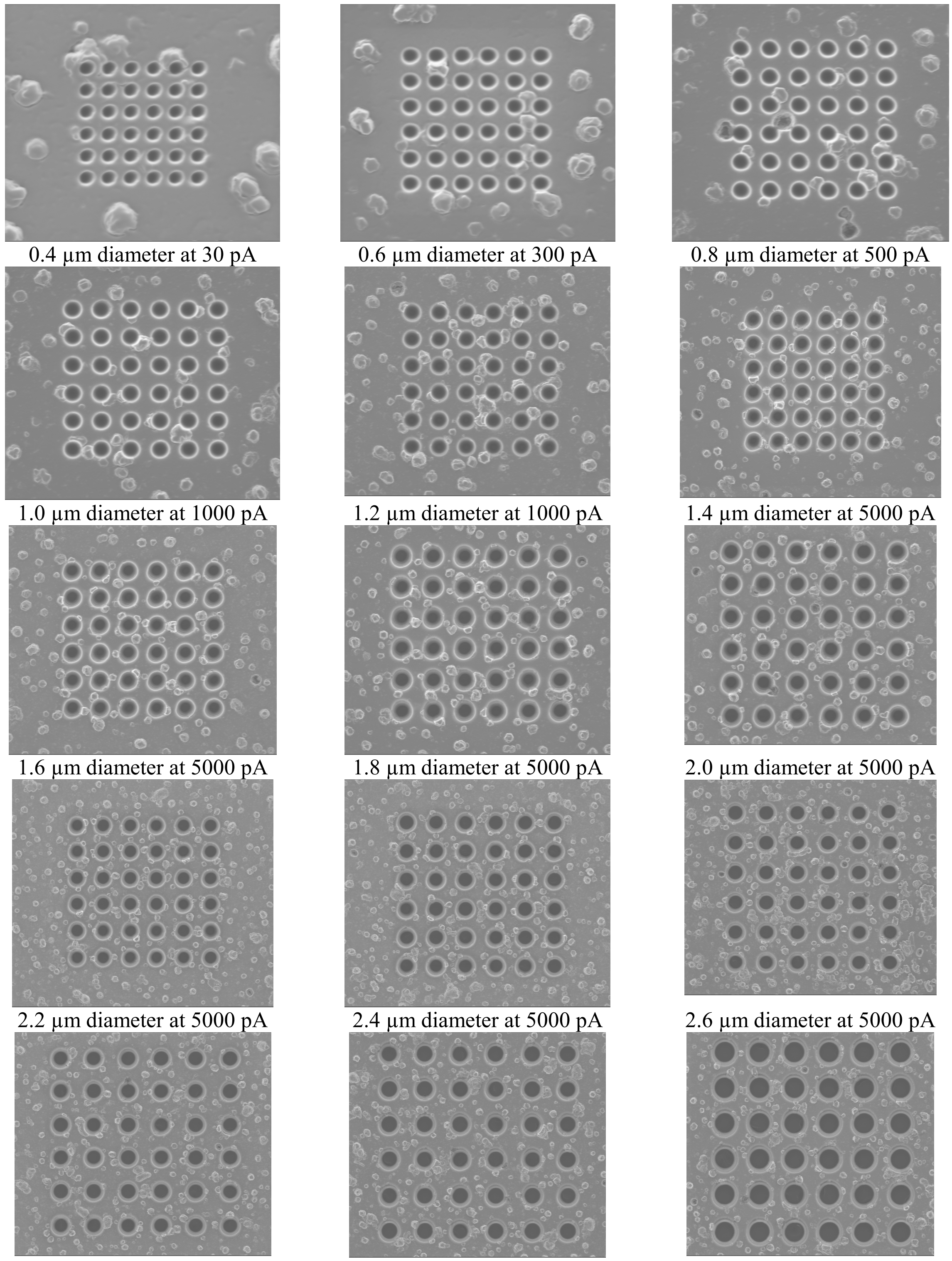

0.4 μm diameter at 30 pA
0.6 μm diameter at 300 pA
0.8 μm diameter at 500 pA
1.0 μm diameter at 1000 pA
1.2 μm diameter at 1000 pA
1.4 μm diameter at 5000 pA
1.6 μm diameter at 5000 pA
1.8 μm diameter at 5000 pA
2.0 μm diameter at 5000 pA
2.2 μm diameter at 5000 pA
2.4 μm diameter at 5000 pA
2.6 μm diameter at 5000 pA
2.8 μm diameter at 5000 pA
3.0 μm diameter at 5000 pA
4.0 μm diameter at 5000 pA

Figure 5.15: Negative bit patterns of GaN:Er film with ITO cap layer fabricated by FIB milling process under optimum condition. Holes were drilled at 30 keV ion beam energy, 0.2 μs dwell time, 50% overlapping beam spot with varying beam current.

Low beam current is required to fabricate bits with small circular diameter. Figure 5.16 illustrates the contrast of applying different beam current with sub-micron pattern fabrication. Two arrays of negative bit pattern with 0.4 μm in hole-diameter were fabricated. Pattern on the left was milled at 30 pA and pattern on the right was milled at 100 pA beam current. The resulted negative bit pattern milled at smaller beam current of 30 pA has well defined circular-hole formation than that at 100 pA. Pattern fabricated at 100 pA produces distorted elliptical-shape holes instead.

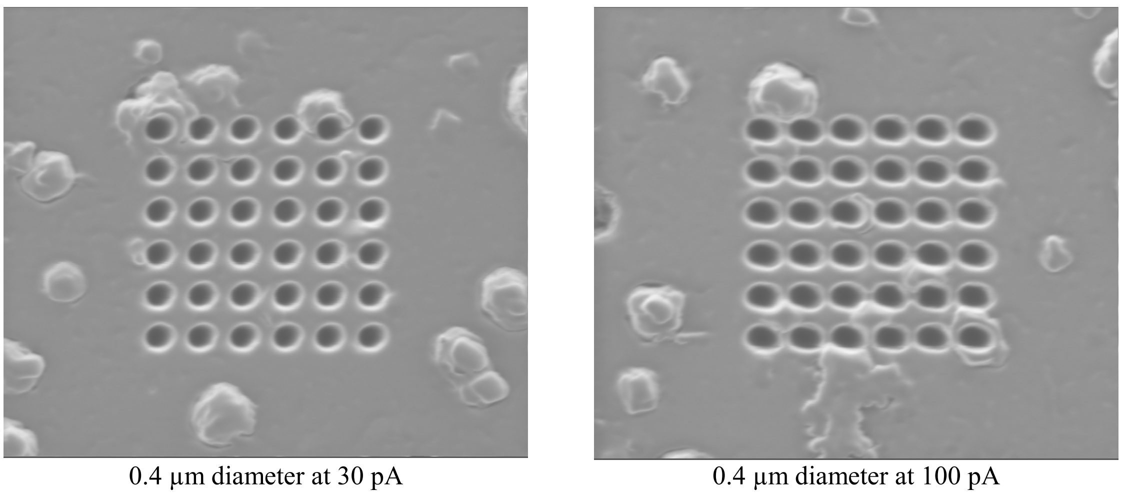

Figure 5.16: Negative bits with circular-hole shape can be distorted to elliptical-hole shape when high a beam current is applied during ion milling process.

Negative bit patterns are easier to make than positive bit patterns. They apparently do not suffer from the same thermal damage by high power IR lasers during data retrieval process. However, upconversion emission from positive bit patterns produces better contrast than that of negative bit patterns. Detection of sub-micron positive bit patterns is relatively easier than that of negative bit patterns.

Optical data retrieving process relies on the detection of upconversion emission from either positive or negative bit patterns. The 1000 nm IR laser was used for stepwise upconversion excitation source. Optical setup for spectral detection as well as the energy transitions involved in the upconversion process is the same as those with the ion implantation approach.[14,15] However, the resulted green upconversion emission has slightly shifted peaks. While upconversion emission at 523 nm and 546 nm wavelength were measured from FIB implanted GaN:Er film, upconversion emission at 537 nm and 558 nm wavelength were measured from MBE in-situ doped GaN:Er film, upon

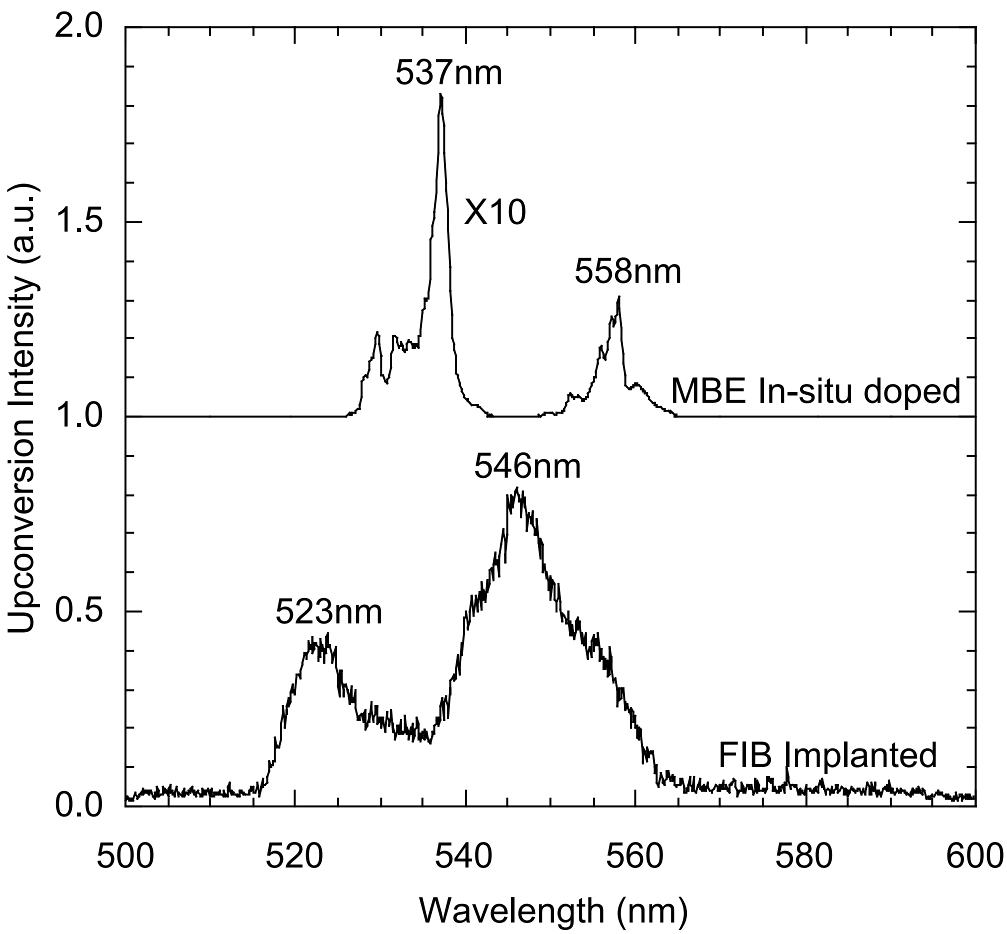

Figure 5.17: High resolution scans of the green upconversion luminescence of an in-situ Er-doped GaN film and an Er FIB implanted GaN film. The FIB implanted film was annealed at 1100 °C for 1 hr in oxygen after implantation. (spectral resolution = 0.4 nm)

excitation of 1000 nm IR laser. The 537 nm emission is related to radiative transition from $^2H_{11/2}$ excited state to $^4I_{15/2}$ ground state, while 558 nm emission is due to transition from $^4S_{3/2}$ to $^4I_{15/2}$ state. The upconversion intensity emitted from the in-situ doped GaN:Er film is approximately ten times stronger than that from the implanted film. Full width at half maximum (FWHM) of in-situ doped film has much narrower bandwidth than that of implanted GaN:Er film. FWHM of MBE doped film is measured to be 2 nm at 537 nm, while FWHM of FIB implanted GaN:Er film is 12 nm at 546 nm. One possible explanation is that disorder induced by FIB implantation has caused the Er ions to have varying local environment.[16] High resolution scan of green upconversion spectral from both MBE in-situ doped and FIB implanted GaN:Er films are shown in Figure 5.17.

Figure 5.18 contains typical upconversion spectra under single and double laser pumping from Er in-situ doped GaN film by MBE. All three spectra show peaks at 535 and 556 nm. The highest intensity spectrum is obtained by pumping at 1000 nm. Upconversion could not be pumped efficiently with 840 nm laser and the emitted intensity is at least 10X weaker than that with 1000 nm laser. Slight increase in upconversion intensity at 535 nm but decrease in intensity at 556 nm is generated when both lasers are used.

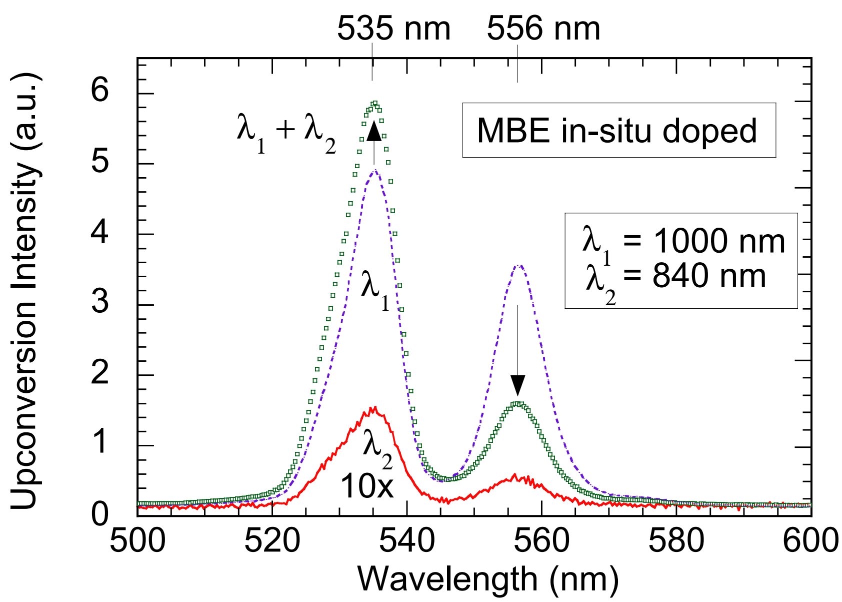

Figure 5.18: Upconversion spectra under single and double laser pumping from MBE grown GaN:Er on sapphire or Si substrate.

Figure 5.19 shows the upconversion emission intensity as a function of cell temperature and corresponding Er concentration in the GaN film. GaN:Er films were excited with 1 µm IR laser at 350 mW. The upconversion intensity increases rapidly with Er concentration up to a level of 0.2–0.3%. The GaN:Er film grown with Er cell temperature at 840 °C had the highest upconversion emission intensity. Further increases in Er concentration lead to the quenching of the upconversion emission. This is very

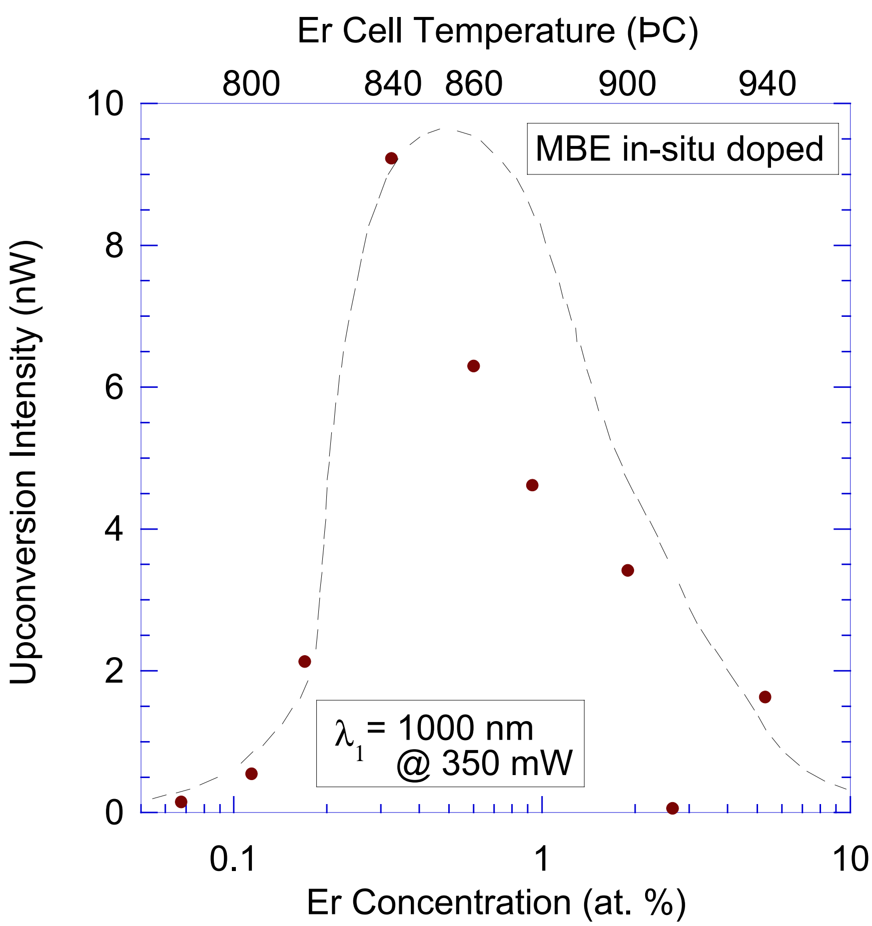

Figure 5.19: Upconversion emission intensity of Er doped GaN as a function of Er cell temperature and corresponding concentration. MBE-grown GaN:Er film on Si was excited by 1 µm laser at 350 mW. Upconversion intensity increases rapidly with Er concentration up to level of 0.2-0.3 atomic %. GaN:Er film grown at 840 °C had the highest upconversion emission intensity.

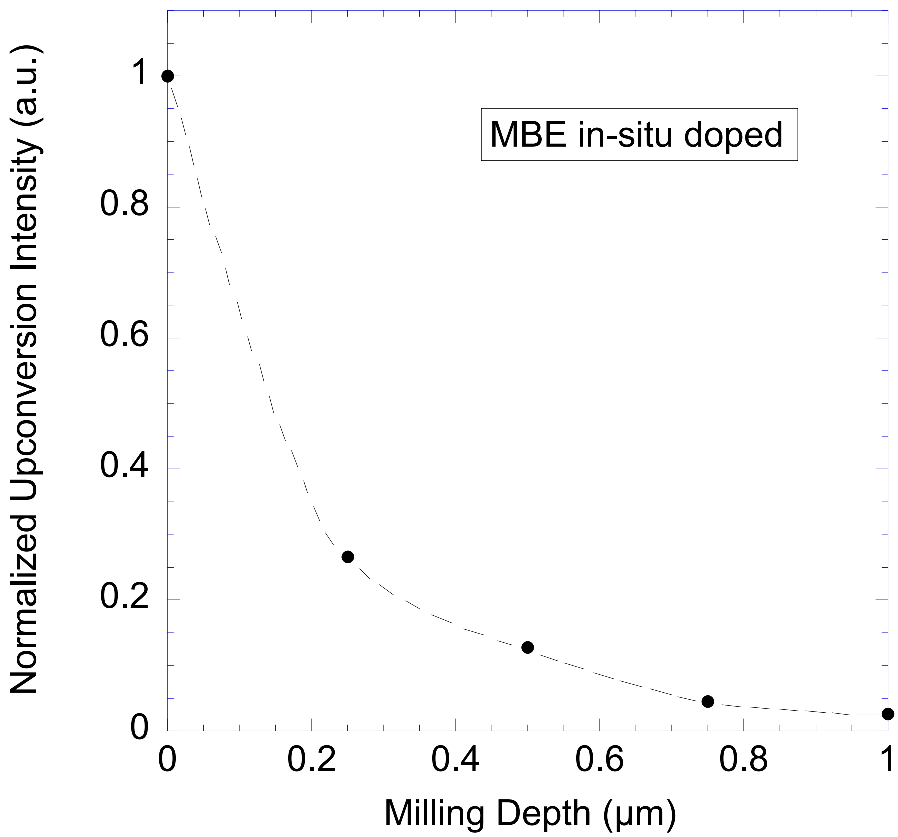

Figure 5.20: Upconversion emission intensity decrease as more GaN:Er on Si film thickness was milled and removed by FIB process. The dimming of emission is thought to be the consequence of damage induced by FIB process and diminishing Er concentration per film.

similar to the maximum in upconversion with concentration (~0.3%) observed[17] in Er-implanted GaN.

Upconversion intensity vary with the milling depth of GaN:Er film. Emission intensity diminish as more layer of GaN:Er film is removed. The intensity diminishing effect could be attributed to two factors. As more layer of film is removed, there is less Er ions available in the dwindling volume of GaN:Er film. Small GaN:Er volume therefore has less Er ion concentration participate for upconversion emission process. Damage to GaN:Er film by FIB milling could occur. Deeper milling depth requires longer total milling time. The extended length of time would inevitably enhance the damage caused by ion bombardment during FIB milling and thus could contribute to the deterioration of upconversion emission intensity. Upconversion intensity as a function of milling depth is plotted in Figure 5.20. The deeper the milling depth, the weaker the upconversion intensity becomes. This relationship could actually be exploited to increase data storage density by encoding data with intensity modulation, where intensity is varied through change of milling depth.

Achieving ultrahigh storage density is a desired goal, which could be satisfied by recording data in small bit size. Nano structure fabrication beyond usual optical diffraction limit can be easily accomplished with FIB milling technique. However, upconverion intensity emitted by each bit gradually diminishes as bit size shrinks. Figure 5.21 shows the inverse relationship between the emission intensity per bit and the bit density of the positive bit pattern. Intensity per bit is derived from the total upconversion intensity excited by a 2 μm diameter laser beam divided by the total number of bits within the coverage of laser beam. Bit density is derived from the total pitch area within a square inch area. A pitch area includes a logic-'1'-bit area and half the space between the bits. As the bit density increases, each bit size decreases and so do the upconversion intensity emitted by each bit.

Figure 5.22 shows the inverse relationship between emission intensity per bit and bit density. Intensity per bit is derived from the total upconversion intensity excited by a 2 μm diameter laser beam divided by the total number of bits within the coverage of laser beam. The highest bit density attained so far is ~150 Mb/cm^2 which is 3X greater than

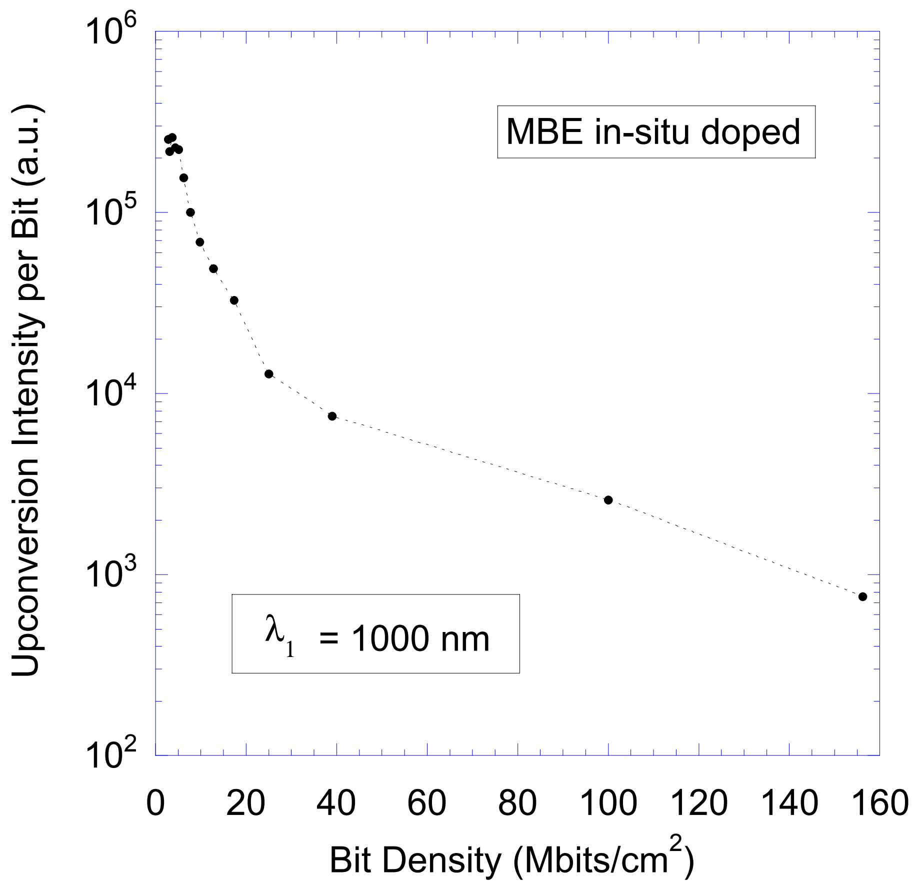

Figure 5.21: Upconversion intensity per bit with respect to bit density. Intensity pre bit is derived from the total upconversion intensity excited by 2 μm in diameter laser divided by total number of bits covered by the laser beam size. Plot shows the inverse relationship between bit density and intensity emitted by each bit.

CD-ROM density but 2X smaller than DVD-ROM. This bit density was obtained with 0.4 µm bit size and 0.8 µm pitch. The extrapolation of 10 Gb/cm^2 bit density requires the FIB milling of bits with 0.1 µm pitch as shown in Figure 5.22. To reach terabyte storage capacity, an 100X improvement on current conditions is needed. To obtain this improvement will require the use of a 980 nm pump laser for more efficient excitation, an

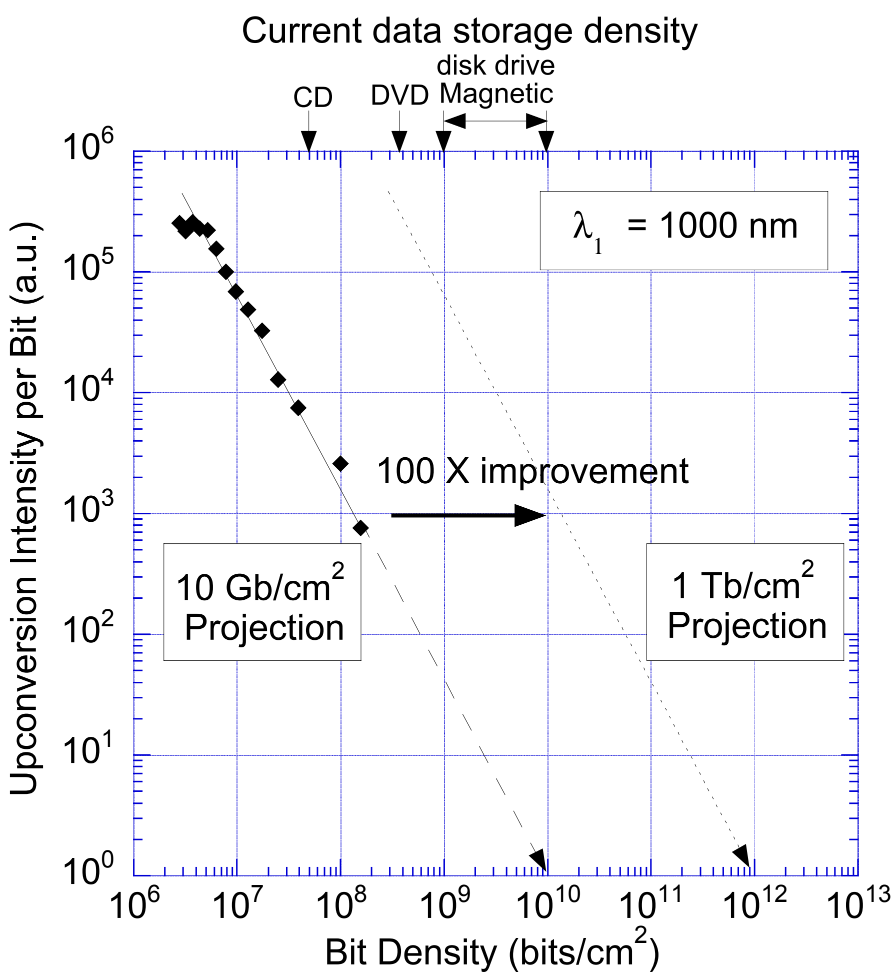

Figure 5.22: Upconversion emission intensity versus current bit density (diamond data points). Maximum bit density of ~10 Gbits/cm^2 is projected with current FIB milling parameters. To achieve terabyte storage capacity, an 100X improvement is required.

increased in the optimum Er concentration, and the utilization of high sensitivity detectors.

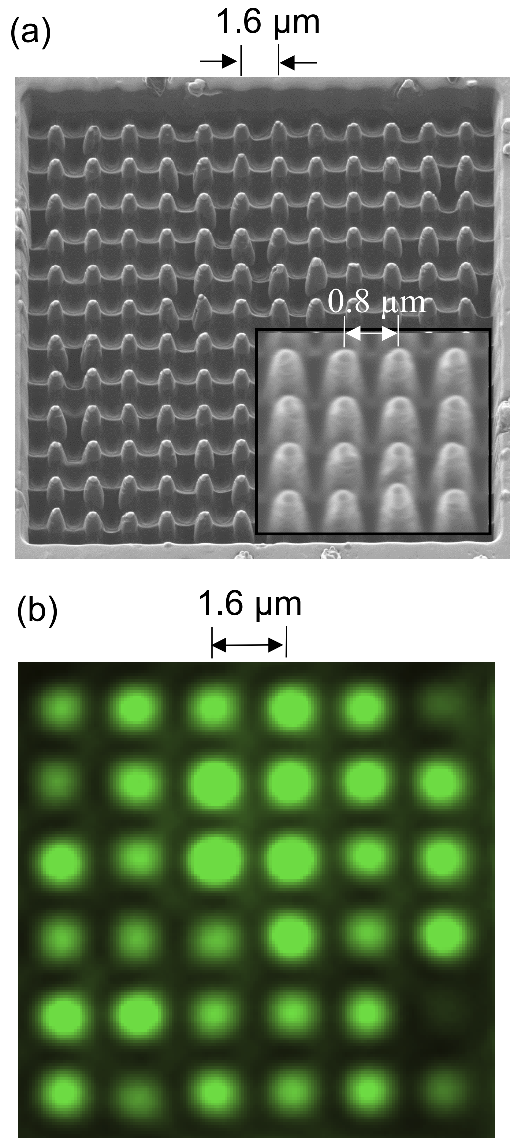

Figure 5.23: (a) Microphotographs of 1.6 μm pitch and 0.8 μm pitch bit patterns.
(b) CCD optical image of upconversion emission from 1.6 μm pitch bit pattern.

The feasibility of parallel readout for positive bit pattern was demonstrated with photo images taken with Spot Color CCD digital camera. Figure 5.23a contains microphotographs of FIB-milled arrays with 0.8 and 1.6 μm pitch. The 0.8 μm bits in the 1.6 μm-pitch pattern were fabricated with an FIB current of 5 nA, while the 0.4 bits array used a 0.5 nA current. The upconversion image of the 1.6 μm-pitch array is shown in Figure 5.23b. The some what nonuniform upconversion intensity of the bits in the array is due primary to the laser Gaussian beam profile. Spatial nonuniformity in the optical properties of the GaN:Er film also play a role. The main reason of this effect is the variation of substrate temperature across the substrate during growth.

5.3 References

[1] R. G. Wilson, R. N. Schwartz, C. R. Abernathy, S. J. Pearton, N. Newman, M. Rubin, T. Fu, and J. M. Zavada, Appl. Phys. Lett. **65**, 992 (1994).

[2] C. H. Qiu, M. W. Leksono, J. I. Pankove, J. T. Torvik, R. J. Feuerstein, and F. Namavar, Appl. Phys. Lett. **66** (5), 562 (1995).

[3] S. Kim, S. J. Rhee, D. A. Turnbull, E. E. Reuter, X. Li, J. J. Coleman, and S. G. Bishop, Appl. Phys. Lett. **71**, 231 (1997).

[4] D. M. Hansen, R. Zhang, N. R. Perkins, S. Safvi, L. Zhang, K. L. Bray, and T. F. Kuech, Appl. Phys. Lett. **72**, 1244 (1998).

[5] J. D. MacKenzie, C. R. Abernathy, S. J. Pearton, U. Hömmerich, J. T. Seo, R. G. Wilson, and J. M. Zavada., Appl. Phys. Lett. **72** , 2710 (1998).

[6] A. J. Steckl and R. Birkhahn, Appl. Phys. Lett. **73**, 1700 (1998).

[7] R. Birkhahn and A. J. Steckl, Appl. Phys. Lett. **73**, 2143 (1998).

[8] A. J. Steckl, M. Garter, R. Birkhahn, and J. Scofield, Appl. Phys. Lett. **73**, 2450 (1998).

[9] M. Garter, J. Scofield, R. Birkhahn and A. J. Steckl, Appl. Phys. Lett. **74**, 182(1999).

[10] H. J. Lozykowski and W. M. Jadwisienczak, Appl. Phys. Lett. **74**, 1129 (1999).

[11] R. Birkhahn, M. Garter and A. J. Steckl, Appl. Phys. Lett. **74**, 2161(1999).

[12] L. C. Chao and A. J. Steckl, Appl. Phys. Lett. **74**, 2364(1999).

[13] J. Heikenfeld, M. Garter, D. S. Lee, R. Birkhahn and A. J. Steckl, Appl. Phys. Lett. **75**, August 1999.

[14] L. C. Chao and A. J. Steckl, J. Vac. Sci. Technol. B **17** (3), 1056 (1999).

[15] B.K. Lee, C.J. Chi, L.C. Chao, J. Cheng, I. Chyr, F.J. Beyette, and A.J. Steckl, Submitted for Applied Optics, (2000).

[16] L. C. Chao, B. K. Lee, C. J. Chi, J. Cheng, I. Chyr, and A. J. Steckl, Appl. Phys. Lett. **75** (13), 1833 (1999).

[17] L. C. Chao, B. K. Lee, C. J. Chi, J. Cheng, T. Chyr, and A. J. Steckl, Appl. Phys. Lett. **75** (13), 1833 (1999).

Chapter 6
Summary and Future Challenge

Thus far, we have successfully demonstrated the feasibility of optical storage method based on GaN:Er. Data can be recorded either with FIB implantation or ion milling. Issues such as power conversion efficiency, luminescence lifetime, signal-to-noise ratio, storage density, and data rate are subjected for further investigation and exploration. Future work should include improving storage density, signal-to-noise ratio, and stimulating data rate. Er is not the only RE element that can be doped and implanted into GaN. The effectiveness of other RE species, such as Pr, Tm, Eu, and Sm, as potential candidates for optical storage device are to be evaluated. Codoping with several RE species is of great interest. This is because codopant method could not only improve the upconversion efficiency, but also present additional method to increase storage density. Preliminary data of our research show that upconversion efficiency is higher with MBE in-situ doped than with FIB implanted GaN:Er film. However FIB implantation technique is preferable for the construction of 3-D volumetric data storage, whereas ion-milling technique is more adequate for building near-field 2-D planar data storage.

In this work, we have demonstrated the concept of RE doped GaN optical memory device base on upconversion process. By using upconversion process, bits can be read in visible emission with IR laser sources. With FIB implantation approach, though we have only demonstrated a 2-D optical storage method, a 3-D model can be build by growing multilayer GaN films, with each layer written with FIB implanted RE. Besides the obvious increase of storage density ($\sim 10^{12}$ bits/cm^3) due to more effectively use of three-dimensional space. Our research results have also showed that upconversion intensity changed with implanted RE dose. At least 2^2 gray scale levels for each written bit can be created. With this scheme, 3-D storage density can be further boasted. Furthermore, more than one RE species can be implanted into GaN films. For each additional n number of species used, a 2^n increase of storage states is possible. It is therefore possible to construct an ultrahigh density 3-D optical storage devices based on RE doped wide band-gap semiconductor.

On the other hand, the potential for making near-field planar optical storage through FIB milling process has also been proven. Simulation of parallel read concept has been demonstrated with CCD color camera. FIB milled Er doped GaN optical storage architecture is based on the premise that data are recorded in nano bit size and can be retrieved with near-field detection of nonlinear stepwise upconversion optical emission intensity. Data density can be further increased by encoding them with intensity modulation method through precious control of milling depth. Near-field signal detection through upconversion emission should attain higher signal to noise (SNR) level than through the usual small light beam reflection. With bit as small as 0.4 μm^2 in size, storage density of 10^{12} bit/in^2 could be achieved. Furthermore, this design presents two distinct advantages, data mastering process based on existing proven semiconductor fabrication technology, and ability to capitalize the reliable, economical, and commercialized IR laser sources. These advantages can lead to reduction of research, development, and production cost, and extended utilization of existing technology. To improve data rate, parallel readout Si detector system is also under developed. To improve readout SNR and to simplified readout process, IR lasers should be substituted with visible lasers once semiconductor lasers at resonant emission wavelength are available.

In conclusion, data storage device based on RE doped GaN semiconductor has great promising future. The potential for creating ultrahigh portable optical storage with RE doped GaN warrant further research study.